Title
Modeling the Effects of Fire on Streamflow in a Chaparral Watershed

Author
McMichael, Christine E.

Publication Date
2004-06-01

Peer reviewed

UNIVERSITY OF CALIFORNIA, SANTA BARBARA

SAN DIEGO STATE UNIVERSITY

Modeling the Effects of Fire on Streamflow in a Chaparral Watershed

A Dissertation submitted in partial satisfaction of the

requirements for the degree Doctor of Philosophy

in Geography

by

Christine Eleana McMichael

Committee in charge:

Professor Allen Hope, Chair

Professor Janet Franklin

Professor Hugo Loaiciga

Professor Dar Roberts

June 2004

The dissertation of Christine Eleana McMichael is approved.

_____

Dar Roberts

_____

Hugo Loaiciga

_____

Janet Franklin

_____

Allen Hope, Chair

May 2004

Modeling the Effects of Fire on Streamflow in a Chaparral Watershed

by

Christine Eleana McMichael

ACKNOWLEDGEMENTS

There are so many people who have contributed in a multitude of ways towards helping me complete my dissertation – yet without God's blessings, love and guidance in my life it would not have been possible, and I give thanks to Him for all He has given me.

I thankful for my husband, Casey, whose love and complete support made it possible to pursue my graduate career in Geography and to fulfill my dream of earning a Ph.D. Casey, 'thank-you' seems like so little to say for all you are to me – I love you. I am also indebted to my entire family for their love and support throughout my academic career, most especially as I completed my dissertation. Special thanks to my brother, Jason, Mom and Jim, Dad and Mary, Joyce and Gary, Aunt Karen and Uncle Ken, and all of my grandparents for your love, prayers and encouragement over the years – I am very grateful for each of you.

My dissertation committee – it was a privilege to work with each one of you and I am most grateful for your dedication, encouragement and guidance throughout my dissertation. I am especially thankful for Dr. Allen Hope (SDSU), my chair, who helped me in so many ways to build the confidence and skills I now have, who believed in my potential even when I doubted it, and whose example I hope to emulate as I pursue my own career in academia. He has left a lasting impression on my life and I am grateful for having had the chance to work with him and to learn from him.

I am also indebted to Dr. Janet Franklin of SDSU for her support and guidance throughout my graduate career, and especially as I worked on my dissertation. She has been, and will continue to be, a role model for me – a successful woman scientist who enjoys research, teaching and working with her students. I am also very thankful for having had the opportunity to work closely with two outstanding professors at UCSB, Dr. Hugo Loaiciga and Dr. Dar Roberts. I spent many enjoyable hours with Dr. Loaiciga discussing hydrology and hydrologic modeling, the dissertation process, and working in academia. I learned a great deal from these talks and am grateful for all of his advice and encouragement throughout my dissertation. I am indebted to Dr. Roberts for sharing his remote sensing expertise with me and for his heroic assistance with processing satellite imagery. His advice and ideas were always a great help in moving my research forward. Together, Dr. Loaiciga and Dr. Roberts helped make my year at UCSB a tremendous learning experience.

I have spent a great deal of my adult life in the Geography Department at San Diego State University. I started at SDSU in the Fall of 1990 as an undergraduate Accounting major. However, I converted to Geography following an Introductory Meteorology class with Dr. Aguado – and I've never looked back! Dr. Aguado has been a wonderful friend over the years and I have greatly benefited from his timely, supportive counsel throughout my student career.

Since coming to the SDSU Geography Department I have completed a B.A., M.A., and now a Ph.D., in Geography. It is hard to express in words how

truly thankful I am for the privilege of having spent all these years with such a special group of people. Of course, people came and went over the years, but the spirit of the Department has never changed. It is an open, collegial, and stimulating place to learn and work – and I will always treasure memories of my time there. I would like to thank ALL of the faculty, staff and students it has been my pleasure to work over the years. Special thanks to Dr. Stow, Dr. O'Leary, Dr. Wright, Dr. Getis, Dr. McArthur, and Dr. Tague for all of your advice, encouragement, and collaboration - and for always taking the time to help me when I needed it. In addition, thank-you to some very special staff who made life smoother in countless ways – Yumiko Tsuneyoshi, Bonnie Golden, Jean Colburn, Lilia Ortiz, Dave McKinsey, Harry Johnson, Pete Coulter, Marcus Chiu, and John Kaiser. I am also very grateful for the many friends I've made in the department over the years, people who were never to busy to help, who made me laugh, and who made my graduate experience so very memorable – especially Ryan Engstrom, Cat Stylinski, Jennifer Swenson, Alex Syphard, Mike Anaya, Robyn Clark, John Rogan, Eric West, Luc Claessens, Mary Henry, Sally Westmoreland and Jeff Fleming.

Special thanks to all of the faculty, staff and students in the Geography Department at UCSB for making me feel welcome and for their support of my research, especially Dr. Mertes, Dr. Michaelsen and Dr. Chadwick. Thank-you, too, to the staff of the Map and Imagery Library at UCSB for their help and advice with image data. I would also like to thank the following people and agencies

from whom I have received data, assistance, and funding during my dissertation – their contributions, large and small, helped make this research possible: Dr. Moritz (UC Berkeley); National Aeronautical and Space Administration (NASA); National Science Foundation (NSF); Phi Beta Kappa, Nu Chapter (San Diego, CA); California Sea Grant College (University of California); Dr. Watson and Dr. Pierce (CSU-Monterey Bay); Dr. Oechel (SDSU); Jon Ahlroth and Matt Naftaly (Santa Barbara County Water Agency); Dr. Stoms (UCSB); Bill Ferguson (Santa Barbara Public Works Department); Ken Oster (USDA-NRCS, California); the support staff at the Danish Hydraulic Institute; Jared Aldstadt (SDSU); Dr. Zachary Bortolot and Joe Grubb (Morehead State University). [Additional acknowledgements can be found at the end of each dissertation chapter.]

Finally, I would like to express my gratitude to Dr. David Rudy and all of the faculty and staff in the Institute for Regional Analysis and Public Policy and in the Department of Geography, Government and History at Morehead State University for their support and encouragement as I completed my dissertation.

This dissertation is based upon work supported by an Earth System Science Fellowship (No. NGT5-30335) provided by NASA, a Doctoral Dissertation Improvement Grant (No. BCS-0000233) provided by NSF, and a Graduate Fellowship provided by the Nu Chapter of Phi Beta Kappa (PBK). In addition, funding support was provided by a NASA Land Use Land Cover Change Grant (No. NAG5-11141) to Drs. Allen Hope and Christina Tague (SDSU). Any opinions, findings, conclusions or recommendations expressed in this dissertation are those of the author and do not necessarily reflect the views of NASA, the NSF or PBK.

VITA of CHRISTINE ELEANA MCMICHAEL
June 2004

EDUCATION

Associate of Arts in Economics, Santa Barbara City College, June 1990
Bachelor of Arts in Geography, San Diego State University, May 1993 (*summa cum laude*)
Master of Arts in Geography, San Diego State University, December 1995
Doctor of Philosophy in Geography, University of California, Santa Barbara and San Diego State University, (expected) June 2004.

PROFESSIONAL EMPLOYMENT

Aug. 2003 - present	Assistant Professor of Geography, Institute for Regional Analysis and Public Policy, Morehead State University
Sept. 2000 - June 2003	NASA Earth System Science Fellow, Department of Geography, San Diego State University / University of California, Santa Barbara
July 1999 - June 2003	Ph.D. Teaching/Research Associate, Department of Geography, San Diego State University / University of California, Santa Barbara;
June 1997 - June 1999	California Sea Grant Trainee, Department of Geography, San Diego State University
Aug. 1995 - May 1997	Ph.D. Teaching/Research Associate, Department of Geography, San Diego State University / University of California, Santa Barbara
Aug. 1993 – July 1995	Graduate Research Assistant, Department of Geography, San Diego State University

COURSES TAUGHT

Remote Sensing of Environment (GEO 355 at Morehead State University)
Physical Geography (GEO 101 at Morehead State University)
Seminar in Regional Analysis (RAPP 300 at Morehead State University)
Introductory Remote Sensing of Environment (GEOG 488 at San Diego State University)
Introduction to Physical Geography (GEOG 101 at San Diego State University)

JOURNAL PUBLICATIONS

Tague, C., McMichael, C., Hope, A., and Choate, J. (in press). Application of the RHESSys model to a California semi-arid shrubland watershed. Journal of the American Water Resources Association.

McMichael, C.E., Hope, A.S., Stow, D.A., Fleming, J.B., Vourlitis, G., and Oechel, W.C. (1999). "Estimating CO2 exchange in two arctic tundra ecosystems using a spectral vegetation index." International Journal of Remote Sensing, 20(4):683-698.

McMichael, C.E., Hope, A.S., Stow, D.A., and Fleming, J.B. (1997). "The relationship between active layer depth and a spectral vegetation index in arctic tundra landscapes of the North Slope of Alaska." International Journal of Remote Sensing, 18(11):2371-2382.

FUNDED GRANTS, FELLOWSHIPS and CONTRACTS

2003	Morehead State University, Internal Grant: "A Remote Sensing-based Assessment of Recent Ice Storm Damage in Eastern Kentucky Forests": $4600.
	Consortium of Appalachian Centers-Appalachian Regional Commission, Contract: "Appalachaian Teaching Project": $2700.
2000-2003	NASA Earth System Science Fellowship: $62,000.
2000	NSF Doctoral Dissertation Research Improvement Grant: $5,400.
	Phi Beta Kappa, Epsilon Association, Graduate Fellowship: $3,000.

AWARDS

McKnight Professional Paper Presentation Award (2000)
California Sea Grant Traineeship (1997-1999)
Calif. Geographical Soc. D.W. Lantis Graduate Student Award (1994)
William and Vivian Finch Award for Remote Sensing (1994)
Graduate Equity Award (1994)
University Scholar Award (1993-1994)
Outstanding Graduating Senior – Department of Geography (1993)
Calif. Geographical Soc. D.W. Lantis Undergraduate Student Award (1993)
Phi Beta Kappa, Nu Chapter, Brian Billotte Memorial Scholarship (1993)
Lauren C. Post Memorial Scholarship (1992-1993)
Academic Achievement Award (1990)
Santa Barbara Scholarship Foundation Undergraduate Scholarship (1988-89)

FIELDS OF STUDY

Major Fields: Environmental Remote Sensing, Hydrologic Modeling, and Physical Geography

Studies in Environmental Remote Sensing, Hydrologic Modeling and Physical Geography with *Professor Allen Hope*

Studies in Environmental Remote Sensing and Chaparral Ecology with *Professor Janet Franklin*

Studies in Hydrologic Modeling with *Professor Hugo Loaiciga*

Studies in Environmental Remote Sensing with *Professor Dar Roberts*

ABSTRACT

Modeling the Effects of Fire on Streamflow in a Chaparral Watershed

by

Christine Eleana McMichael

A comprehensive understanding of the effects of fire and post-fire succession on streamflow dynamics in California chaparral watersheds is needed to facilitate effective planning and management in these semi-arid shrublands. Watershed experiments have provided insights into the hydrologic effects of fire and post fire succession in chaparral watersheds, however extrapolation of these results is constrained by the small number of studies and the limited space and/or time scales examined. As it was not logistically or economically feasible to conduct additional field experiments for this research, an integrated remote sensing-distributed hydrological modeling strategy was utilized to advance our understanding of the effects of fire and post-fire succession on streamflow dynamics in these ecosystems. A wide range of inputs was derived for a modified version of the distributed, physically-based MIKE-SHE model using remote sensing and geographic information systems (GIS) techniques, including the development of a remote sensing-chronosequence approach for estimating the post-fire recovery sequence of chaparral leaf area index (a key input given that approximately 75% of incoming rainfall is returned to the atmosphere via evapotranspiration). The Monte Carlo-based Generalized Likelihood Uncertainty

Estimation (GLUE) methodology provided the framework for model calibration, testing, and predictive uncertainty estimation. Model simulations were performed using a suite of fire size-weather regime combinations to investigate the impacts of fire on annual and seasonal streamflow dynamics.

Over two-thirds of the observations (comprising over 90% of the total observed flow) in the calibration and test periods were contained within the GLUE-based predictive uncertainty bounds, an acceptable level of model performance relative to total period flow; prediction errors were generally associated with large rainfall and fire events. Model simulation results demonstrated that seasonal and annual streamflow response increased approximately linearly with fire size under both the wet and dry weather regimes. Moreover, the sensitivity of streamflow response to fire size varied with annual rainfall condition and stand age. However, these predictions were largely indistinguishable from the predictive uncertainty associated with the calibrated model used to make them - highlighting the importance of analyzing hydrologic predictions for altered land cover conditions in the context of model uncertainty.

TABLE OF CONTENTS

LIST of FIGURES

LIST of TABLES

PREFACE

Chaparral shrublands in California cover approximately 3.4 million hectares of land from sea level to about 2000m in regions dominated by a semi-arid climate. Fires in these watersheds dramatically alter land cover conditions and initiate a complex matrix of vegetation recovery sequences that span many decades. Future climate- and anthropogenic-induced changes may modify the current fire regime in these ecosystems and, consequently, post-fire vegetation recovery patterns and related streamflow dynamics. Catchment experiments have provided insights into the effects of fire and post-fire succession on streamflow in these shrublands, however extrapolation of these results is constrained by the small number of studies and the limited space and/or time scales examined. A more comprehensive understanding of these effects is required in order to facilitate effective planning by those charged with protecting and managing California's chaparral watersheds for water supply, water quality and wildlife/vegetation habitat. It is not feasible to conduct the field experiments required to investigate the impacts of fire size on streamflow dynamics at the larger spatio-temporal scales of interest. Therefore, this dissertation utilized an integrated remote sensing-distributed hydrological modeling strategy to examine these effects for a medium size chaparral catchment in central California.

Organization of the dissertation

Chapter One discusses the importance of the leaf area index (LAI) vegetation parameter in modeling the eco-hydrological effects of land cover change (e.g., due

to fire), as well as the scant availability of chaparral LAI values in the literature. This limitation is addressed in Chapter One via the development and application of a remote sensing-based chronosequence approach for estimating LAI recovery sequences following fire in central California chaparral shrublands.

Chapter Two explains the concept of equifinality, that acceptable model predictions might be achieved using different parameter sets, and describes the application of a methodology (the Generalized Likelihood Uncertainty Estimation (GLUE) technique) that explicitly recognizes this phenomenon and provides a framework for model calibration, testing and predictive uncertainty estimation. The GLUE-based evaluation of the spatially distributed, physically based MIKE-SHE hydrologic model is presented in Chapter Two for the Jameson catchment, a 34 km^2 chaparral-dominated basin in central California.

Despite the widespread use of remote sensing-based LAI estimates in hydrological modeling, there is little understanding of how uncertainty in these inputs translates into uncertainty in model predictions (predictive uncertainty) or affects the sensitivity of model output to individual parameters (parameter sensitivity). Chapter Three examines the effects of uncertainty in LAI inputs on the predictive uncertainty and parameter sensitivity of the MIKE-SHE model using the Monte Carlo-based GLUE and Generalized Sensitivity Analysis (GSA) methodologies, respectively, for the Jameson catchment.

Fire is a major agent of land cover transformation in chaparral watersheds, however little is known about the relationship between fire size and seasonal and

annual streamflow response in these semi-arid basins. Chapter Four describes the application of the calibrated MIKE-SHE model to examine these relationships over a range of fire sizes in the Jameson catchment for both a wet and a dry period. Chapter Four also introduces the concept of 'inherent predictive uncertainty' (i.e., the predictive uncertainty associated with a GLUE-calibrated model) and evaluates model predictions for each fire size-period combination relative to the inherent predictive uncertainty of the calibrated MIKE-SHE model.

CHAPTER ONE

Post-fire recovery of leaf area index in California chaparral: a remote sensing-chronosequence approach

Abstract. Fire is a major driver of land surface transformation in California Mediterranean-type shrublands (i.e. chaparral). The re-growth of leaves following fire impacts a wide variety of ecosystem processes and information on the post-fire recovery of leaf area index (LAI) is often required in eco-hydrologic modelling studies. A few studies have reported LAI values for chaparral, but none have tracked LAI dynamics over the entire post-fire recovery sequence. In this study we used a chronosequence approach with satellite imagery to determine the post-fire development sequence of LAI for chaparral shrublands in central California. Moreover, we explored how LAI varied with differences in annual antecedent precipitation conditions (APC) and physical site factors. LAI recovery following fire was most rapid during the first 10-15 years, after which it remained relatively constant with increasing stand age. For a given stand age, LAI varied non-linearly with annual APC, while spatial variations in LAI were associated with differences in topographic aspect and landscape wetness potential. However, a better understanding of the nature and interaction of these controls on LAI is needed if realistic post-fire LAI trajectories (for historic, present and future periods) for eco-

hydrological modelling studies in chaparral catchments are to be developed in the future.

1. Introduction

Fire is a major driver of land surface transformation in California Mediterranean-type shrublands, i.e. chaparral (Keeley *et al*. 1999). The removal and re-growth of green leaves following fire impacts a wide variety of ecosystem processes including canopy light interception (Henry and Hope 1998), river discharge (Rambal 1994, Loaiciga *et al*. 2001) and soil nutrient cycling (Christensen 1994). Consequently, information on the spatio-temporal dynamics of green leaf area is often required in physically based, spatially distributed eco-hydrologic models to study the effects of land-cover change (e.g. due to fire) on ecosystem and catchment processes. The parameter most widely used to represent changes in green leaf abundance in these types of studies is the leaf area index (LAI), which is the total (one-sided) area of the transpiring leaf surface above a given ground area. While a number of authors have reported LAI values for chaparral shrublands (Table 1-1), these data are typically restricted to a single species (or community type), a few observations over a limited area and/or to one point in time. Observations of LAI at the spatio-temporal scales required to study landscape- and catchment-level impacts of fire and vegetation recovery in chaparral are not practical given the considerable sampling and logistical difficulties associated with such a field campaign.

1.1. Remote Sensing of LAI

Previous work has demonstrated the viability of using remote sensing-based techniques to characterise the spatio-temporal patterns of LAI over large areas and/or multiple time periods (Nemani and Running 1989, Spanner *et al*. 1990, Curran *et al*. 1992, Friedl *et al*. 1994, Watson *et al*. 1999). Remote sensing-based estimates of LAI are typically made using site specific empirical relationships that have been established between ground-based measurements of LAI and vegetation indices derived from multi-spectral satellite data (de Jong 1994, Hoff *et al*. 1995, Chen and Cihlar 1996, Turner *et al*. 1999). These spectral vegetation indices (SVIs) generally take the form of a ratio or linear combination of sensor bands and represent a means of reducing multi-spectral information to a single value for estimating vegetation characteristics (e.g. LAI). The SVI most widely used to estimate LAI is the Normalized Difference Vegetation Index, NDVI (1):

$$\mathrm{NDVI} = \frac{\mathrm{NIR} - \mathrm{R}}{\mathrm{NIR} + \mathrm{R}} \qquad (1)$$

where, NIR and R refer to the near-infrared and red regions of the electromagnetic spectrum, respectively; values of NDVI range between -1 and 1. Green leaves exhibit strong absorption in the red region and high reflectance in the near-infrared region of the electromagnetic spectrum. The NDVI has been shown to be linearly related to the fraction of photosynthetically active radiation absorbed by the canopy which, in turn, is nonlinearly related to LAI (Asrar *et al*. 1984, Sellers

1985, 1987). The relationship between NDVI and LAI generally has a near-linear form for LAIs between zero and three, becoming asymptotic as values approach four to five (Asrar *et al*. 1984, Sellers 1985, Fassnacht *et al*. 1997). Based on published values of chaparral LAI (Table 1-1) it is unlikely that the relationship between NDVI and LAI would reach saturation levels.

A generalized NDVI-LAI model developed by Baret *et al*. (1989) has been applied in Mediterranean Basin ecosystems using multi-temporal satellite data to estimate LAI inputs for carbon and water flux models (Hoff *et al*. 1995, Lacaze *et al*. 1996, Teixeira-Filho *et al*. 1996). Gamon *et al*. (1995) examined the relationship between the NDVI and LAI in a California Mediterranean-type ecosystem using ground-based measurements. Although a strong relationship between the NDVI (hand-held radiometer) and the LAI (destructive harvesting) was reported when measurements from evergreen shrubs and trees were combined (Gamon *et al*. 1995), the uncertainties associated with extrapolating these plot-level results to large chaparral catchments over successional time periods may be large.

1.2. Post-fire succession in chaparral

One of the most striking and consistent observations regarding chaparral growth patterns is its rapid recovery during the first 10-15 years following fire. A number of measures of evergreen shrub growth have been shown to increase rapidly during the first 10-15 years following fire, including vegetation cover fraction (Horton

and Kraebel 1955, Hanes 1971), above-ground biomass (Rundel and Parsons 1979, Mooney 1981), live above-ground biomass (Black 1987), foliage biomass (Rundel and Parsons 1979, Riggan *et al*. 1988) and LAI (Rundel and Parsons 1979). Descriptions regarding changes in biomass and LAI after age 15 are mixed. Some evidence suggests that small increases in aboveground biomass occur through age 30, after which it remains relatively constant for the remainder of the shrubs' lifespan (Mooney 1981). In contrast, Rundel and Parsons (1979) documented a consistent decline in aboveground biomass, leaf biomass and LAI between ages 16 and 60, while Black (1987) reported an initial increase in live biomass after age 30, followed by a decline, followed by another increase.

In addition to stand age, chaparral shrub re-growth has been shown to respond to differences in precipitation conditions. Observations of percent vegetation cover (Keeley and Keeley 1981), NDVI (Henry and Hope 1998) and model simulations of LAI (Miller 1981) have demonstrated that chaparral shrub recovery for sites in southern California responds to inter-annual variability in precipitation. Measurements of aboveground biomass (Black 1987) and estimates of percent vegetation cover (Hanes 1971) in chaparral have also been shown to vary with topographic aspect (in response to differences in energy and soil moisture balances).

Depending upon the post-fire regeneration strategy employed (i.e. seedling recruitment or re-sprouting), evergreen chaparral shrubs typically live 30-50 years (seeders) or 50+ years (re-sprouters – the above-ground portion) (Horton and

Kraebel 1955, Hanes 1971, Black 1987). Some authors have reported evergreen shrub stands as old as 80-100 years (e.g. Keeley and Keeley 1977, Keeley 1992, Zammit and Zedler 1992). As a result, it is necessary to relate LAI to stand age over at least an 80 year period in order to characterise the entire post-fire successional sequence. To date, it has not been possible to monitor this entire sequence in chaparral shrublands due to the relatively short length of the satellite era (1972-present) and the timing of fires within this period. Problems related to image acquisition (e.g. cloudiness and limited anniversary date coverage) have further confounded such attempts. An alternative strategy is to use a chronosequence approach to relate satellite-based estimates of chaparral LAI to stand age at a given point in time (after Rundel and Parsons 1979). The entire post-fire sequence of LAI may be characterized via this exchange of space for time given a sufficient range of stand ages.

1.3. Research objectives

In this study we used a chronosequence approach with satellite imagery to investigate the relationship between chaparral LAI and stand age following fire. It was expected that the post-fire trajectory of LAI development would follow chaparral re-growth trends reported in the literature and increase most rapidly during the first 10-15 years after fire. However, temporal differences in annual antecedent precipitation conditions (APC) and spatial variability in site energy and moisture balances imply a range of possible LAI values for any given stand age.

Therefore, we also expected LAI to vary with differences in annual APC and physical site characteristics.

2. Methods

Satellite imagery and fire history maps were used to develop an empirical procedure for determining the trajectory of chaparral LAI development following fire in the Coast Range of central California. The general NDVI-LAI model proposed by Baret *et al*. (1989) was used to convert NDVIs into LAI values for ten fall Landsat Thematic Mapper (TM) and Enhanced Thematic Mapper+ (EMT+) images. In each image the mean LAI was extracted from eleven chaparral stands and plotted against stand age (chronosequence approach). The general relationship between LAI and stand age was examined using LAI-stand age data pairs from all images (the pooled data set). The impact of differences in annual APC on LAI was determined by stratifying the pooled data by image date. Variability in LAI resulting from differences in site energy and moisture balances was investigated by examining the relationships between LAI, topographic aspect and an index of landscape wetness.

2.1. Study area

This study was carried out over an approximately 3200 km^2 area in the San Rafael Mountains (Coast Range) north of Santa Barbara, California, USA (Figure 1-1). The Mediterranean-type climate of this non-urbanized region is characterized by

cool, wet winters and warm, dry summers. Annual average precipitation and river discharge are approximately 780 mm and 233 mm, respectively. Elevation ranges between 238 m and 2083 m. Rocky, nutrient-poor sandy-loam soils are typically found on the relatively steep, rugged hillslopes (average slope ~ 43%), while somewhat deeper soils are found in ravines, valley bottoms and along gentle foothill slopes (O'Hare and Hallock 1988). Serpentine soils occur in limited areas (O'Hare and Hallock 1988). The combination of stands in different stages of post-fire succession with spatial variability in physical site characteristics (e.g. terrain and soils) produces a complex vegetation mosaic dominated by evergreen shrub and tree species (e.g. *Adenostoma fasiculatum*, *Ceanothus leucodermis*, *Arctostaphylos glauca*, *Quercus spp.*), intermixed with herbs/grasses, summer deciduous sub-shrubs (e.g. *Salvia mellifera*, *Artemisia californica*, *Eriogonum fasiculatum*), and winter-deciduous riparian trees (e.g. *Salix spp*. and *Populus spp*.) (Stephenson and Calcarone 1999). Fires in this region generally occur towards the end of the dry summer period, with the largest events coinciding with extreme weather conditions (Moritz 1997, Moritz 2003).

2.2. Satellite imagery

Nine Landsat TM images and one Landsat ETM+ image (28.5 m pixel resolution) were obtained from the Earth Resources Observation Systems (EROS) Data Center in South Dakota, USA (Table 1-2). All images were terrain-corrected using a co-registered 28.5 m digital elevation model (DEM). Fall

(August/September) imagery was selected in order to minimise the contribution of non-evergreen vegetation types to the spectral signal. The fall 2002 ETM+ image was selected as the base image for both the geo-referencing and relative radiometric registration procedures. Each of the nine remaining images was spatially registered to the fall 2002 image using Digital Imaging Made Easy (DIME) software and a minimum of 700 tie points. Root mean square errors (RMSE) for the geo-referenced image set ranged between 0.30-0.65 pixels.

Atmospheric correction and conversion of DN images to apparent surface reflectance (hereafter referred to as reflectance) was performed using ACORN (Atmospheric CORrection Now) software. ACORN pre-processing involved preparing the required image metadata files (i.e. image spectral response, image acquisition parameters, and atmospheric conditions) and converting the fall 2002 scene into radiances using the gains and offsets provided with the image. ACORN was used in Mode 5 (atmospheric correction of calibrated multispectral data) with a 'Mid-latitude summer' atmospheric model to convert the fall 2002 radiance image into apparent surface reflectances. 'Relative radiometric calibration' standardizes an image dataset with respect to atmospheric, illumination and sensor effects so that image-derived products can be compared over time (Roberts *et al*. 1998). Thirty temporally invariant targets (each 2x2 pixels in size) were selected across the range of image brightness (rock outcrops, runways, buildings, deep ocean) and used to radiometrically intercalibrate each of the fall images to the base fall 2002 image. A minimum of 25 targets was used to develop the linear

calibration equations (the presence of clouds and/or outliers in the linear regressions occasionally reduced the number of available targets). The mean digital number (DN) and reflectance value were extracted from each band for each target for the 'uncalibrated' image and the fall 2002 (base) image, respectively. Reflectance values for each target from the 2002 image were regressed against the DNs from the paired image for each band to derive a set of calibration equations; adjusted R^2 values were greater than 0.88 for all equations.

Differences in surface illumination conditions caused by topography have been shown to cause variability in surface spectral response that is independent of actual changes in land cover (Teillet *et al*. 1982, Civco 1989, Gu and Gillespie 1998, Dymond *et al*. 2001). Given the rugged nature of our study area, an illumination correction algorithm was applied to each of the 10 Landsat reflectance-based images to normalise for topographic effects. The C-correction algorithm (Teillet *et al*. 1982) was used for this procedure given its superior performance (Meyer *et al*. 1993, McDonald *et al*. 2000) over other widely-used illumination corrections (e.g., cosine correction, Smith *et al*. 1980, Teillet *et al*. 1982; Minnaert correction, Minnaert 1941, Smith *et al*. 1980).

Following illumination correction, the 3200 km^2 study area was subset from each image in the set. Image pixels located in topographic shadows were identified and masked out using the 28.5 m DEM. Each reflectance-based image was then converted into an NDVI image using ERDAS IMAGINE software. Finally, since this research focused on the post-fire recovery of evergreen

chaparral shrubs, all other vegetation types were masked out of the NDVI images using an existing digital vegetation map of the area (2 ha minimum mapping unit) (Franklin *et al*. 2000).

2.3. Approach

2.3.1. NDVI-LAI model

The following general model (2) has been used to estimate LAI from NDVI values in Mediterranean-type ecosystems (Baret *et al*. 1989, Hoff *et al*. 1995, Lacaze *et al*. 1996):

$$LAI = -\frac{1}{k} * \ln\left(\frac{NDVI_{\infty} - NDVI}{NDVI_{\infty} - NDVI_{back}}\right) \quad (2)$$

where, k is a parameter related to the extinction of solar radiation through a vegetation canopy, $NDVI_{\infty}$ is the maximum NDVI observed for 'infinite' vegetation, and $NDVI_{back}$ is the background NDVI. Parameterized values used in previous Mediterranean-type ecosystem studies are given in Table 1-3. In this study the value of $NDVI_{\infty}$ was set equal to the maximum chaparral NDVI observed in study area over the entire image set (0.850). This value of $NDVI_{\infty}$ corresponds closely to those reported in Table 1-3. A value for $NDVI_{back}$ was selected by examining the near-infrared vs. red feature space for the driest image in the set (September 3, 2002, Table 1-2). To avoid potential bias introduced by outliers, $NDVI_{back}$ was set equal to the average NDVI of the 20 brightest pixels located

along the soil line (0.123). While our value of $NDVI_{back}$ is different from those cited in Table 1-3, Lacaze *et al*. (1996) indicated that values of this parameter may be highly variable from site to site as a result of local differences in canopy understory, soil surface conditions and litterfall.

Ideally the NDVI-LAI model should be calibrated with respect to k using paired observations of LAI and NDVI for a range of representative vegetation sites. As discussed previously, observations of this type are not available for California chaparral ecosystems, especially at scales consistent with pixels in satellite imagery. Moreover, such a set of observations is not likely to be collected in the near future as a result of the considerable logistical difficulties involved in carrying out such a comprehensive field study in this landscape, including the potential uncertainties associated with accurately characterising LAI for 88.5 m x 88.5 m plots. The absence of paired LAI-NDVI observations is not critical to this study since we are more concerned with the relationship between LAI and stand age than with the absolute magnitude of predicted LAIs. However, in order to model LAI values as realistically as possible, we adopted the following strategy for selecting a value of k.

Miller (1981) stated that LAI values for evergreen chaparral shrubs generally range between one and two, but may rise to three or four as annual precipitation increases. LAI values reported in the chaparral literature (1- 1) range between approximately one and three. Based on this information, we assumed that mature chaparral stands in this region reach a LAI of two under average annual

precipitation conditions. The value of *k* for which NDVI-LAI model predictions corresponded to this LAI value was found to be 0.365. This value of *k* was used when applying the NDVI-LAI model to each satellite image under the assumption that it was equally valid for all stands and antecedent precipitation conditions.

2.3.2. Vegetation stand age

Digital fire history maps of the study area were used to delineate fire perimeters and determine dates of ignition (CDF/USDA 2001, M. Moritz, *personal communication*). These maps were intersected with each LAI image to determine the vegetation age mosaic in the study area at each point in time. Eleven different fires were identified in this area for the time period encompassing the satellite imagery. For purposes of this research the area associated with each fire was referred to as a 'stand'. We restricted our analysis to fires larger than 30 km^2 as the recovery of small areas may be strongly affected by local site conditions. The impact of human activities on vegetation re-growth dynamics was assumed to be negligible given the non-urbanized state of the study area.

2.3.3. LAI-stand age relationship: antecedent precipitation and site characteristics

Ten LAI images were generated by applying the calibrated NDVI-LAI model to each of the NDVI images. The average LAI was calculated for each stand in each image and plotted against the corresponding stand age to examine the general

relationship between LAI and stand age over all images. This pooled data set was then stratified by image date to assess how values of LAI for a given stand age were affected by differences in annual APC, the total precipitation for the water year (October-September) preceding the satellite image date. An image was classified as 'average' if its corresponding annual APC was within ½ standard deviation (390mm) of the long term average annual APC (715mm); images with annual APC values greater or less than ½ standard deviation were classified as 'wet' or 'dry', respectively (Table 1-2).

An examination of the relationship between LAI and two variables representing site energy and moisture availability - topographic aspect and landscape wetness potential – was conducted for a mature stand in one image (this approach standardized the analysis for both stand age and APC). The stand with the highest average standard deviation (1.093) over the four average APC images (1986, 1988, 1997 and 2000) was selected for this analysis. In order to facilitate the comparison of continuous variables (LAI, aspect and wetness) across the landscape we divided the 'mature' stand into three separate sub-units on the basis of 'relative landscape productivity'. Differences in relative landscape productivity (RLP) across the mature stand were assumed to follow the spatial variability in the mean LAI image for this stand (computed using all 10 LAI sub-scenes for this stand). Pixels in the mature stand were assigned to a RLP-unit (low, moderate and high) via an equal-value division of the mean LAI image histogram. An aspect grid for the mature stand was derived from the 28.5 m DEM. A grid of landscape

wetness for this stand was generated by calculating the compound topographic index (CTI) from the 28.5 m DEM (3):

$$CTI = \ln (A / \tan (\beta)) \quad (3)$$

where, A is the upslope contributing area and β is the landscape slope. The CTI is commonly used in hydrologic analysis to characterise the potential for different areas in a catchment to develop saturated conditions (Beven and Kirkby 1979); typical values of CTI range between 1 (dry) and 15 (saturated). Polar plots were used to examine the relationships between aspect and CTI for each RLP unit in the mature stand.

3. Results and discussion

3.1. The general LAI-stand age relationship

Plotting mean LAI versus stand age for all stands in all images yielded the scatter of points shown in Figure 1-2. An exponential growth function (broken line) was fit to this pooled dataset to illustrate the general shape of the relationship between mean LAI and stand age. [Note: all fitted lines in this paper are for illustrative purposes only; they are not predictive models.] This function was forced through LAI = 0 at stand age = 0 based on the assumption that all photosynthetically active vegetation within a mapped perimeter was completely consumed by fire. In reality some green vegetation may have survived fire, however information regarding its

location and extent was not available for our study area (nor is this information generally available for fires in this region). Fires analyzed in this study occurred in the summer and chaparral re-growth does not usually begin until the following spring when temperatures rise and soil moisture supplies are adequate. Consequently, LAI values in the fall immediately following fire could reasonably be expected to equal zero.

The general relationship depicted in Figure 1-2 indicates that LAI increased most rapidly during the first 15 years following fire, with the largest change in LAI occurring between ages zero and five. LAI remained essentially constant from age 15 through age 81 (the oldest stand in the image set). The rapid increase in mean LAI during the first 10-15 years is consistent with the trend in LAI reported by Rundel and Parsons (1979) for this age span [and with measurements of biomass (Rundel and Parsons 1979, Mooney 1981, Black 1987, Riggan *et al*. 1988) and estimates of percent cover (Horton and Kraebel 1955, Hanes 1971).] Rundel and Parsons (1979) measured LAI for five *Adenostoma fasiculatum*-dominated chaparral stands of different ages (2, 6, 16, 37 and 60) in Sequoia National Park, California and documented an increase in LAI between ages 2 and 16. The agreement between our results and those of Rundel and Parsons (1979) suggests that, despite differences in species composition between sites, the post-fire recovery dynamics of chaparral in the Sequoia and San Rafael Mountain areas are broadly similar for stands younger than 16 years of age.

In contrast to the decline in LAI between ages 16 and 60 reported by Rundel and Parsons (1979), our results indicate that mean LAI remained steady between ages 15 and 81 (similar to findings reported by Mooney (1981) for above-ground biomass). This difference in LAI dynamics after age 16 could be a result of site-to-site variability in species composition. Rundel and Parsons (1979) measured LAI for pure stands (3-5 shrubs) of *Adenostoma fasiculatum*, while each large stand used in this study contained a mix of evergreen shrub species (from which a mean LAI was obtained). The resulting variability in life history strategies, life span, morphology and physiology modifies stand composition over time, potentially maintaining a nearly constant mean LAI value for a given stand as some species thrive and expand while others senesce and die. In contrast, LAI values for mono-specific stands are directly tied to changes in the structure and function of a single vegetation type.

3.2. Antecedent precipitation condition and LAI

The effect of variability in annual APC on the general LAI-stand age relationship was examined by stratifying the pooled data pairs in Figure 1-2 by satellite image date (Figure 1-3). This APC-based stratification greatly reduced the variability in the relationship between mean LAI and stand age. As before, an exponential growth curve was fit through each image-based set of points to illustrate the form of the relationship. Post-fire LAI recovery was most rapid over the first 10-15 years under each antecedent precipitation condition, with the largest gains

generally taking place in the first five years after fire. There was very little to no change in LAI after age 15 in each case.

From Figure 1-3 it is clear that the relationship between mean LAI and stand age responded to differences in annual APC. For stand ages between zero and 30 in the 'dry' image set (Figure 1-3a), mean LAI values were smallest in the driest year (fall 2002). Mean LAI values for stands older than age 30 were approximately the same in 1985 and 2002 despite the fact that 148 mm more rain fell in 1985 than in 2002 (Table 1-2). Values of mean LAI were largest for all stand ages in the 1994 image, approaching 30% larger for stands older than 30 years. Although we expected the antecedent precipitation from the preceding year to have a large effect on leaf productivity, two-year antecedent precipitation may be the critical period associated with leaf production. The leaves of evergreen chaparral shrubs remain on the plants for an average of two years following leaf initiation (Miller 1981, Kummerow and Ellis 1989). Hence, the very wet conditions in water year 1993 (1260 mm) may have enhanced leaf production (and/or limited leaf drop) in 1994 relative to the 1985 and 2002 images, which had drier 2-year antecedent precipitation conditions.

Stands older than 20 years had approximately the same mean LAI values in each of the four 'average' APC images (Figure 1-3b). Younger stands in this image set followed one of two post-fire recovery trajectories, one reaching peak values more rapidly (1986 and 1988) than the other (1997 and 2000). The young stand ages in 1986 and 1988 are associated with a fire in 1985, while the young

stand ages in 1997 and 2000 correspond to a fire that occurred in 1994. Differences in the two post-fire trajectories are likely due to variability in fire properties (e.g., intensity), physical site characteristics (e.g., slope/aspect) and/or rainfall conditions between stands.

Values of mean LAI were different across nearly all stand ages for the three 'wet' APC images (Figure 1-3c). The 1-year and 2-year antecedent precipitation conditions were larger for the 1995 image than for the 1992 image, while both APC values were greatest preceding the 1998 image. However, despite wetter conditions, the 1998 image had the lowest mean LAI values over all stand ages. A potential explanation for this phenomenon may be related to observed differences in rainfall patterns between water years. In particular, 1998 experienced over 50 percent more days with rainfall totals above 50 mm than either 1992 or 1995. Moreover, there were 30 percent and 78 percent more days with rainfall totals over 25 mm in 1998 than in 1992 and 1995, respectively. It is possible that the occurrence of more days with high rainfall totals in 1998 may have been associated with greater cloudiness and cooler temperatures, conditions which may have constrained and/or delayed chaparral productivity that year.

Overall, the response of the LAI-stand age curves to differences in APC was not linear (Figure 1-3). This finding agrees with Miller's (1981) LAI simulation results which predict an asymptotic relationship between LAI and annual precipitation, i.e. beyond some value, further additions of precipitation to the land surface do not greatly affect the magnitude of LAI. This precipitation

threshold effect is illustrated in Figure 1-4 for three different stand ages (5, 10 and 20 years old). A logarithmic curve was fit to the set of points for each stand age in order to illustrate the diminishing effect of increasing precipitation on mean LAI.

The ten satellite images used in this study encompass the range of annual APC observed in the study area over the past forty-five years. While representative, this is not a comprehensive set of imagery and we do not fully understand the non-linear response of LAI to annual antecedent precipitation condition. Future research will analyse additional imagery (including spring imagery) in an attempt to more completely characterise the nature of this response. In addition to the one-year, two-year and cumulative antecedent precipitation conditions, the effect of intra-annual variability in precipitation on LAI will be examined.

3.3. LAI, topographic aspect and landscape wetness

The relationship between topographic aspect and landscape wetness potential (i.e. CTI) for each RLP-unit is displayed in Figure 1-5. It is clear from these plots that both aspect and landscape wetness potential influence the spatial distribution of chaparral LAI. The polar plots show that each RLP-unit (i.e. LAI class) was dominated by different topographic aspects. The majority of pixels in the low RLP-unit were located in the south-west quadrant, while most pixels in the high RLP-unit were found on north-west facing slopes. The moderate RLP-unit was almost equally dominated by south-west and north-west facing pixels. Overall,

these patterns correspond closely to those found in the literature, where above-ground biomass (Black 1987) and percent cover (Hanes 1971) were greater on north-facing slopes than on south-facing slopes.

The range of CTI values was similar among all three RLP-units, however the concentration and spatial distribution of values within each range varied between units (Figure 1-5). The mean (and standard deviation) CTI increased from 1.2 (1.5) to 1.6 (1.8) to 2.7 (2.5) for the low, moderate and high RLP-units, respectively. CTI values in the low RLP-unit were generally less than 5 (fairly dry), while larger values (wetter conditions) were more common in the moderate and high RLP-units. This shift in landscape wetness potential with increasing RLP reflects the fact that water is the limiting resource for vegetation productivity in chaparral ecosystems. Differences in the spatial distribution of low, medium and high CTI values between RLP-units suggest that variability in soil moisture across the landscape is controlled both by slope drainage characteristics and incoming radiation (aspect). Future work will examine this hypothesis in more detail and will investigate the role that other physical site characteristics (e.g. soil type and elevation) play in controlling the spatial variability of LAI in this environment.

4. Conclusions

Our remote sensing-based results indicate that chaparral LAI recovers rapidly during the first 10-15 years after fire. However, after this point, stand age seems to have a very small impact on changes in LAI and differences in annual APC and

physical site characteristics (aspect and landscape wetness potential) appear to emerge as the primary controls on LAI dynamics. A better understanding of the nature and interaction of these controls is needed if future efforts to develop realistic post-fire LAI trajectories (for historic, present and future periods) for hydro-ecological modelling studies in chaparral catchments are to be successful.

Efforts are underway to obtain field-based estimates of LAI in order to improve the calibration of the Baret *et al*. (1989) NDVI-LAI model. At a minimum, this sampling strategy should include LAI estimates for each of the major shrub species for each functionally significant combination of terrain and soil attributes. Although the present study focused on evergreen shrubs, other vegetation types typically intermix with these shrubs in the study basin and surrounding areas – types which may be ecologically and/or hydrologically significant at particular spatio-temporal scales. For example, annual herbaceous species dominate the immediate post-burn environment in chaparral, yet nearly disappear after three to four years as they are shaded out by the recovering shrubs (Keeley and Keeley 1981, Keeley *et al.* 1981). Therefore, additional LAI sampling of the non-shrub vegetation (e.g. grasses and summer deciduous sub-shrubs) should be carried out whenever possible.

Finally, in order to extend our analysis to additional years and seasons, future work will also investigate the potential of applying the NDVI-LAI model to multi-spectral imagery from other remote sensing platforms (e.g. the Advanced Visible and Infrared Imaging Spectrometer (AVIRIS)). In conjunction with this

effort, additional remote sensing-based measures of 'green vegetation abundance' will be related to field-based LAI estimates in an attempt to identify the most accurate remote sensing-based LAI model for chaparral. In general, spectral vegetation indices (SVIs, of which the NDVI is the most widely applied) may be affected by extraneous variables such as the presence of non-photosynthetic material (Gamon *et al*. 1995), variability in illumination conditions (Deering *et al*. 1994) and soil background (Elvidge and Lyon 1985, Huete *et al*. 1985) in image pixels. As a result, a NDVI-based LAI model may not, ultimately, be the most appropriate approach in chaparral shrublands that contain a large proportion of woody material and favour steep slopes. Moreover, SVIs are only capable of providing single spectral ratio information for each, usually 'mixed', pixel. An alternative to SVIs is linear spectral mixture analysis (LSMA), which can be used to identify sub-pixel components (e.g. green vegetation abundance, woody material and shade) that are largely independent of extraneous conditions (Roberts *et al*. 1993, Roberts *et al*. 1997). It is possible that the green vegetation abundance component derived from LSMA may provide improved estimates of chaparral LAI, however additional work is needed to develop and calibrate a LSMA-based LAI model for these ecosystems.

Acknowledgements

Funding for this research was provided in part by a NASA Earth System Science Fellowship (No. NGT5-30335), a NSF Doctoral Dissertation Research Improvement Grant (No. BCS-0000233) and a NASA Land Use Land Cover Change Grant (No. NAG5-11141).

Thanks are due to Dr. Max Moritz for assistance with digital fire history data; Drs. Janet Franklin and Christina Tague for valuable comments in preparing the manuscript; Dr. David Stoms for assistance with satellite data; Lisa Levien, Chris Fischer and John Rogan for help with satellite and digital vegetation data; David McKinsey for compiling the digital elevation model; and Harry Johnson for designing the study area map.

References

Asrar, G., Fuchs, M., Kanemasu, E.T., and Hatfield, J.L., 1984. Estimating absorbed photosynthetic radiation and leaf area index from spectral reflectance in wheat. Agronomy Journal. 76, 300-306.

Baret, F., Olioso, A., Luciani, J.L., and Hanocq, J.F., 1989. Estimation de l'énergie photosynthétiquement active absorbée par une culture de blé à partir de données radiométriques. Agronomie. 9, 885-895.

Beven, K.J. and Kirkby, M.J., 1979. A physically based, variable contributing area model of basin hydrology. Hydrological Sciences Bulletin 24, 43-69.

Black, C.H., 1987. Biomass, nitrogen, and phosphorus accumulation over a southern California fire cycle chronosequence. In Plant Response to Stress, edited by J.D. Tenhunen, F.M. Catarino, O.L. Lange, and W.C. Oechel (Berlin: Springer-Verlag), pp. 445-458.

CDF/USDA (California Department of Forestry and Fire Protection, USDA Forest Service), 2001. Fire Perimeters, http:\frap.cdf.ca.gov\data.

Chen, J.M., and Cihlar, J., 1996. Retrieving leaf area index of boreal conifer forests using Landsat TM images. Remote Sensing of Environment 55, 153-162.

Christensen, N.L., 1994. The effects of fire on physical and chemical properties of soils in Mediterranean-climate shrublands. In The Role of Fire in Mediterranean-type Ecosystems, edited by J.M. Moreno and W.C. Oechel (New York: Springer-Verlag), pp. 79-95

Civco, D.L., 1989. Topographic normalization of Landsat Thematic Mapper digital imagery. Photogrammetric Engineering and Remote Sensing 55, 1303-1309.

Curran, P.J., Dungan, J.L., and Gholz, H.L., 1992. Seasonal LAI in slash pine estimated with Landsat TM. Remote Sensing of Environment 39, 3-13.

De Jong, S.M., 1994. Derivation of vegetative variables from a Landsat TM image for modeling soil erosion. Earth Surface Processes and Landforms 19, 165-178.

Deering, D.W., Middleton, E.M., and ECK, T.F., 1994. Reflectance anisotropy for a spruce hemlock forest canopy. Remote Sensing of Environment 47, 242-260.

Dymond, J.R., Shepard, J.D., and Qi, J., 2001. A simple physical model of vegetation reflectance for standardising optical satellite imagery. Remote Sensing of Environment 77, 230-239.

Elvidge, C.D., and Lyon, R.J.P., 1985. Influence of rock-soil spectral variation on the assessment of green biomass. Remote Sensing of Environment 17, 265-279.

Fassnacht, K.S., Gower, S.T., MacKenzie, M.D., Nordheim, E.V., and Lillesand, T.M., 1997. Estimating the leaf area index of north central Wisconsin forests using the Landsat Thematic Mapper. Remote Sensing of Environment 61, 229-245.

Franklin, J., Woodcock, C.E., and Warabington, R., 2000. Digital vegetation maps of forest lands in California: integrating satellite imagery, GIS modeling, and field data in support of resource management. Photogrammetric Engineering and Remote Sensing 66, 1209-1217.

Friedl, M.A., Michaelsen, J., davis, F.W., Walker, H., and Schimel, D.S., 1994. Estimating grassland biomass and leaf area index using ground and satellite data. International Journal of Remote Sensing 15, 1401-1420.

Gamon, J.A., Field, C.B., Goulden, M.L., Griffin, K.L., Hartley, A.E., Joel, G., Penuelas, J., and Valentini, R., 1995. Relationships between NDVI, canopy structure, and photosynthesis in three Californian vegetation types. Ecological Applications 5, 28-41.

Gray, J.T., 1982. Community structure and productivity in *Ceanothus* chaparral and coastal sage scrub of southern California. Ecological Monographs 52, 415-435.

Gu, D., and Gillespie, A., 1998. Topographic normalization of Landsat TM images of forest based on sub-pixel sun-canopy-sensor-geometry. Remote Sensing of Environment 64, 166-175.

Hanes, T.L., 1971. Succession after fire in the chaparral of southern California. Ecological Monographs 41, 27-52.

Henry, M.C., and Hope, A.S., 1998. Monitoring post-burn recovery of chaparral vegetation in southern California using multi-temporal satellite data. International Journal of Remote Sensing 19, 3097-3107.

Hoff, C., Bachelet, D., Rambal, S. Joffre, R., and Lacaze, B., 1995. Simulating leaf area index of Mediterranean evergreen oak ecosystems: comparison with remotely sensed estimation. Proceedings of the International Colloquium Photosynthesis and Remote Sensing 28-30 August 1995, (Montpellier, France), pp. 313-321.

Horton, J.S., and Kraebel, C.J., 1955. Development of vegetation after fire in the chamise chaparral of southern California. Ecology 36, 244-262.

Huete, A.R., Jackson, R.D., and Post, D.F., 1985. Spectral response of a plant canopy with different soil backgrounds. Remote Sensing of Environment 17, 37- 53.

Keeley, J.E., 1992. Demographic structure of California chaparral in the long-term absence of fire. Journal of Vegetation Sciences 3, 79-90.

Keeley, J.E., Fotheringham, C.J., and Morias, M., 1999. Reexamining fire suppression impacts on brushland fire regimes. Science 284, 1829-1832.

Keeley, J.E., and Keeley S.C., 1977. Energy allocation patterns of sprouting and non-sprouting species of *Arctostaphylos* in the California chaparral. American Midland Naturalist 98, 1-10.

Keeley, J.E., and Keeley, S.C., 1981. Post-fire regeneration of California chaparral. American Journal of Botany 68, 524-530.

Keeley, S.C., Keeley, J.E., Hutchinson, S.M., and Johnson, A.W., 1981. Post-fire succession of the herbaceous flora in southern California chaparral. Ecology 62, 1608-1621.

Kummerow, J., and Ellis, B.A., 1989. Structure and function in chaparral shrubs. In The California Chaparral: Paradigms Reexamined, edited by S.C. Keeley (Los Angeles: Natural History Museum of Los Angeles County), Science Series No. 34, pp. 140-150.

Lacaze, B., Caselles, V., Coll, C., Hill, J., Hoff, C., de Jong, S., Mehl, W., Negendank, J.F.W., Riezebos, H., Rubio, E., Sommer, S., Teixeira-Filho, J., and Valor, E., 1996. DeMon: Integrated Approaches to Desertification Mapping and Monitoring in the Mediterranean Basin, Final Report of the DeMon-1 Project, edited by J. Hill (Brussels: European Commission), pp. 176.

Lawrence, W.T., 1975. A radiation model for chaparral canopies. M.S. Thesis, San Diego State University.

Loaiciga, H.A., Pederos, D., and Roberts, D.A., 2001. Wildfire-streamflow interactions in a chaparral watershed. Advances in Environmental Research 5, 295-305.

McDonald, E.R., Wu, X., Caccetta, P.A., and Campbell, N.A., 2000. Illumination correction of Landsat TM data in south east NSW. In: Proceedings of the Tenth Australasian Remote Sensing and Photogrammetry Conference, Adelaide, Australia, 21-25 August [CDROM].

Meyer, P., Itten, K., Kellenberger, T., Sandmeier, S., and Sandmeier, R., 1993. Radiometric corrections of topographically induced effects on Landsat TM data in an alpine environment. ISPRS Journal of Photogrammetry and Remote Sensing 48, 17-28.

Miller, P.C., 1981. Similarities and Limitations of resource utilization in Mediterranean type ecosystems. In Resource Use by Chaparral and Matorral, edited by P.C. Miller (New York: Springer-Verlag), pp. 369-407.

Minnaert, M., 1941. The reciprocity principle in Lunar photometry. Astrophysical Journal 93, 403-410.

Mooney, H.A., Kummerow, J., Johnson, A., Parsons, D., Kelley, S., Hoffman, A., Hays, R., and Giliberto, J., 1977. The producers – their resources and adaptive responses. In Convergent Evolution in Chile and California, edited by H.A. Mooney (Stroudsburg, PA: Dowden, Hutchinson and Ross), pp. 85-143.

Mooney, H.A., 1981. Primary production in Mediterranean-climate regions. In Ecosystems of the world. II. Mediterranean-type shrublands, edited by F. di Castri, D.W. Goodall, and R.L. Specht (New York: Elsevier Scientific), pp. 249-255.

Moritz, M., 1997. Analyzing extreme disturbance events: fire in Los Padres National Forest. Ecological Applications 7, 1252-1262.

Moritz, M., 2003. Spatiotemporal analysis of controls on shrubland fire regimes: age dependency and fire hazard. Ecology 84, 351-361.

Nemani, R.R., and Running, S.W., 1989. Testing a theoretical climate-soil-leaf area hydrologic equilibrium of forests using satellite data and ecosystem simulation. Agricultural and Forest Meteorology 44, 245-260.

O'Hare, J.P., and Hallock, B.G., 1988. Soil Survey of the Los Padres National Forest Area, California. United States Department of Agriculture, Forest Service and Soil Conservation Service: University of California; 148.

Rambal, S., 1994. Fire and water yield: a survey and predictions for global change. In The Role of Fire in Mediterranean-type Ecosystems, edited by J.M. Moreno and W.C. Oechel (New York: Springer-Verlag), pp. 96-116.

Riggan, P.J., Goode, S., Jacks, P.M., and Lockwood, R.N., 1988. Interaction of fire and community development in chaparral of southern California (USA). Ecological Monographs 58, 155-176.

Roberts, D.A., Smith, M.O., and Adams, J.B., 1993. Discriminating green vegetation, non-photosynthetic vegetation, and soils in AVIRIS data. Remote Sensing of Environment 44, 255-269.

Roberts, D.A., Green, R.O., and Adams, J.B, 1997. Temporal and spatial patterns in vegetation and atmospheric properties from AVIRIS. Remote Sensing of Environment 62, 223-240.

Roberts, D.A., Batista, G.T., Pereira, J.L.G., Waller, E.K., and Nelson, B.W., 1998. Change identification using multi-temporal spectral mixture analysis: applications in eastern Amazonia. In Remote Sensing Change Detection: Environmental Monitoring Methods and Applications, edited by R.S. Lunetta and C.D. Elvidge (Michigan: Ann Arbor Press), pp.137-161.

Rundel, P.W., and Parsons, D.J., 1979. Structural changes in chamise *Adenostoma fasciculatum* along a fire-induced age-gradient. Journal of Range Management 32, 462-466.

Schlesinger, W.H., and Gill, D.S., 1980. Biomass, production, and changes in the availability of light, water, and nutrients during the development of pure stands of the chaparral shrub, *Ceanothus megacarpus*, after fire. Ecology 61, 781-789.

Sellers, P.J., 1985. Canopy reflectance, photosynthesis, and transpiration. International Journal of Remote Sensing. 6, 1335-1372.

Sellers, P.J., 1987. Canopy reflectance, photosynthesis, and transpiration II: the role of biophysics in the linearity of their interdependence. Remote Sensing of Environment 21, 143-183

Smith, J.A., Lin, T.L., and Rasnson, K.J., 1980. The Lambertian assumption and Landsat data. Photogrammetric Engineering and Remote Sensing 46, 1183-1189.

Spanner, M.A., Pierce, L.L., Peterson, D.L., and Running, S.W., 1990. Remote sensing of temperate coniferous forest leaf area index: the influence of canopy closure, understory vegetation and background reflectance. International Journal of Remote Sensing 11, 95-111.

Stephenson, J. R., and Calcarone, G. M., 1999. Southern California mountains and foothills assessment: habitat and species conservation issues. General Technical Report GTR-PSW-172, Pacific Southwest Research Station, Forest Service, U.S. Department of Agriculture.

Teillet, P.M., Guindon, B., and Goodenough, D.G., 1982. On the slope-aspect correction of multispectral scanner data. Canadian Journal of Remote Sensing 8, 84-106.

Teixeira-Filho, J., Rambal, S., Lacaze, B., and Lointier, M., 1996. Mapping maximal canopy transpiration over a Mediterranean watershed. Proceedings EARSeL Workshop on Satellite Meteorology and Hydrology. 6-7 September 1996, (Netherlands: A.A. Balkema).

Turner, D.P., Cohen, W.B., Kennedy, R.E., Fassnacht, K.S., and Briggs, J.M., 1999. Relationship between leaf area index and Landsat TM spectral vegetation indices across three temperate zone sites. Remote Sensing of Environment 70, 52-68.

Watson, F.G.R., Vertessy, R.A., and Grayson, R.B. 1999. Large scale modelling of forest hydrological processes and their long term effect on water yield, Hydrological Processes 13, 689-700.

Zammit, C.A, and Zedler, P.H., 1992. Size structure and seed production in even- aged populations of *Ceanothus greggii* in mixed chaparral. Journal of Ecology 81, 499-511

TABLES

Table 1-1. LAI values reported in the chaparral literature, by species/stand type and age/life stage.

Species / Stand Type	Age (years) / Life Stage	LAI	Citation
Adenostoma fasciculatum	20	2.65	Lawrence 1975
Ceanothus greggii	20	1.62	Lawrence 1975
Adenostoma fasciculatum	21	3.09	Mooney et al. 1977
Evergreen shrub	mature	2.50	Mooney et al. 1977
Adenostoma fasciculatum	2	1.79	Rundel and Parsons 1979
Adenostoma fasciculatum	6	1.53	Rundel and Parsons 1979
Adenostoma fasciculatum	16	2.20	Rundel and Parsons 1979
Adenostoma fasciculatum	37	1.23	Rundel and Parsons 1979
Adenostoma fasciculatum	60	1.22	Rundel and Parsons 1979
Adenostoma fasciculatum	5	0.80	Schlesinger and Gill 1980
Adenostoma fasciculatum	21	1.60	Schlesinger and Gill 1980
Adenostoma fasciculatum	22	2.10	Gray 1982
Adenostoma fasciculatum	21	2.20	Riggan et al. 1988
Ceanothus oliganthus	21	1.70	Riggan *et al*. 1988
Evergreen shrub	mature	~2	Gamon *et al*. 1995

Table 1-2. Acquisition dates for Landsat TM and ETM+ imagery.

Year	Month / Day	Annual Precipitation* (mm)	APC class
1985	09 / 12	413	Dry
1986	08 / 30	804	Average
1988	09 / 04	634	Average
1992	09 / 15	993	Wet
1994	08 / 20	498	Dry
1995	09 / 24	1498	Wet
1997	08 / 28	621	Average
1998	08 / 31	1855	Wet
2000	08 / 20	760	Average
2002	09 / 03	265	Dry

* Annual precipitation is reported on a water year basis (October-September); see *Section 2.3.3* for description of APC classes.

Table 1-3. NDVI-LAI model parameters for studies conducted in Mediterranean-type ecosystems.

Source	$NDVI_{\infty}$	$NDVI_{back}$	k	Vegetation Type	Sensor
de Jong (1994)*	0.859	0.224	0.213	Oak woodlands	Landsat TM
Hoff *et al*. (1995)*	0.862	0.225	0.212	Oak woodlands	NOAA AVHRR#
This study	0.850	0.123	0.365	Evergreen shrublands	Landsat TM/ETM+

* Cited in Lacaze *et al*. (1996).
# National Oceanic and Atmospheric Administration (NOAA) Advanced Very High Resolution Radiometer (AVHRR).

FIGURES

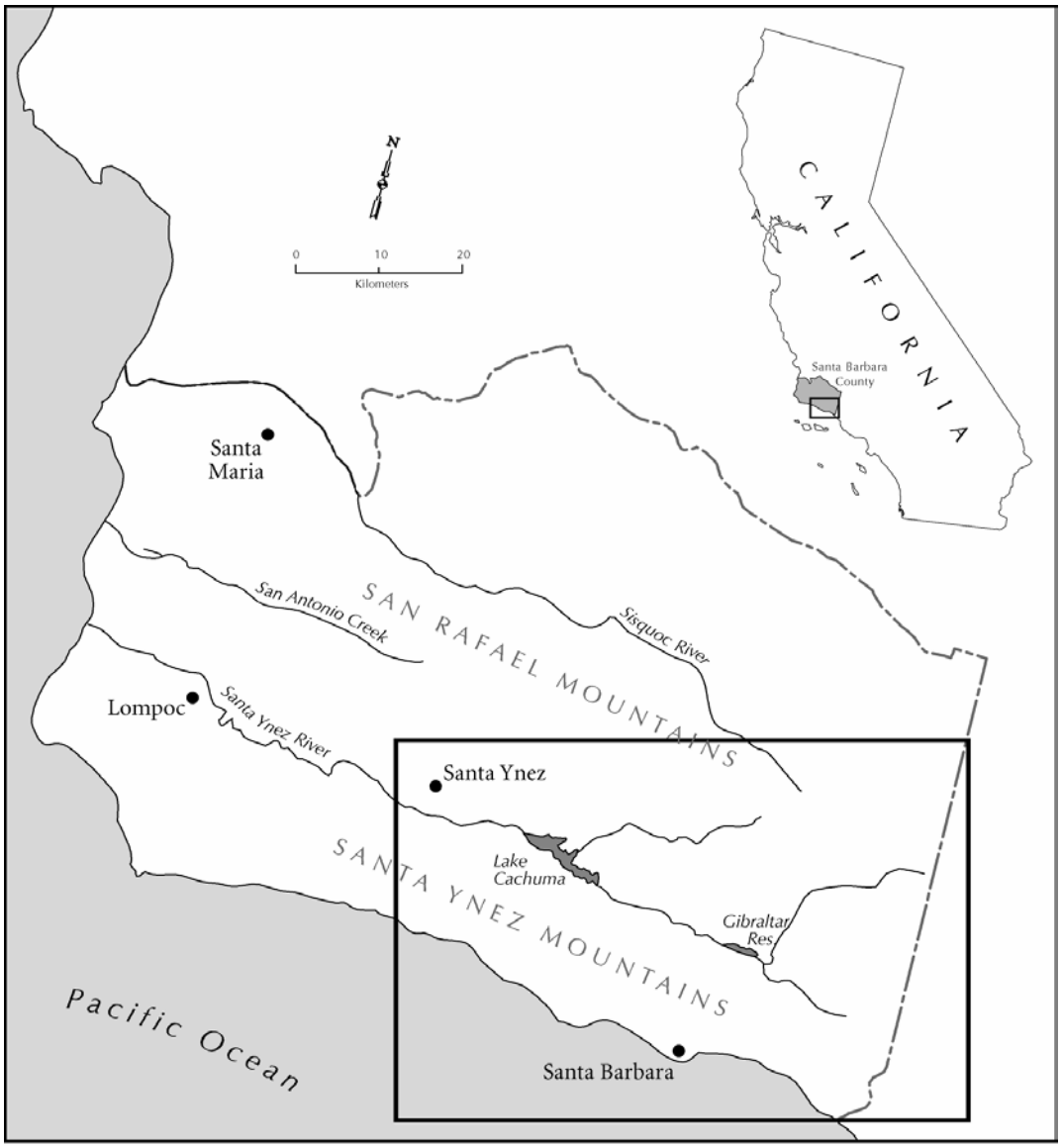

Figure 1-1. Study region near Santa Barbara, California (boxed area).

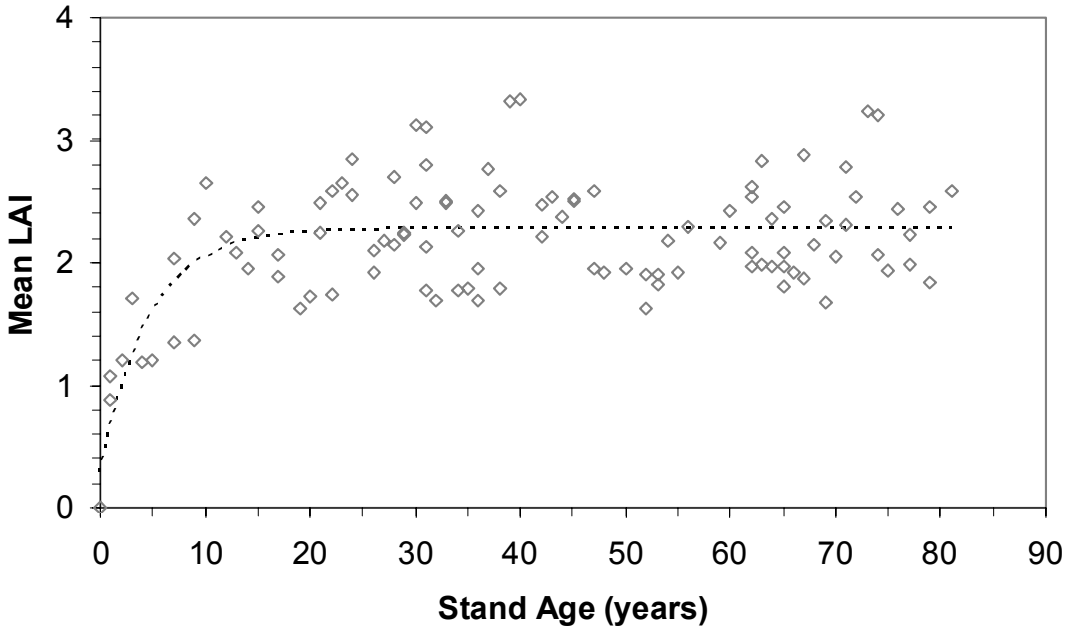

Figure 1-2. Mean LAI vs. stand age – pooled data set. [The line is for illustrative purposes only; it is not a predictive model.]

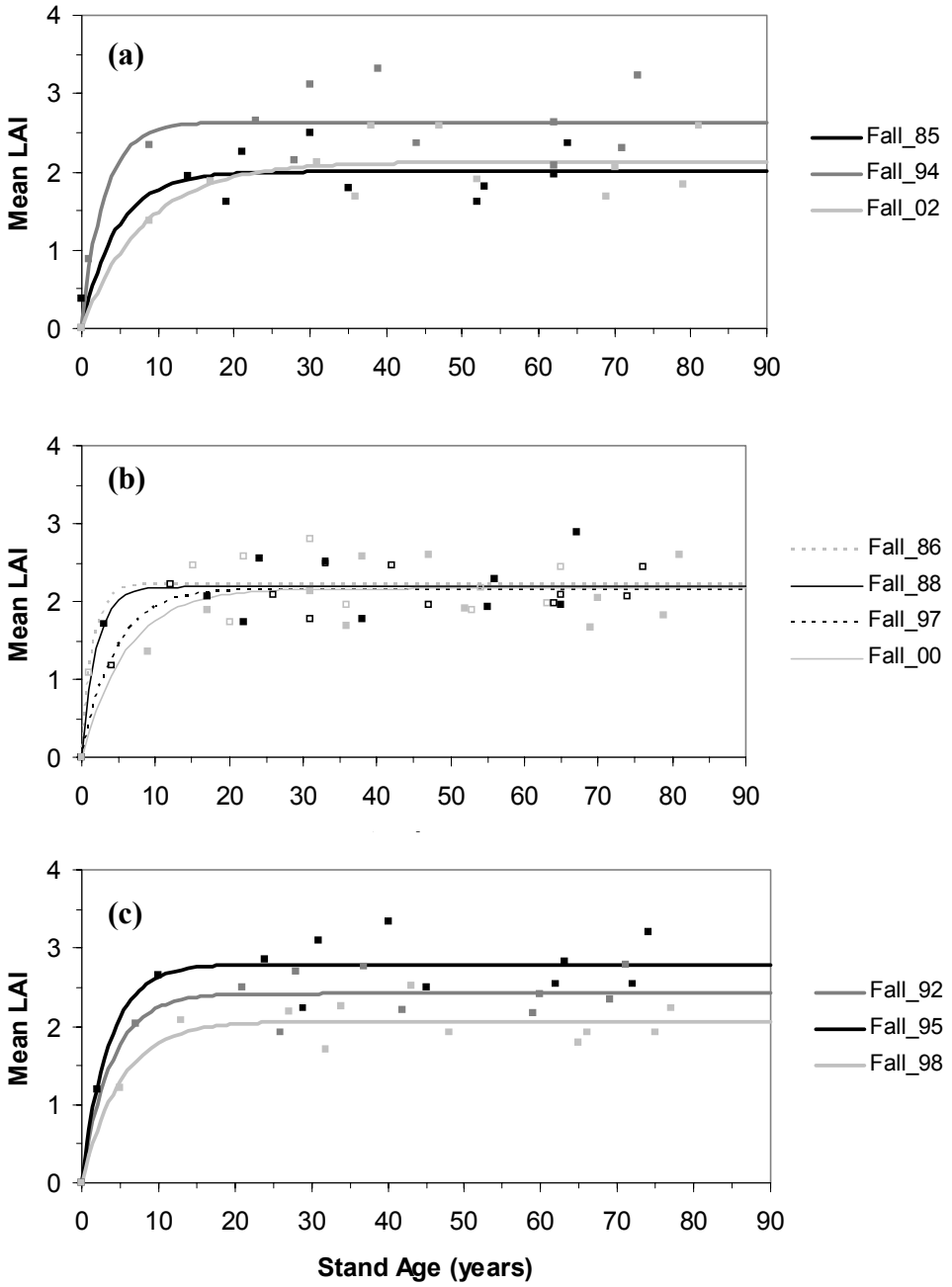

Figure 1-3. Mean LAI vs. stand age – by APC class and image date: (a) 'dry' APC; (b) 'average' APC; (c) 'wet' APC. Point symbol colors correspond to line colors; closed boxes in (3b) correspond to solid lines and open boxes correspond to dashed lines. [Lines are for illustrative purposes only; they are not predictive models.]

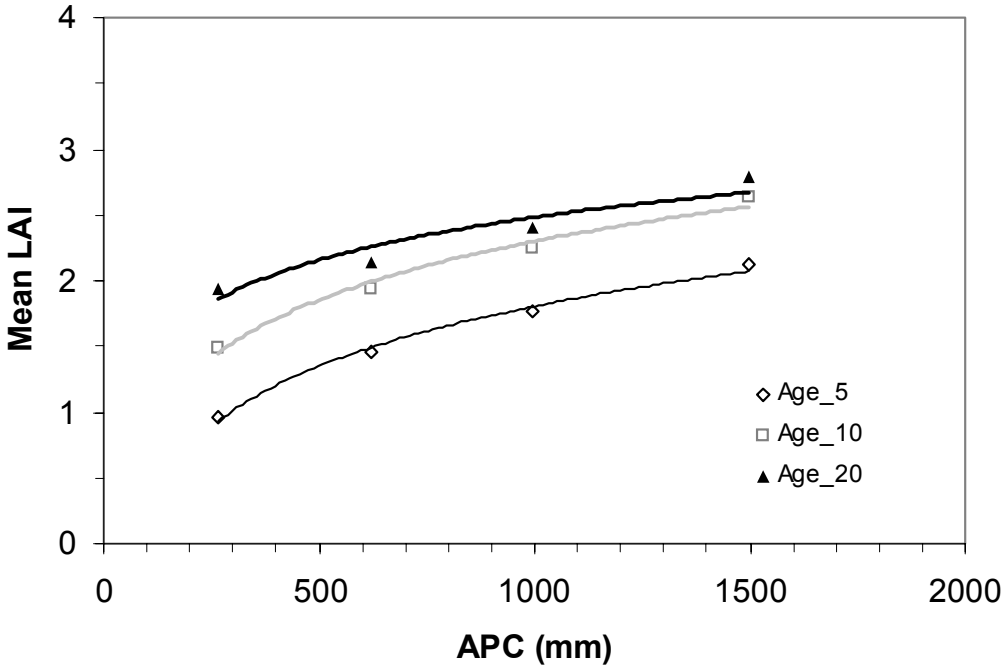

Figure 1-4. The relationship between mean LAI and antecedent precipitation condition (APC) for three stand ages. APC values used in this figure correspond to the 2002 (265 mm), 1997 (621 mm), 1992 (993 mm), and 1995 (1498 mm) Landsat images.

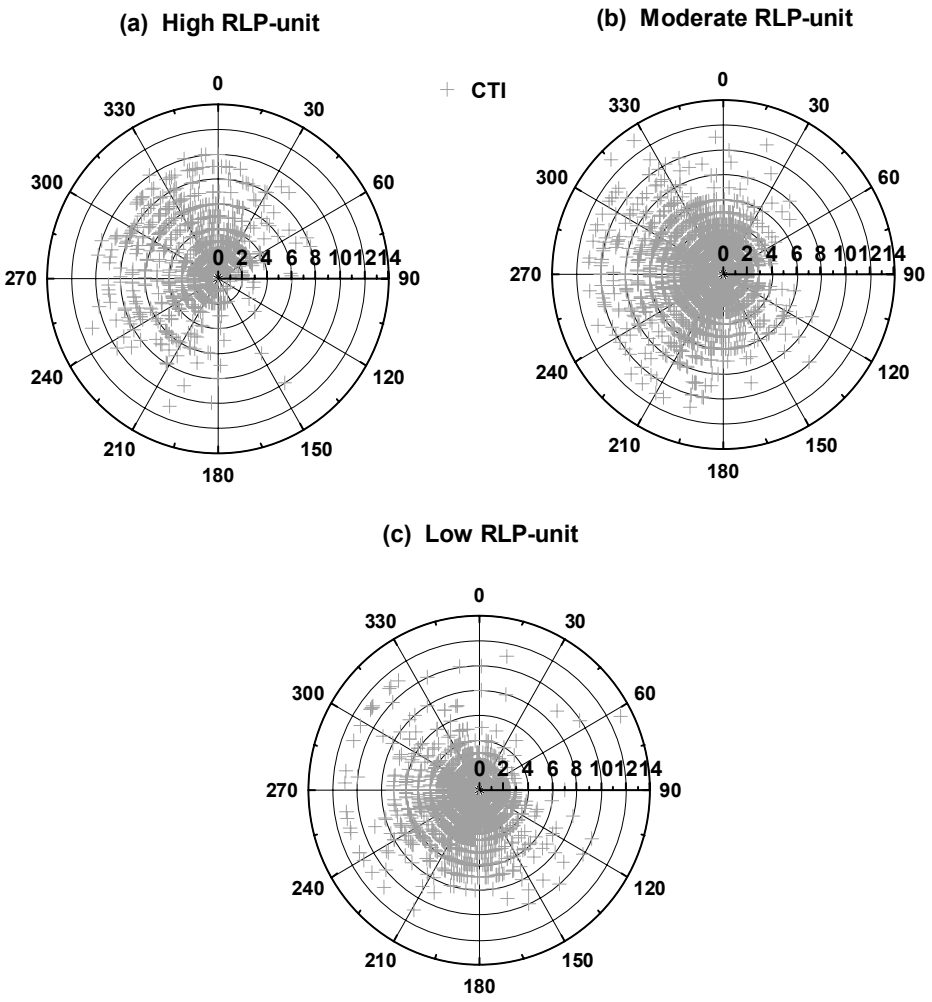

Figure 1-5. Relationship between the compound topographic index (CTI) and topographic aspect (in degrees) for the: (a) High RLP-unit, (b) Moderate RLP-unit, and (c) Low RLP-unit.

CHAPTER TWO

Distributed hydrological modeling in chaparral shrublands: MIKE SHE model calibration and uncertainty estimation

Abstract. Manual and automatic calibration approaches in distributed hydrological modeling have traditionally focused on identifying a single parameter set which optimizes the agreement between observed and predicted values. In recent years the concept of equifinality, that acceptable model predictions might be achieved using different parameter sets, has gained recognition as a more appropriate framework for hydrological simulations. In this study the Generalized Likelihood Uncertainty Estimation (GLUE) methodology was used for model calibration, testing and predictive uncertainty estimation in the application of the MIKE-SHE model for estimating monthly streamflow in a semi-arid shrubland catchment in central California. One thousand randomly generated parameter sets were used to make Monte Carlo simulations for a 20 year calibration period encompassing variable climatic and wildfire conditions. One hundred and nine behavioral parameter sets were retained following model calibration and uncertainty bounds were established using the resulting ensemble of model predictions. Two thirds of the observations in this period fell between the calculated uncertainty bounds. This group of 109 behavioral parameter sets was subsequently used to make streamflow predictions and construct uncertainty

bounds for a 12 year test period with different climatic and fire characteristics. Again, more than two-thirds of the observations fell between the uncertainty bounds. Predictive uncertainty bounds were wide for most months in each evaluation period. Prediction errors (i.e., observations falling outside the uncertainty bounds) were generally associated with large rainfall and/or fire events. Observations outside the uncertainty bounds are indicative of deficiencies in model structure and/or errors in input and/or observed data.

1. Introduction

Mediterranean-type ecosystems (MTEs) are transitional areas between the arid and mesic regions of the world. These semi-arid ecosystems comprise a vegetation form with worldwide distribution and are of special interest to global change research for a variety of reasons related to population growth, biodiversity, land use/land cover change and water resources (Moreno and Oechel 1995, Davis *et al*. 1996, Mittermeier *et al*. 1998). The large, expanding human populations in these regions are expected to exert ever-greater pressure on the environment, resulting in significant changes in land cover condition and dynamics (Verstraete and Schwartz 1991, Hill *et al*. 1995). Moreover, as MTE water relations are predicted to be among the most sensitive to global change (Moreno and Oechel 1995), the potential impacts that land cover change may have on hydrologic processes in MTEs are of particular concern.

Fires in California MTE shrublands dramatically alter catchment land cover and initiate a complex matrix of vegetation recovery sequences that span many decades. Future climate- and anthropogenic-induced changes may modify the current fire regime in this region (Ryan 1991, Davis and Michaelsen 1995) and, consequently, post-fire vegetation recovery patterns and related streamflow dynamics. Catchment experiments have provided insights into the effects of fire on streamflow in MTE shrublands (Hoyt and Troxell 1932, Scott 1993; Lavabre *et al.* 1993, Loaiciga *et al*. 2001), however, extrapolation of these results is constrained by the limited space and/or time scales examined. A more comprehensive understanding of these effects is required in order to facilitate effective planning by those charged with protecting and managing California's shrubland catchments for water supply, water quality and wildlife/vegetation habitat. It is not feasible to conduct the field experiments required to improve our understanding of the hydrological impacts of fire and post-fire succession at the space (tens to hundreds of square kilometers) and time (seasonal and annual) scales most relevant to water resource managers in this semi-arid environment. Rather, a distributed hydrological modeling approach is required, one capable of representing changes in vegetation patterns following fire and the concomitant effects on catchment hydrological processes.

Application of a distributed hydrological model requires calibrating on historical records, as well as a number of assumptions related to the model structure, input data and parameters. Manual and automatic approaches

traditionally used to calibrate distributed hydrological models focus on identifying a single parameter set which optimizes the agreement between observed and predicted values. However, the goal of identifying a single optimum parameter set may be ill-founded in rainfall-runoff modeling as a result of uncertainties related to process representation, catchment parameterization, input data, the specification of initial/boundary conditions and the measurement of discharge data used in calibration (Beven 1989, Binley and Beven 1991). Given these uncertainties, it should be expected that multiple parameter sets and/or model structures might provide acceptable predictions – this is the concept of equifinality (Beven 1993, 1996, Beven and Freer 2001).

The Generalized Likelihood Uncertainty Estimation (GLUE) methodology (Binley and Beven 1991, Beven and Binley 1992, Beven and Freer 2001) is a Bayesian Monte Carlo-based approach that recognizes the equifinality of parameter sets and model structures and provides an alternative strategy for distributed model calibration and uncertainty estimation. The GLUE framework recognizes that multiple acceptable parameter sets can be identified and used to generate a range of model predictions which serves as the basis for uncertainty estimation. In contrast, the single optimum parameter set identified using a traditional calibration approach provides only a single prediction sequence.

In this research we used a GLUE-based approach to characterize the uncertainty and error associated with MIKE-SHE (Refsgaard and Storm 1995) predictions of monthly streamflow for a semi-arid shrubland catchment near Santa

Barbara, California, USA. Specifically, we investigated how predictive uncertainty varied from season to season, under different rainfall and fire conditions, and between model calibration and test periods.

2. Methods

2.1. MIKE-SHE modeling system

MIKE-SHE (a derivative of the Systeme Hydrologique Europeen, SHE, Abbott *et al*. 1986a, b) is a physically-based, spatially distributed model that has been widely used to study a variety of water resource and environmental problems under diverse climatological and hydrological regimes (Refsgaard and Storm 1995). MIKE-SHE comprises five process-oriented modules, each representing a major component of the hydrologic cycle including: a) interception/evapotranspiration, b) overland and channel flow, c) unsaturated zone flow, d) saturated zone flow and e) aquifer-river exchange. The user creates an application-specific model by including all or some of (or portions of) these modules in the model setup. The catchment is subdivided into grid cells of equal size and time steps are allowed to vary between modules in order to account for the varied time scales of different flow processes (Refsgaard and Storm 1995).

A modified version of MIKE-SHE (after Andersen *et al*. 2001) was used in this study. The major differences between the original (MIKE-SHE) and modified (MSHE_m) versions of the model are found in the representations of flow in the unsaturated and saturated zones. In MIKE-SHE vertical flow in the unsaturated

zone is modeled using the full Richard's equation, whereas in MSHE_m it is calculated using a 'simplified' Richard's equation where the tension term is ignored. Within each grid cell the soil column is divided into a number of layers, each with associated parameters based on soil type. Groundwater flow in the original version is represented by a three-dimensional saturated zone module that is dynamically coupled to the unsaturated zone module. In MSHE_m a net vertical drainage from the unsaturated zone is accumulated in a series of linear interflow reservoirs; thus, there is a many-to-one mapping between unsaturated zone grids and the set of cascading interflow reservoirs. The interflow reservoirs model lateral subsurface throughflow using a reservoir threshold parameter and a set of horizontal time constants. A vertical time constant is used to compute drainage from each interflow reservoir to the single catchment groundwater reservoir. Finally, baseflow from this groundwater reservoir is modeled as a function of current storage and a horizontal time constant. The decision to implement MSHE_m was necessitated by the lack of knowledge and data regarding groundwater processes in the study catchment.

Interception of rainfall in MSHE_m (and MIKE-SHE) is computed as a function of the canopy interception storage capacity and the leaf area index (LAI) – a key input variable in this fire-prone environment given that greater than 70% of annual rainfall is returned to the atmosphere via evapotranspiration (Poole *et al*. 1981). Evaporation from canopy storage is governed by the potential evapotranspiration (PE) rate; stem flow occurs once the storage is filled. Three

separate, non-linear functions control plant transpiration (T): a) f_1(LAI), b) f_2(soil volumetric moisture content, θ) and c) f_3(rooting depth/density); each function can take on a value between zero and one. These functions express the dependence of plant transpiration on the abundance of green leaves, the amount of water available in the root zone, and the distribution of roots with depth, respectively. Transpiration is calculated by successively multiplying PE by the value of each function (after Kristensen and Jensen 1975). Soil evaporation is calculated as a function of soil moisture in the upper layer of the soil column and is added to T in order to compute actual evapotranspiration (AE) (Refsgaard and Storm 1995).

2.2. GLUE methodology

The limitations of current physically-based, distributed hydrological models have been discussed by Beven (1989) and others (Grayson *et al*. 1992, Refsgaard and Storm 1996) in some detail. Many studies have demonstrated the prevalence of equifinality in physically-based hydrological modeling resulting from uncertainties in model structure, boundary conditions, catchment parameterization and errors in input and observed variables (Freer and Beven 1996, Zak and Beven 1999, Brazier *et al*. 2000, Beven and Freer 2001). Consequently, the traditional search for an optimal parameter set is no longer considered an appropriate approach to the problem of model calibration. The GLUE methodology (Binley and Beven 1991, Beven and Binley 1992) explicitly recognizes the equifinality of parameter sets (and models) in physically-based modeling and provides a more suitable

framework for model calibration and uncertainty estimation. An overview of GLUE is given below, the reader is referred to Beven and Binley (1992), Freer and Beven (1996) and Beven and Freer (2001) for additional details.

A number of decisions need to be made when implementing GLUE in the context of a particular physically-based modeling application. First, realistic ranges are selected for each parameter included in model calibration on the basis of prior model applications and/or physical reasoning. The goal is to create a parameter space which maximizes the number of good (behavioral) model runs without generating unnecessary (non-behavioral) model runs. Monte Carlo simulations are made using a large number of parameter sets whose values are randomly selected from uniform distributions across the defined range for each parameter (non-uniform distributions may used if supported by available information or previous experience). The relative performance of each parameter set is evaluated on the basis of a likelihood measure (or measures) calculated by comparing model predictions with observed data. It should be noted that, in the context of GLUE, the meaning of 'likelihood' is broader than that found in classical statistics (Beven and Binley 1992). A parameter set is classified as behavioral if the corresponding likelihood value is equal to or greater than a specified threshold value; parameter sets that do not meet this criterion are rejected as non-behavioral.

The final step in the GLUE procedure is to establish predictive uncertainty bounds (or, prediction limits) for comparison with observed values. First, the set

of behavioral likelihood values is rescaled to unity by dividing each value by the sum of likelihood values. Next, behavioral model predictions for each time step are ranked in ascending order and each prediction is assigned to a user-specified bin. The rescaled likelihood values corresponding to the ranked predictions in each bin are summed to give the height of each bar in the density plot. A cumulative density plot may be constructed by graphing the cumulative sum of the likelihood values versus the ranked model predictions. Typically, the 5^{th} and 95^{th} percentiles calculated at each time step are used to generate the uncertainty bounds over the period of observations (Binley and Beven 1991, Beven and Binley 1992, Zak and Beven 1999, Ratto *et al*. 2001), however, other values may be used (Brazier *et al*. 2000). Prediction limits calculated in this manner capture the uncertainty in model output associated with errors in model parameterization; observations falling outside the uncertainty bounds are likely the result of errors in input data, model structure and/or observed variables (Beven and Freer 2001).

It should be emphasized that the decisions made at each step in the GLUE methodology are subjective. For example, the choice of both the likelihood measure and corresponding threshold value has been shown to influence the number of behavioral parameter sets retained following Monte Carlo simulations which, in turn, directly impacts the calculation of prediction limits (Beven and Binley 1992, Freer and Beven 1996). However, a major advantage of the GLUE framework is that, while subjective, these decisions are made explicit so that they are both repeatable and subject to critique by the wider modelling community.

2.3. Study site

The Jameson catchment (34 km^2), located in the San Rafael Mountains north of Santa Barbara, California, USA (Figure 2-1), is one of the few remaining non-urbanized catchments in this region. There is a comprehensive geo-spatial dataset available for the study site including digital maps of fire history, vegetation type, soil type and elevation. The semi-arid climate of this region is characterized by cool, wet winters and warm, dry summers. Annual average precipitation and streamflow in the Jameson catchment are 780 mm and 233 mm, respectively. Elevation ranges from 677 m at the catchment outlet to 1771 m at the highest point along the ridge. Sandy-loam soils are typically found on the steep, rugged hillslopes (average slope ~ 43%), while somewhat deeper sandy-loam and loam soils are found on gentler slopes. The combination of stands in different stages of post-fire succession with spatial variability in physical site characteristics (e.g. terrain and soils) produces a complex vegetation mosaic dominated by evergreen shrubs (chaparral) intermixed with oak woodlands, summer deciduous sub-shrubs (coastal sage scrub), conifer forest and grassland (Stephenson and Calcarone 1999).

2.4. Input data

Model grid cell size for the Jameson catchment was fixed at 270 m. This spatial scale was selected to allow for the most accurate representation of catchment

attributes without placing excessive demands on computer run time required for Monte Carlo simulations. Model predictions of streamflow were made at a daily time step and aggregated to monthly values for comparison with observed streamflow data. Observed values of monthly streamflow were obtained from the United States Geological Survey gage (#11121010) located at the catchment outlet (daily values were not available). Input time series and spatially distributed datasets are described below.

2.4.1. Time series data

Daily temperature and precipitation data from water years (October – September) 1961 to 1993 were obtained from National Climate Data Center (NCDC) gages in and around the Jameson catchment. Temperature data were quality checked and missing values were interpolated by developing linear regression equations between individual stations; separate regressions were developed for minimum and maximum temperatures. Precipitation data were also quality checked and missing values were interpolated using daily precipitation data from neighboring gages maintained by the Santa Barbara County Water Agency. Less than one percent of the temperature and precipitation values were missing and had to be estimated using these techniques.

It was assumed that the spatial distribution of individual precipitation events across the catchment corresponded to the spatial pattern of mean annual precipitation (MAP). Five distinct precipitation zones were identified in the study

catchment based on a digital MAP map of Santa Barbara County (J. Michaelsen, *personal communication*). The ratio between MAP at the NCDC stations (located in Zone 1) and the MAP for each of the remaining four zones was calculated and used as the basis for redistributing observed (point) values of precipitation to each zone. A time series of daily rainfall values was generated for each zone using this approach.

MSHE_m also requires daily inputs of potential evapotranspiration (PE). The lack of measured wind speed, net radiation and relative humidity data precluded the use of the Penman equation (Penman 1956) in the study catchment. Instead, PE was estimated using the Hargreaves-Samani (1985) model with observed, lapse-rate adjusted daily temperature data and daily estimates of slope-aspect adjusted extraterrestrial radiation (Dingman 1994). Daily values of PE calculated using the Penman model were obtained from a California Irrigation and Management Information System (CIMIS) meteorological station (No. 64) located approximately 30 km to the west. These CIMIS-based values were used to calibrate and validate the Hargreaves-Samani PE model for this environment. Values of the coefficient of efficiency (Nash and Sutcliffe 1970) for the calibration and verification periods were 0.99 and 0.94, respectively. Spatial variation in PE across the Jameson catchment was characterized using twelve different zones, defined using three slope (low, moderate and high) and four aspect (North, East, South and West) classes. A daily time series of PE was calculated separately for each zone using the calibrated Hargreaves-Samani model.

2.4.2. Spatially distributed data

A time sequence of LAI maps was used to represent chaparral growth and recovery in MSHE_m. These maps were derived using an integrated remote sensing-chronosequence approach (Chapter One). The basis of this approach was to convert values of the normalized difference vegetation index (NDVI) into LAI values using the generalized model of Baret *et al*. (1989). In this model LAI is calculated as a function of the maximum NDVI, the minimum NDVI and k, a coefficient representing the extinction of solar radiation through the canopy. In Chapter One a time series of ten (near-anniversary date) fall Landsat Thematic Mapper (TM) and Enhanced Thematic Mapper (ETM+) satellite images was converted from NDVI to LAI using this model (calibrated to regional conditions). Mean LAI values were recorded for a series of fires and used to derive a relationship between LAI and chaparral stand age for each image date. An average LAI-Stand Age trajectory was computed from the ten individual relationships and used as the basis for developing input sequences of chaparral LAI for MSHE_m. While inter-annual variability in chaparral LAI was captured using this approach, intra-annual variability was not represented in the hydrological model given: (a) the exclusive use of fall imagery to develop the LAI-Stand Age relationships in Chapter One, and (b) the absence of information on seasonal LAI in the chaparral literature. However, adjustments (small increases) were made to input LAI values in each of the first four years following fire (successively smaller increases each year) in order to account for the presence

of herbaceous vegetation that normally occurs on post-burn chaparral sites during this period (Keeley *et al*. 1981, Keeley and Keeley 1981). Input LAI sequences for non-chaparral vegetation types were derived using information from the literature (Gray and Schlesinger 1981, Gamon *et al*. 1995).

Temporally varying vegetation rooting depths were specified using information from the literature (Kummerow *et al*. 1977, Hellmers *et al*. 1985) and results from a previous application of MSHE_m (using manual calibration) in the Jameson catchment (Tague *et al*. in press). Existing digital vegetation, soils and elevation maps were used to delineate vegetation, soil and topographic units within the catchment. Vegetation stand age was determined by intersecting the vegetation type map (Franklin *et al*. 2000) with the digital fire history map. A soil profile (texture and depth of each horizon) was specified for each model grid cell using available soil survey data (3^{rd} Order) for the study catchment (O'Hare and Hallock 1988).

2.5. Calibration parameters

The actual number of parameters in MSHE_m depends on which modules are included in the model setup and how the catchment is discretized (horizontally and vertically). Eleven parameters were used for model calibration and uncertainty estimation in this study (Table 2-1 and Appendix B) based on previous applications of MIKE-SHE (Xevi *et al*. 1997, Christiaens and Feyen 2002, Vazquez *et al*. 2002, Vazquez and Feyen 2003) and MSHE_m (Andersen *et al*.

2001, Tague *et al*. in press), and the MIKE-SHE user's manual (DHI Water and Environment 2000). The range for each parameter varied in model calibration was set using previous studies and/or physical reasoning.

The parameters C_1 and C_2 control the distribution of actual evapotranspiration between transpiration and soil evaporation, while C_3 influences the value of the moisture content function (f_2). The saturated hydraulic conductivity (K_s) and exponent (n) parameters are used to compute the hydraulic conductivity as a function of effective saturation for the sandy loam (*K_s_SandyLoam* and *n_SandyLoam*) and loam (*K_s_Loam* and *n_Loam*) soil types. The remaining four parameters (IF_t, IF_h, IF_v and GW_h) control interflow (IF) and groundwater (GW) dynamics in MSHE_m. The interflow reservoir threshold (IF_t) sets the storage capacity of the reservoir. The horizontal time constant (IF_h) regulates interflow between reservoirs, or between a reservoir and the river, and the vertical time constant (IF_v) controls interflow contribution to groundwater. The groundwater reservoir time constant (GW_h) governs the rate of baseflow contribution to streamflow

The following assumptions were made in order to minimize the number of parameters used in model calibration. First, only the values of C_1, C_2 and C_3 for shrubland vegetation types were used in calibration since more than 85% of the catchment area was classified as shrubland and it was the only vegetation impacted by fire. Parameter values for other vegetation types were held constant. In addition, we assigned the same values of IF_t, IF_h, and IF_v to each interflow

reservoir (after Andersen *et al*., 2001) given that no information was available to guide a separate parameterization for each reservoir.

2.6. Model calibration, testing, and uncertainty estimation

The number of Monte Carlo runs implemented in a particular application is a function of the interactions between catchment size, model structure (including grid cell size), the number of calibration parameters and the available computer resources. Tens of thousands (Zak and Beven 1999) to millions (Brazier *et al*. 2000) of runs can be made when model codes are less complex, grid cell size is large, few parameters are used in calibration, extensive computing power is available, and/or for smaller catchments. The physically-based, distributed MSHE_m model code is very complex and, therefore, extremely computer intensive. This fact, coupled with the large number of calibration parameters and catchment grid cells used in this study, constrained the number of Monte Carlo simulations possible given available computer resources to 1000.

One thousand randomly generated parameter sets were used to make Monte Carlo simulations for a 20 year calibration period (water years 1962-1981) encompassing a wide range of climatic conditions and containing one small fire (one percent of the catchment area, October 1971) and one medium size fire (20% of the catchment area, September 1964). A standard performance metric, the Nash-Sutcliffe (1970) coefficient of efficiency, E (1), was used to evaluate model performance following each run:

$$E = \frac{\sum (O - \overline{O})^2 - \sum (O - P)^2}{\sum (O - \overline{O})^2}$$

where, O is the observed flow, $\bar{O}$ is the mean observed flow, and P is the predicted flow. We selected the widely used coefficient of efficiency as our likelihood measure in order to evaluate the accuracy of both the magnitude and timing of predicted flows (e.g., Andersen *et al*. 2001, Beven 2001, Vasquez *et al*. 2002, Tague *et al*. in press). The first two water years in each simulation period were used to spin-up model storages and, thus, were excluded from the calculation of E. The 'behavioral' threshold value of E used in this application of MSHE_m followed Andersen *et al*. (2001), where 'good' model runs were those with $E \geq 0.80$. Parameter sets identified as behavioral were used to make predictions for a second (test) period in order to evaluate the robustness of the behavioral parameter sets for the study catchment. This second period (water years 1982-1993) contained one very large fire (78% of the catchment area, July 1985) and experienced widely varying climatic conditions. The range of behavioral model predictions made for each period were used to calculate the 5th and 95th percentiles using the GLUEWIN software package (Ratto and Saltelli 2001); the resulting uncertainty bounds were compared with observed streamflow values for each period.

3. Results and discussion

3.1. Model calibration

One hundred and nine of the 1000 Monte Carlo-based calibration runs were classified as behavioral, with values of E ranging from 0.80 to 0.92. This proportion of behavioral parameter sets is comparable to that found in other GLUE-based modeling studies (e.g., Brazier *et al*. 2000, Beven and Freer 2001). The distribution of E for behavioral parameter sets was positively skewed (Figure 2-2) with approximately 50% of the simulations having values of E less than or equal to 0.84; only five of the 109 behavioral runs had a value of E greater than 0.90.

Predicted monthly streamflow values for each of the 109 behavioral parameter sets (excluding the first two water years) were used to compute the 5% and 95% uncertainty bounds. Sixty-eight percent of the observed streamflow values fell within these bounds (Figure 2-3a); the remaining 32% of the observations comprised just over six percent of the total observed streamflow. This level of flow prediction error (i.e., < 10%) was considered acceptable for the calibration period as a whole (after Andersen *et al*. 2001).

The average range between the upper and lower uncertainty bounds (R_{avg}) was largest in wet season months (November-April, Figure 2-3b), with values decreasing steadily through the transition (May-June) and dry (July-October) seasons. That is, greater predictive uncertainty was associated with high flows than with low flows. The variability around R_{avg} (Figure 2-3b) results from year to

year differences in predictive uncertainty, and is particularly high in the wet season. On the other hand, values of the normalized average range (NR_{avg}) (computed by dividing the uncertainty range for each time step by the observed flow depth and re-calculating R_{avg}) were largest (i.e., uncertainty was greatest) in transition and dry season months (Figure 2-3c); variability around NR_{avg} was also greatest in these months.

Observed streamflow values in four of the 18 water years were completely contained within the uncertainty bounds. Considering the large variability in rainfall totals for these years, ranging from low (1968 and 1981) to moderate (1979) to very high (1969), it is apparent that the group of 109 behavioral parameters sets was capable of accurately representing integrated catchment behavior (streamflow) under different rainfall conditions. However, catchment behavior was not always well modeled and some degree of prediction error (under- and/or over-estimation) occurred in each of the remaining water years.

The largest under-estimation errors (observed values above the 95% bound) and over-estimation errors (observed values below the 5% bound) occurred in wet season months (Figure 2-4). Sixty-eight percent of the total calibration period under-estimation error was found in just three months, November 1971 (8%), January 1974 (39%) and February 1976 (21%). Thirty-four percent of the total period over-estimation error occurred in March (6%) and April (28%) 1967; much of the remaining over-estimation error (44%) occurred in February, March and April 1978. Under-estimation errors occurred in both average and high

rainfall years, generally in association with very large events (e.g., 316 mm over five days in 1974). On the other hand, over-estimation errors occurred primarily in high rainfall years and were associated with a range of event sizes.

3.2. Model testing

Each of the 109 behavioral parameter sets from the calibration period was used to make daily streamflow predictions for the test period in order to evaluate their robustness under different fire and rainfall regimes. Uncertainty bounds for this period were calculated using predicted monthly flows. Sixty-seven percent of the observed streamflow values fell within the 5% and 95% uncertainty bounds (Figure 2-5a); the remaining 33% of observed values comprised approximately nine percent of the total observed flow. Thus, nearly the same proportion of observed values was contained within the uncertainty bounds in each period, and the overall level of prediction error (< 10%) in each period was considered acceptable.

The trend in (and magnitude of) R_{avg} for the test period (Figure 2-5b) was very similar to that seen in the calibration period. Predictive uncertainty was largest in wet season months, progressively declining through the transition and dry season months. As before, normalizing for observed streamflow (NR_{avg}) reversed this trend such that the greatest uncertainty was found in the dry season months (Figure 2-5c). Variability around R_{avg} and NR_{avg} was again highest in wet season and dry season months, respectively.

No water years in the test period were error-free, in contrast to the calibration period. As with predictions in the calibration period, most under- and over-estimation error in the test period occurred during wet season months (Figure 2-6). Nearly 40% of the total under-estimation error occurred in January 1993, with an additional 46% in January (11%) and February (35%) 1986 following a very large fire in 1985. Twenty percent of the total over-estimation error occurred in March 1988 when 135 mm of rain fell over three days. Sixty percent of the remaining over-estimation error corresponded to a very large storm event in February 1992 (458 mm over six days). Under- and over-estimation errors in the test period, as in the calibration period, were associated primarily with large events (e.g., 390 mm of rainfall over six days in 1993) in wet rainfall years. In addition, a large portion of the total under-estimation error in the test period was associated with the 1985 fire.

3.3. Discussion

Virtually the same proportion of observed monthly streamflow values was captured by the 5% and 95% uncertainty bounds in each evaluation period, despite quite different rainfall patterns and fire conditions. The total prediction error (i.e., the sum of over- and under-estimation errors) for each period as a whole was considered acceptable as it represented less than 10% of the observed flow. Seasonal trends in R_{avg} and NR_{avg} were very similar in both periods, demonstrating a level of consistency in the ability of MSHE_m to predict high, moderate and low

flows across periods. Differences in the magnitude of, and variability in, R_{avg} and NR_{avg} between evaluation periods were generally small.

Average predictive uncertainty (R_{avg}) was greatest, and most variable, in wet season months, declining through the transition and dry seasons. However, the opposite pattern was seen once R_{avg} was normalized for observed flow (NR_{avg}), indicating that the mean relative predictive uncertainty was greatest in dry season months. That is, model predictions were most uncertain, relative to observed values, in months when streamflow was low to non-existent; the relative variability in predictive uncertainty was also greatest in the dry season. In wet season months NR_{avg} was generally less than 5% of the observed flow and the relative variability in predictive uncertainty was small. Overall, the fact that NR_{avg} was less than 10% of observed flow in all seasons (Figures 2-3c and 2-5c) suggests that (on average) MSHE_m predictions of monthly streamflow in this catchment were *relatively* certain for both evaluation periods. Even so, the wide *absolute* uncertainty bounds observed in many wet season months, and following the large fire in 1985, indicate that the group of behavioral parameter sets used in this application of MSHE_m does not adequately represent the full range of hydrologic processes in the Jameson catchment.

Over-estimation errors in dry months (July – October) represented less than 1.5% of the total prediction error for each evaluation period. Monthly streamflow was not under-estimated during the dry season in either period. Absolute over- and under-estimation errors in transition months (May-June) were

also very small, comprising just 1% and 2.5% of the total error in the calibration and test period, respectively. Overall, total streamflow in both transition and dry months was modeled with acceptable errors by MSHE_m using the group of 109 behavioral parameter sets, indicating that the moderate and low flow conditions were generally well characterized by the model structure.

Estimation errors (over and under) were largest in wet season months (November-April), comprising 98% of the total estimation error for each period. In contrast to findings for the transition and dry seasons, catchment processes in the wet season were not always characterized adequately by MSHE_m, particularly in relation to large storms and extensive fire. The patterns of over- and under-estimation were notably different between wet season months in the calibration and test periods (Figures 2-4 and 2-6). Over- and under-estimation errors generally increased from November through April in the calibration period, while nearly the opposite pattern was seen in the test period. This phenomenon is somewhat difficult to explain given that errors in both periods were associated with (often very) large rainfall events.

Differences in under- and over-estimation errors following fire in September 1964 (20%), October 1971 (1%) and July 1985 (78%) are most likely a function of the variability in fire size. The lack of appreciable estimation error in water years 1965 (597 mm of rainfall) and 1972 (417 mm of rainfall) indicates that the GLUE-based calibration of MSHE_m successfully captured post-fire catchment behavior over a range of fire size (1 – 20%) and rainfall conditions

(including large storm events). On the other hand, nearly half of the total test period under-estimation error occurred in water year 1986 (830 mm of rainfall) following the massive fire in July 1985. Errors that year were largely associated with sizable rainfall events (e.g., 196 mm in three days in February 1986) in wet season months. While these errors represent only 3% of the total observed flow in the test period, they highlight deficiencies in the ability of the model structure and/or input data to adequately characterize successional dynamics in this catchment following very large fires.

3.4. Sources of uncertainty and error

Previous work has demonstrated that the identification of behavioral parameter sets is directly influenced by the choice of likelihood measure and/or the corresponding threshold value (Beven and Binley 1992, Freer and Beven 1996). In this study 109 parameter sets out of 1000 were classified as behavioral based on a 0.80 threshold of the coefficient of efficiency. As stated earlier this number of behavioral parameter sets is proportional to that found in other GLUE-based studies, but the absolute number of sets identified in this study is much smaller. A larger number of Monte Carlo simulations (e.g., 10,000) would likely yield additional behavioral parameter sets and provide a more complete sampling of the parameter space. However, a substantial increase in computing resources would be required to make this number of runs for such a complex model. The number

of behavioral parameter sets might also be increased by selecting a different likelihood measure and/or threshold value.

The 5% and 95% bounds represent predictive uncertainty arising from errors associated with specifying values and ranges for calibration parameters. Monthly observations falling between these uncertainty bounds denote time steps at which acceptable streamflow predictions were made using the selected group of behavioral parameter sets. Observations not captured by the uncertainty bounds (i.e., prediction errors) are indicative of deficiencies in model structure and/or errors in input and/or observed data which prevented acceptable streamflow predictions from being made for those time periods (Beven 2001, Beven and Freer 2001). A number of factors which may have contributed to predictive uncertainty and/or prediction error in this study are discussed below.

The general lack of information and data for subsurface conditions in the study catchment precluded the use of the 3-D groundwater module available in the full version of MIKE-SHE. Instead, we implemented the semi-distributed Linear Reservoir groundwater module (MSHE_m) with three interflow reservoirs and one ground reservoir. The Linear Reservoir module does not allow interactions and feedback between the saturated and unsaturated zones and, consequently, may not adequately represent subsurface flow dynamics under all conditions. Moreover, MSHE_m is not capable of representing time-varying soil properties. This may be an important limitation of the model as fire has been shown to alter soil physical

properties in California semi-arid shrublands (DeBano and Conrad, 1978), potentially modifying soil water-holding capacity.

The grid cell size used in this study (270 m) was somewhat coarse given the rugged nature of the terrain in the study area. However, results from previous studies using MIKE-SHE and MSHE_m demonstrate that overall model performance is marginally sensitive to changes in grid cell size for small (1 km^2, MIKE-SHE, Xevi *et al*. 1997), medium (34 km^2, MSHE_m, Tague *et al*. in press), and large catchments (568 km^2, MIKE-SHE, Vasquez *et al*. 2002). For example, Vazquez *et al*. (2002) found little change in a number of model performance measures when MIKE SHE was applied over a range of grid cell sizes (300-1200 m) in a large catchment. The manual calibration and application of MSHE_m at 30 m and 270 m grid cell resolutions in the Jameson catchment resulted in very similar values of E, 0.96 and 0.93, respectively (Tague *et al*. in press).

Errors associated with observed data and model inputs may also have contributed to predictive uncertainty and prediction errors in this study. For example, LAI inputs may contain errors associated with satellite image processing and/or NDVI-LAI model calibration (Chapter One). The use of LAI values derived from fall (i.e., dormant season) imagery may have contributed to greater absolute predictive uncertainty in wet season months, compared with transition and dry season months, due to the possible under-estimation of growing season LAI. For example, Riggan *et al*. (1988) reported quite different LAI values in the peak season and dormant season for two California evergreen shrub species.

Additional research is needed to examine the potential of new remote sensing datasets, e.g., the daily Earth Observing System Moderate Resolution Imaging Spectrometer (EOS-MODIS) LAI product, to help refine the representation of chaparral LAI phenology in future MIKE-SHE model applications.

The LAI-Stand Age trajectory has also been shown to vary with annual antecedent precipitation conditions (Chapter One), a dynamic not accounted for in this study due to the use of an average recovery trajectory. In addition, uncertainties in the approach used to increase input LAI values in the immediate post-fire years (to account for herbaceous vegetation) may have contributed to the large under-prediction errors observed in the wet season months following the large fire event in 1985. Errors and uncertainty associated with the procedures used to develop spatially distributed precipitation and potential evapotranspiration inputs for this rugged catchment may also have influenced MSHE_m model performance in this study.

4. Conclusions

Results from the GLUE-based calibration and testing of MSHE_m provide insights into both the strengths and weaknesses of the combined model structure, parameters and input data as a tool for predicting integrated catchment behavior in Jameson. Over two-thirds of the observations (comprising over 90% of the total observed flow) in each period were contained within the uncertainty bounds, an acceptable level of model performance relative to total period flow. However, the

fact that the greatest (absolute) prediction errors were associated with critical catchment events, i.e., large storms and large fires, suggests that refinements are needed to improve MSHE_m performance and reduce predictive uncertainty at the monthly/seasonal time scales prior to future application in this fire-prone environment. Sources of uncertainty and error discussed above will be investigated in future work.

GLUE provides a useful modeling approach for advancing beyond the flawed concept of parameter optimization. Working within an equifinality framework allows modelers to explicitly recognize and quantify the effects of uncertainties on model predictions. Future versions of commercially available modeling systems should incorporate the flexibility to conduct GLUE-based modeling and uncertainty estimation – particularly given the use of distributed model predictions as a basis for environmental decision-making.

Acknowledgements

Funding for this research was provided in part by a NASA Land Use Land Cover Change Grant (No. NAG5-11141), a NASA Earth System Science Fellowship (No. NGT5-30335), and a NSF Doctoral Dissertation Research Improvement Grant (No. BCS-0000233).

The authors would like to thank: Drs. Joel Michaelsen and Max Moritz, Dave McKinsey, Jon Ahlroth, Matthew Naftaly, Ken Oster and Bill Ferguson for help with dataset compilation, Robyn Clark, Michael Anaya and W. Casey McMichael for assistance with data processing, Harry Johnson for designing the study site map, and the software technical support staff at the Danish Hydraulic Institute.

References

Abbott, M.B., Bathurst, J.A., Cunge, P.E., O'Connell, J., and Rasmussen, J., 1986a. An introduction to the European Hydrological System – Systeme Hydrologique Europeen 'SHE 1: history and philosophy of a physically based distributed modeling system. Journal of Hydrology 87, 45-59.

Abbott, M.B., Bathurst, J.A., Cunge, P.E., O'Connell, J., and Rasmussen, J., 1986b. An introduction to the European Hydrological System – Systeme Hydrologique Europeen 'SHE' 2: structure of a physically based distributed modelling system. Journal of Hydrology 87, 61-77.

Andersen, J., Refsgaard, J.C., and Jensen, K.H., 2001. Distributed hydrological modelling of the Senegal River Basin – model construction and validation. Journal of Hydrology 247, 200-214.

Baret, F., Olioso, A., Luciani, J.L., and Hanocq, J,F. 1989. Estimation de l'énergie photosynthétiquement active absorbée par une culture de blé à partir de données radiométriques. Agronomie 9, 885-895.

Beven, K., 1989. Changing ideas in hydrology – the case of physically-based models. Journal of Hydrology 105, 157-172.

Beven , K., 1993. Prophecy, reality and uncertainty in distributed hydrological modelling. Advances in Water Resources 16, 41-51.

Beven, K., 1996. Equifinality and uncertainty in geomorphological modelling. Proceedings of the 27th Binghamton Symposium in Geomorphology: the Scientific Nature of Geomorphology, 27-29 September 1996. Rhoads, B.L., and Thorn, C.E. (eds). John Wiley & Sons, Ltd., pp. 289-313.

Beven, K.J., 2001. Rainfall-Runoff Modelling: the Primer. John Wiley & Sons Ltd.: West Sussex, England; 360.

Beven, K., and Binley, A., 1992. The future of distributed models: model calibration and uncertainty prediction. Hydrological Processes 6, 279-298.

Beven, K., and Freer, J., 2001. Equifinality, data assimilation, and uncertainty estimation in mechanistic modelling of complex environmental systems using the GLUE methodology. Journal of Hydrology 249, 11-29.

Binley, A.M., and Beven, K.J., 1991. Physically-based modelling of catchment hydrology: a likelihood approach to reducing predictive uncertainty. In Computer Modelling in the Environmental Sciences, Farmer, D.G., and Rycroft, M.J. (eds). Clarendon Press: Oxford, pp. 75-88.

Brazier, R.E., Beven, K.J., Freer, J., and Rowan, J.S., 2000. Equifinality and uncertainty in physically based soil erosion models: an application of the GLUE methodology to WEPP- the Water Erosion Prediction Project – for sites in the UK and USA. Earth Surface Processes and Landforms 25, 825-845.

Christiaens, K., and Feyen, J., 2002. Constraining soil hydraulic parameter and output uncertainty of the distributed hydrological MIKE SHE model using the GLUE framework. Hydrological Processes 16, 373-391.

Davis, F.W., and Michaelsen, J., 1995. Sensitivity of fire regime in chaparral ecosystems to global climate change. In Global Change and Mediterranean-Type Ecosystems, Oechel, W.C., and Moreno, J.M. (eds). Springer-Verlag: New York, pp. 435-456.

Davis, G.W., Richardson, D.M., Keeley, J.E., and Hobbs, R.J., 1996. Mediterranean-type ecosystems: the influence of biodiversity on their functioning. In Functional Roles of Biodiversity: a Global Perspective, Mooney, H.A., Cushman, J.H., Medina, E., Sala, O.E., and Schulze, E-D. (eds). John Wiley and Sons Ltd., pp. 151-183.

DeBano, L.F., and Conrad, C., 1978. The effect of fire on nutrients in a chaparral ecosystem. Ecology 59, 489-497.

DHI Water and Environment, 2000. MIKE-SHE: Pre- and Postprocessing User Manual.

Dingman, S.L., 1994. Physical hydrology. Prentice Hall: New Jersey, USA, pp. 575.

Franklin, J., Woodcock, C.E., and Warbington, R., 2000. Digital vegetation maps of forest lands in California: integrating satellite imagery, GIS modeling, and field data in support of resource management. Photogrammetric Engineering and Remote Sensing 66, 1209-1217.

Freer, J., and Beven, K., 1996. Bayesian estimation of uncertainty in runoff prediction and the value of data: an application of the GLUE approach. Water Resources Research 32, 2161-2173.

Gamon, J.A., Field, C.B., Goulden, M.L., Griffin, K.L., Hartley, A.E., Joel, G., Penuelas, J., and Valentini, R., 1995. Relationships between NDVI, canopy structure, and photosynthesis in three Californian vegetation types. Ecological Applications 5, 28-41.

Gray, J.T., and Schlesinger, W.H., 1981. Biomass, production and litterfall in the coastal sage scrub of southern California. American Journal of Botany 68, 24-33.

Grayson, R.B., Moore, I.D., and McHahon, T.A., 1992. Physically based hydrologic modelling. 2. Is the concept realistic? Water Resources Research 28, 2639-2658

Hargreaves, G.H., and Samani, Z.A., 1985. Reference crop evapotranspiration from temperature. Applied Engineering in Agriculture 1, 96-99.

Hellmers, H., Horton, J.S., Juhren, G., and O'Keefe, J., 1985. Root systems of some chaparral plants in southern California. Ecology 36, 667-678.

Hill, J., Megier, J., and Mehl, W., 1995. Land degradation, soil erosion and desertification monitoring in Mediterranean ecosystems. Remote Sensing Reviews 12, 107-130.

Hoyt, W.G., and Troxell, H.C., 1932. Forests and streamflow. Proceedings of the American Society of Civil Engineers 58, 1037-1066.

Keeley, J.E., and Keeley, S.C., 1981. Post-fire regeneration of southern California chaparral. American Journal of Botany 68, 524-530.

Keeley, S.C., Keeley, J.E., Hutchinson, S.M., and Johnson, A.W., 1981. Post-fire succession of the herbaceous flora in southern California chaparral. Ecology 62, 1608-1621.

Kummerow, J., Krause, D., and Jow, W., 1977. Root systems of chaparral shrubs. Oecologia 29, 163-177.

Kristensen, K.J., and Jensen, S.E., 1975. A model for estimating actual evapotranspiration from potential evapotranspiration. Nordic Hydrology 6, 170-188.

Lavabre. J., Sempere Torres, D., and Cernesson, F., 1993. Changes in the hydrological response of a small Mediterranean basin a year after a wildfire. Journal of Hydrology 142, 273-299.

Loaiciga, H.A., Pedreros, D., and Roberts, D., 2001. Wildfire-streamflow interactions in a chaparral Watershed. Advances in Environmental Research 5, 295-305.

Mittermeier, R.A., Meyers, N., Thomsen, J.B., da Fonseca, G.A.B., and Olivieri, S., 1998. Biodiversity hotspots and major tropical wilderness areas: approaches to setting conservation priorities. Conservation Biology 12, 516-520.

Moreno, J.M., and Oechel, W.C., 1995. Global change and Mediterranean-type Ecosystems. Springer-Verlag: New York.

Nash, I.E., and Sutcliffe, I.V., 1970. River flow forecasting through conceptual models I. Journal of Hydrology 10, 282-290.

O'Hare, J.P., and Hallock, B.G., 1988. Soil Survey of the Los Padres National Forest Area, California. United States Department of Agriculture, Forest Service and Soil Conservation Service: University of California, 148 p.

Penman, H.L., 1956. Evaporation: an introductory survey. Netherlands Journal of Agricultural Science 4, 7-29.

Poole, D.K., Roberts, S.W., and Miller, P.C., 1981. Water utilization. In Resource use by chaparral and matorral: a comparison of vegetation function in two Mediterranean-type ecosystems. Miller, P.C. (ed). Ecological Studies No. 39. Springer-Verlag: Berlin, pp.123-149.

Ratto, M., and Saltelli, A., 2001. IMPACT Deliverable 18: Model Assessment in Integrated Procedures for Environmental Impact Evaluation – Software Prototypes. Joint Research Centre of European Commission. http://webfarm.jrc.cec.eu.int

Ratto, M., Tarantola, S., and Saltelli, A., 2001. Sensitivity analysis in model calibration: GSA-GLUE approach. Computer Physics Communications 136, 212-224.

Refsgaard, J.C., and Storm, B., 1995. MIKE-SHE. In Computer Models of Watershed Hydrology, Singh VP (ed). Water Resources Publications: Colorado, USA, pp. 809-846.

Refsgaard, J,S., and Storm, B., 1996. Construction, calibration and validation of hydrological models. In Distributed Hydrological Modelling, Abbott, M.B., Refsgaard, J.C. (eds). Kluwer Academic, pp. 41-54.

Riggan, P.J., Goode, S., Jacks, P.M., and Lockwood, R.N., 1988. Interaction of fire and community development in chaparral of southern California. Ecological Monographs 58, 155-176.

Ryan, K.C., 1991. Vegetation and wildland fire: implications of global climate change. Environment International 17, 169-178.

Scott, D.F., 1993. The hydrological effects of fire in South African mountain catchments. Journal of Hydrology 150, 409-432.

Stephenson, J.R., and Calcarone, G.M., 1999. Southern California mountains and foothills assessment: habitat and species conservation issues. General Technical Report GTR-PSW-172, Pacific Southwest Research Station, Forest Service, U.S. Department of Agriculture.

Tague, C., McMichael, C., Hope, A., and Choate, J., In press. Application of the RHESSys model to a California semi-arid shrubland watershed. Journal of the American Water Resources Association.

Vasquez, R.F., Feyen, L., Feyen, J., and Refsgaard, J.C., 2002. Effect of grid size on effective parameters and model performance of the MIKE-SHE code. Hydrological Processes 16, 355-372.

Vazquez, R.F., and Feyen, J., 2003. Effect of potential evapotranspiration estimates on effective parameters and performance of MIKE SHE-code applied to a medium-size catchment. Journal of Hydrology 270, 309-327.

Verstraete, M.M., and Schwartz, S.A., 1991. Desertification and global change. Vegetatio 91, 3-13.

Xevi, E., Christiaens, K., Espino, A., Sewnandan, W., Mallants, D., Sorensen, H., and Feyen, J., 1997. Calibration, validation and sensitivity analysis of the MIKE-SHE model using Neuenkirchen catchment as case study. Water Resources Management 11, 219-242.

Zak, S.K., and Beven, K.J., 1999. Equifinality, sensitivity and predictive uncertainty in the estimation of critical loads. The Science of the Total Environment 236, 191-214.

TABLES

Table 2-1. Parameter ranges used in the MSHE_m Monte Carlo simulations.

Parameter		Minimum value	Maximum value
Interflow/Groundwater reservoirs			
IF_t	(m)	0.0001	0.3
IF_h	(days)	0.0001	3
IF_v	(days)	0.0001	80
GW_h	(days)	0.05	100
Soil			
K_s_Sandy Loam	($m\ s^{-1}$)	1.0×10^{-6}	5.0×10^{-4}
n_Sandy Loam		1	30
K_s_Loam	($m\ s^{-1}$)	1.0×10^{-6}	5.0×10^{-4}
n_Loam		1	30
Vegetation			
C_1		0.01	1
C_2		0.01	1
C_3	($mm\ day^{-1}$)	1	60

FIGURES

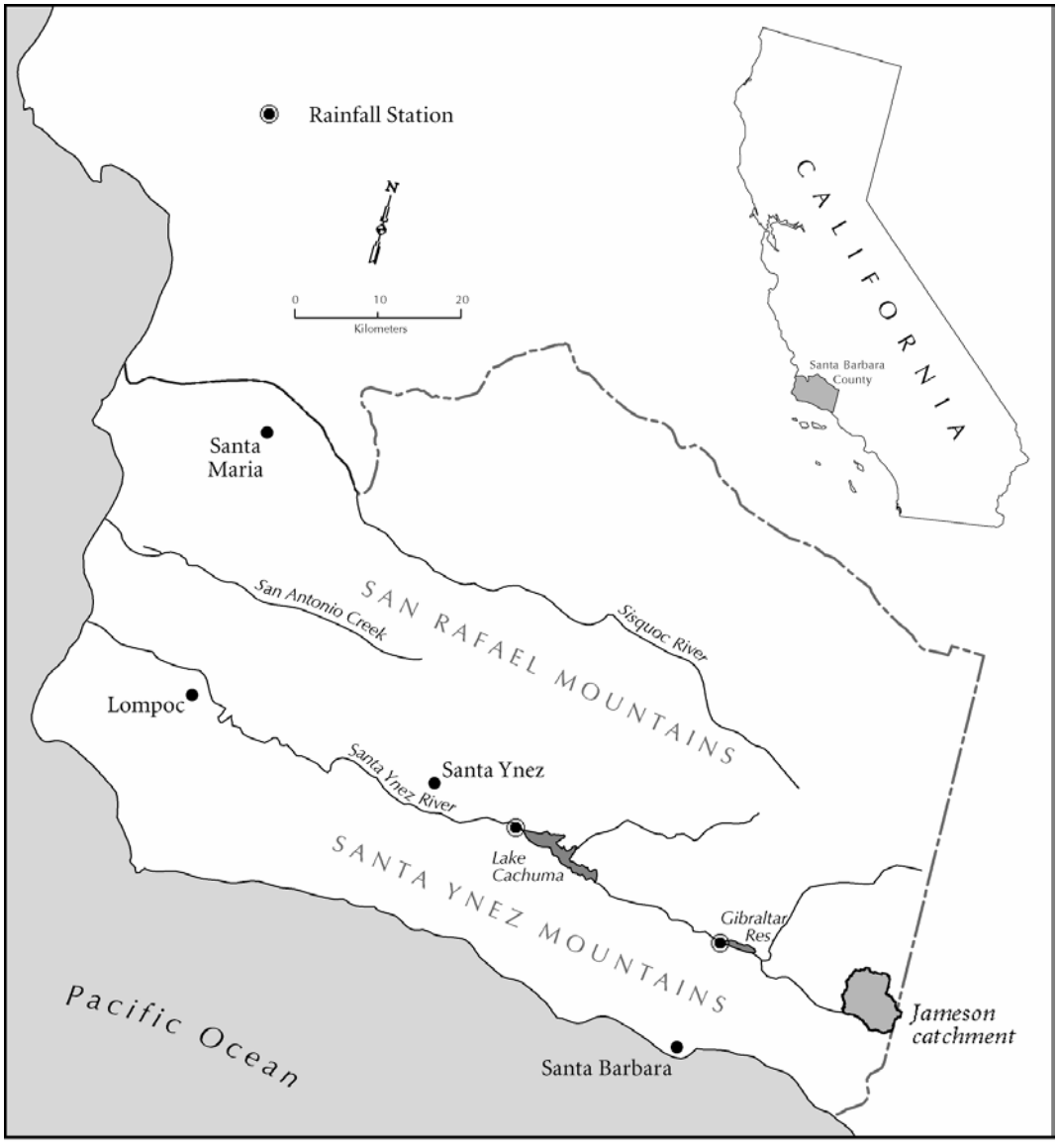

Figure 2-1. The study site - Jameson watershed near Santa Barbara, California.

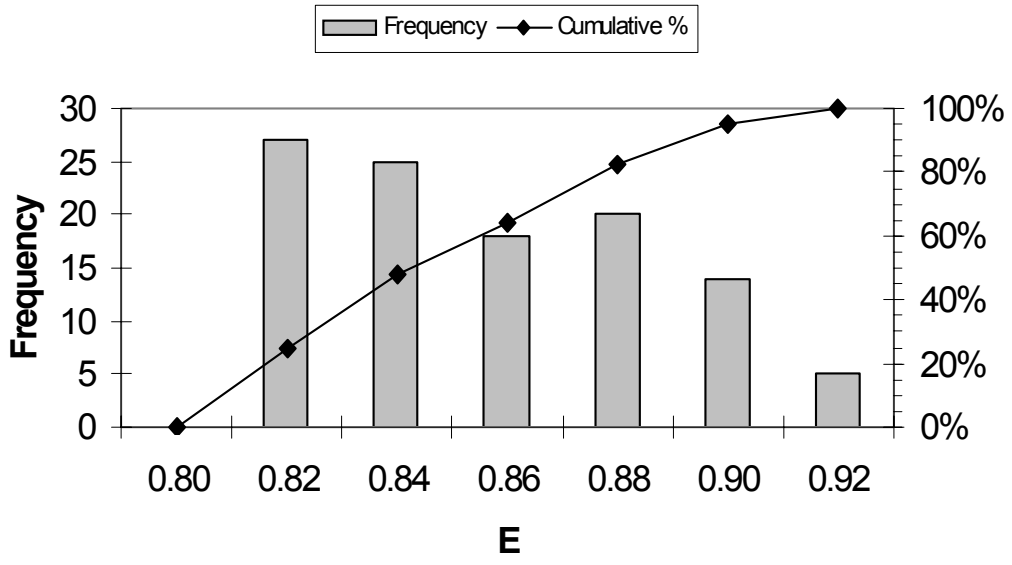

Figure 2-2. Frequency distribution of the coefficient of efficiency, E, for the group of 109 behavioral parameter sets.

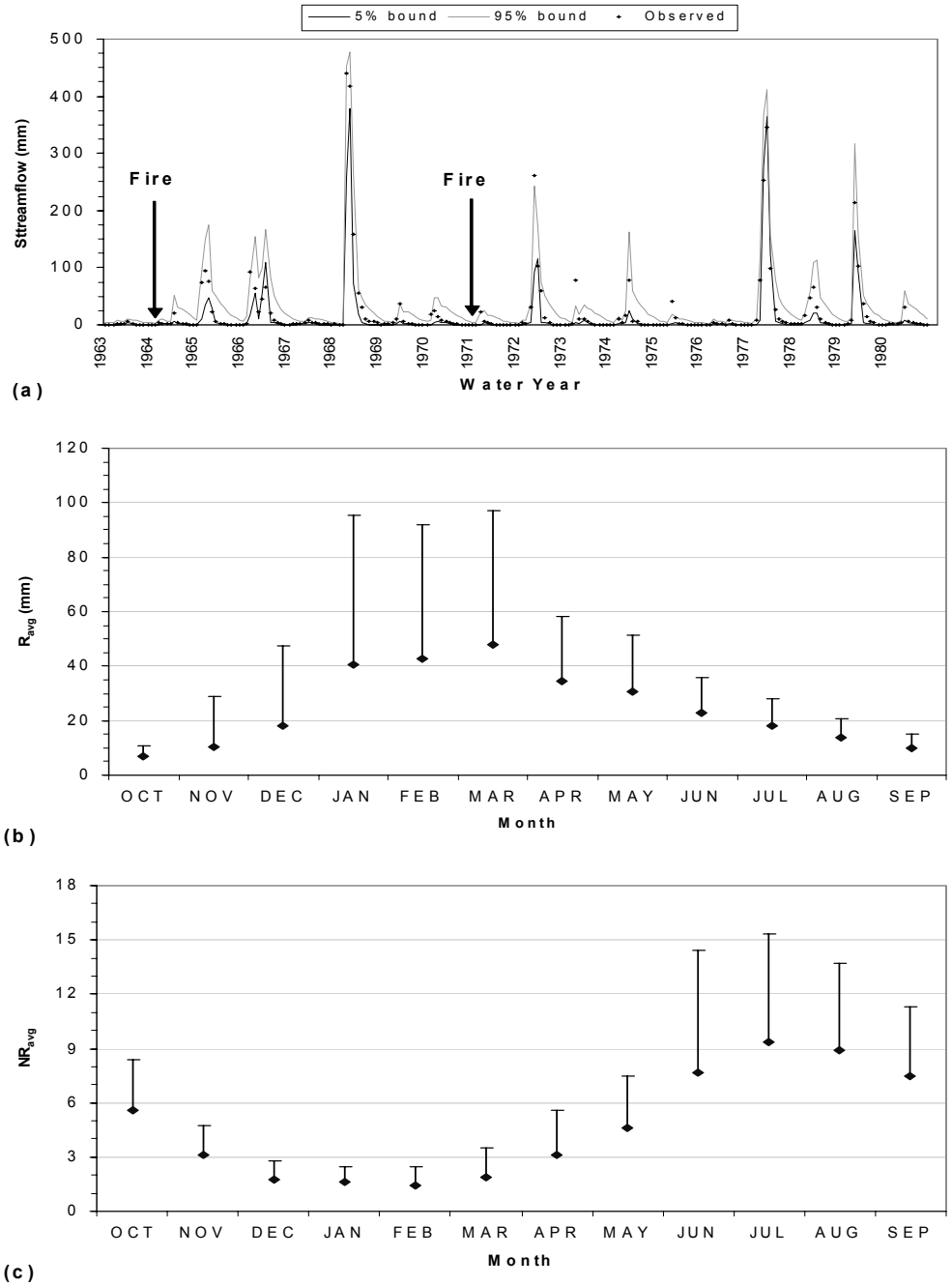

Figure 2-3. Calibration period results: (a) 5% and 95% uncertainty bounds with observed streamflow values, (b) average predictive uncertainty (R_{avg}), by month and (c) R_{avg} normalized for observed streamflow (NR_{avg}), by month. One standard deviation above the mean is shown in (b) and (c) to illustrate the variability in predictive uncertainty for each month.

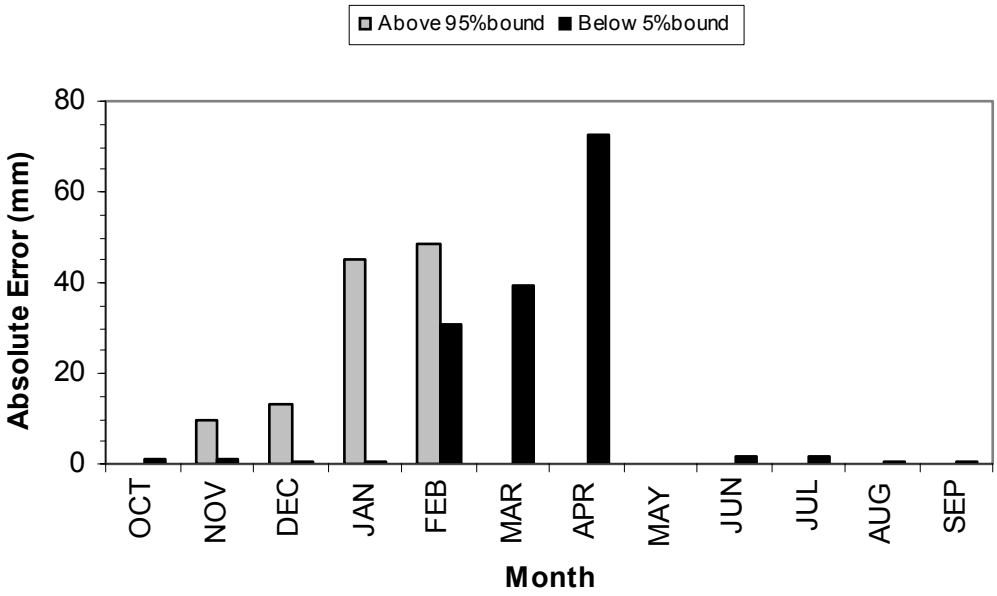

Figure 2-4. The calibration period 'absolute error' was calculated, for each observation not contained by the uncertainty bounds, as the absolute difference between the observed value and the nearest uncertainty bound. Under-estimation occurred when observed values fell above the 95% bound; over-estimation occurred when observations fell below the 5% bound.

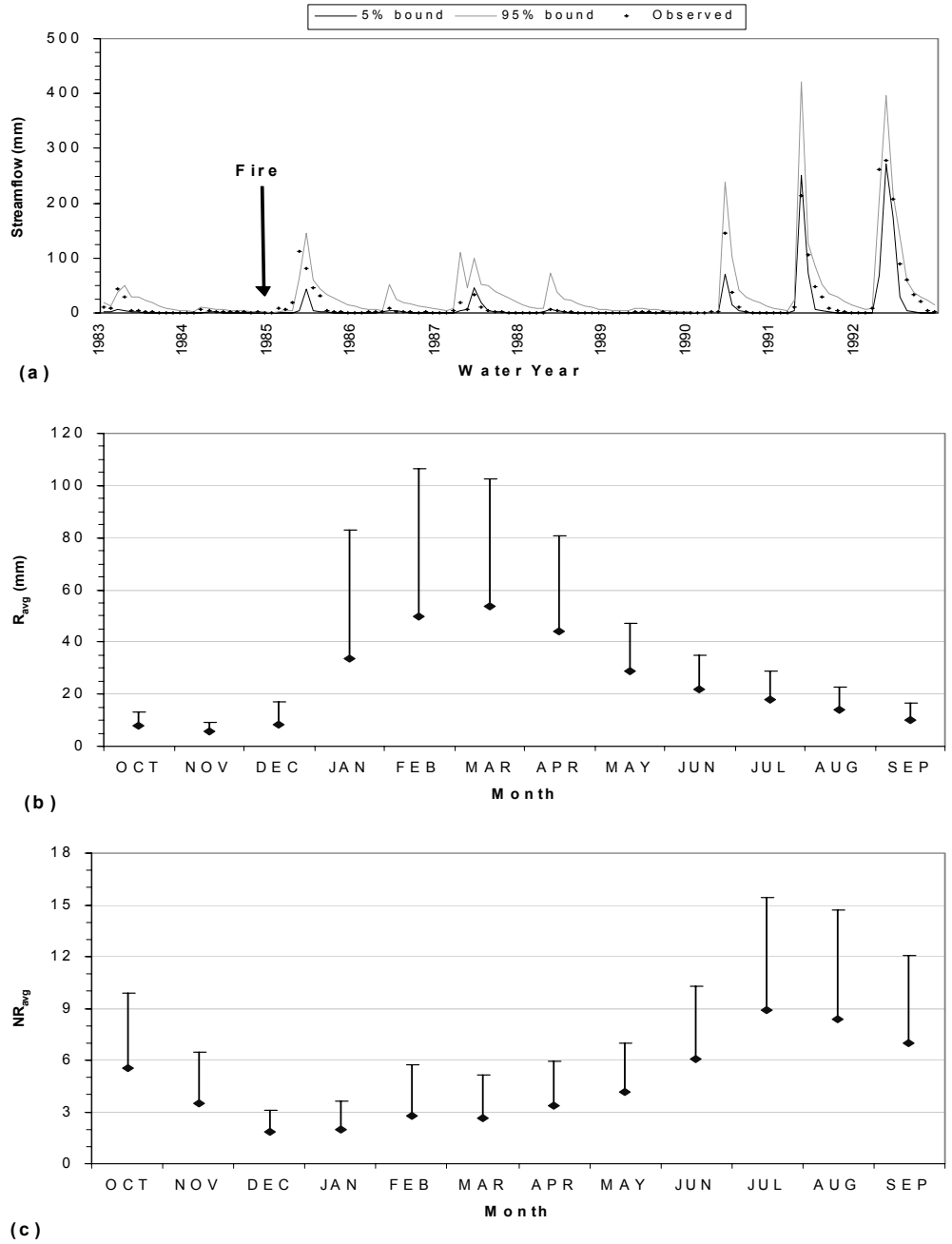

Figure 2-5. Test period results: (a) 5% and 95% uncertainty bounds with observed streamflow values, (b) average predictive uncertainty (R_{avg}), by month and (c) R_{avg} normalized for observed streamflow (NR_{avg}), by month. One standard deviation above the mean is shown in (b) and (c) to illustrate the variability in predictive uncertainty for each month.

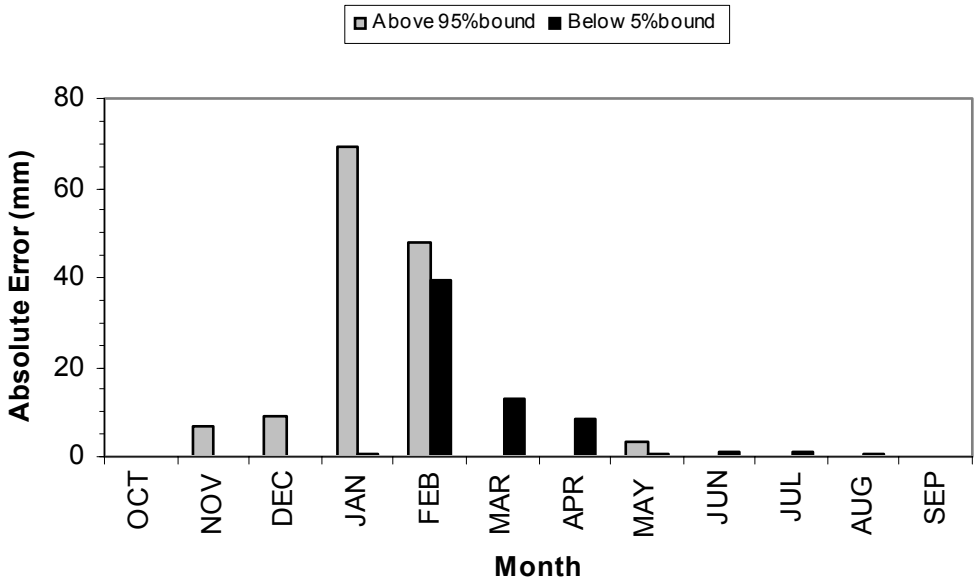

Figure 2-6. The test period 'absolute error' was calculated, for each observation not contained by the uncertainty bounds, as the absolute difference between the observed value and the nearest uncertainty bound. Under-estimation occurred when observed values fell above the 95% bound; over-estimation occurred when observations fell below the 5% bound.

CHAPTER THREE

Uncertainty in leaf area index: effects on predictive uncertainty and parameter sensitivity of the distributed MIKE-SHE model

Abstract. Remote sensing-based estimates of leaf area index (LAI) are often used to represent green vegetation dynamics in distributed hydrological modeling. However, we have little understanding of how uncertainty in these estimates translates into uncertainty in model predictions (predictive uncertainty) or affects the sensitivity of model output to individual parameters (parameter sensitivity). In this study we used the Monte Carlo-based Generalized Likelihood Uncertainty Estimation (GLUE) and Generalized Sensitivity Analysis (GSA) methodologies to examine the effects of uncertainty in LAI inputs on the predictive uncertainty and parameter sensitivity, respectively, of the distributed MIKE-SHE model applied to a semi-arid shrubland catchment in central California.

Overall, uncertainties in LAI inputs did not greatly affect the uncertainty associated with model predictions of streamflow. Relative changes in predictive uncertainty between 'LAI uncertainty scenarios' and the 'baseline' LAI sequence were usually less than ten percent, suggesting that remote sensing-based estimates of LAI are generally appropriate for distributed hydrological modeling in this environment. However, given that some of the largest changes in predictive uncertainty were observed in the first few years following fire, particularly in wet

season months, future work will focus on refining both inter- and intra-annual LAI estimates for this initial recovery period. The influence of uncertainty in LAI on parameter sensitivity was greatest for evapotranspiration and unsaturated zone parameters, highlighting the key role that LAI plays in partitioning rainfall in this model. As expected, model output was relatively insensitive to saturated zone parameters across all LAI uncertainty scenarios.

1. Introduction

Fire in California semi-arid shrublands, i.e., chaparral, dramatically alters catchment land cover and initiates a complex matrix of vegetation recovery sequences that span many decades. The removal and re-growth of vegetation following fire affects the partitioning of rainfall into evapotranspiration and streamflow. Green leaves become increasingly abundant as the vegetation regenerates, altering the relative contributions of canopy evaporation and transpiration and soil evaporation to total evapotranspiration. As a result, information on the spatio-temporal patterns of green leaf area is often required in distributed hydrological models to simulate the impacts of land cover change (e.g., due to fire) on catchment processes. The variable most widely used to represent changes in canopy leaf area in distributed modeling studies is the leaf area index (LAI), the total (one-sided) leaf area per unit ground area. While a number of authors have reported LAI values for chaparral shrublands (e.g., Rundel and Parsons 1979, Schlesinger and Gill 1980, Riggan *et al.* 1988, Gamon *et al*. 1995),

these values are typically restricted to a single species (or community type), a few observations over a limited area and/or to one point in time. As such, these data are not generally suitable for distributed hydrological modelling given the (potentially large) uncertainty associated with extrapolating point measurements over large areas and long periods. This is of particular concern in chaparral shrublands where recurring fires give rise to considerable landscape heterogeneity.

Alternatively, remote sensing-based techniques may be used to characterize catchment LAI dynamics. Remote sensing-based estimates of LAI are typically made using site specific empirical relationships between ground-based measurements of LAI and spectral vegetation indices (SVIs) derived from multi-spectral satellite data (de Jong 1994, Hoff *et al*. 1995, Chen and Chilar 1996, Turner *et al*. 1999). These SVIs generally take the form of a ratio or linear combination of sensor bands and represent a means of reducing multi-spectral information to a single value for estimating vegetation characteristics. The SVI most widely used to estimate LAI is the normalized difference vegetation index (NDVI = (near-infrared – red) / (near-infrared + red)), formulated to exploit the strong absorption (red) and reflectance (near-infrared) properties of green leaves. Remote sensing-based estimates of LAI for chaparral shrublands were made in Chapter One using the generalized NDVI-LAI model of Baret *et al*. (1989). In this model LAI is calculated as a function of the maximum NDVI, the background NDVI and k, a parameter related to the extinction of solar radiation through the vegetation canopy. The general model was calibrated for regional conditions and

used it to convert 10 fall Landsat Thematic Mapper (TM) and Enhanced TM (ETM) images from NDVI into LAI (Chapter One). Values of mean LAI were extracted from eleven large (> 30 km^2) chaparral stands and plotted against stand age (chronosequence approach) to characterize the post-fire recovery sequence of LAI in each image.

There are many advantages to using remote sensing-based approaches for estimating catchment scale LAI dynamics, however, validation of these values is difficult and not often performed – leading to unknown errors in estimated LAI values. Uncertainty in LAI estimates may also arise from errors in image processing procedures and/or uncertainties in calibrating NDVI-based LAI models. Nevertheless, remote sensing-based LAI estimates have been used to characterize catchment vegetation dynamics in distributed hydrological modeling studies in a variety of environments. Mackay and Band (1997) prescribed LAI inputs for the Regional Hydro-ecological Simulation System (RHESSys) using estimates based on Landsat TM NDVI imagery for a 13 km^2 mixed-coniferous catchment in the Central Sierra Nevada, California. Input LAI values for the MIKE-SHE model applied to the 350,000 km^2 Senegal River catchment in West Africa were derived using coarse scale Advanced Very High Resolution Radiometer (AVHRR)-based NDVI images (Sandholt *et al*. 1999, Andersen 2002). Watson *et al*. (1999) used a combination of ground-based measurements and Landsat TM NDVI images to represent vegetation canopy dynamics in the MACAQUE model applied to eucalypt-dominated catchments in southeast

Australia. Finally, the average LAI recovery sequence from Chapter One was used in Chapter Two to characterize post-fire LAI dynamics in an application of the modified MIKE-SHE model to a chaparral catchment in central California. However, despite the widespread use of remote sensing-derived LAI inputs, we have little understanding of how uncertainty in these estimates translates into uncertainty in model predictions (predictive uncertainty) or affects the sensitivity of model output to individual parameters (parameter sensitivity).

Accurate estimation of LAI inputs for distributed hydrological modeling in chaparral shrubland catchments is particularly critical since greater than 70% of annual rainfall is returned to the atmosphere via evapotranspiration (Poole *et al*. 1981). In this study we investigated how uncertainty in remote sensing-derived LAI inputs affects both predictive uncertainty and parameter sensitivity of the distributed MIKE-SHE model applied to a chaparral shrubland catchment in central California. A variety of techniques have been used to perform uncertainty analysis (UA) and sensitivity analysis (SA) in hydrological modelling (e.g., Xevi *et al.* 1997, Christiaens and Feyen 2001, Anderton *et al*. 2002, Vachaud and Chen 2002, Eckhardt *et al*. 2003). However, the prevalence of equifinality in distributed hydrological models, i.e., that multiple parameter sets may provide acceptable model results, necessitates the use of Monte Carlo-based techniques to allow parameter interactions throughout the entire parameter space. Therefore, we implemented the Monte Carlo-based Generalized Likelihood Uncertainty Estimation (GLUE, Beven and Binley 1992, Beven and Freer 2001) and

Generalized Sensitivity Analysis (GSA, Spear and Hornberger 1980, Hornberger and Spear 1981) methodologies for UA and SA, respectively (explained in more detail in sections 3.4 and 3.5). Specifically, we used: (a) a GLUE-based framework to examine the uncertainty associated with model predictions arising from uncertainties in LAI inputs and (b) a GSA-based approach to evaluate how uncertainties in LAI inputs influence parameter sensitivity.

2. Methods

2.1. MIKE-SHE modeling system

MIKE-SHE, a derivative of the Systeme Hydrologique Europeen, SHE (Abbott *et al.* 1986a, b), is a physically-based, distributed hydrological model that has been widely used to study a variety of water resource problems in diverse environments (Refsgaard and Storm 1995). MIKE-SHE comprises a number of sub-modules representing all major phases of the hydrologic cycle. Spatial variation in catchment characteristics is represented using equally sized grid cells, each of which is vertically discretized into a number of sub-layers to represent the soil profile. In this study the model grid cell size was fixed at 270 m to allow the most accurate representation of catchment attributes without placing excessive demands on computer run time. Model predictions of daily streamflow values were summed to monthly totals for comparison with observed monthly values (daily observations were not available). A modified version of the MIKE-SHE model, developed by Andersen *et al*. (2001) for use in catchments with limited data on

subsurface processes, was used in this study. The major differences between the original (MIKE-SHE) and modified (MSHE_m) versions of the model are found in the representations of flow in the unsaturated and saturated zones. A fairly detailed description of the MSHE_m model is provided in Chapter Two and will not be repeated here. However, given this study's focus on LAI inputs, those equations requiring values of LAI are presented below.

Each of the sub-components comprising the total actual evapotranspiration (ET_a), evaporation from canopy storage, plant transpiration and soil evaporation, is calculated within the evapotranspiration module (DHI 2000). Canopy interception of rainfall (1) is a function of the interception storage capacity, I_{max}:

$$I_{\max} = C_{\text{int}} LAI \tag{1}$$

where, C_{int} is an interception parameter and LAI is the input leaf area index; stem flow occurs once I_{max} is filled. Evaporation from canopy storage (2) depends upon the actual amount of water intercepted by the leaves, I, and the rate of potential evapotranspiration, E_p:

$$E_{can} = \min(I, E_p \Delta t) \tag{2}$$

where, E_{can} is the canopy evaporation and Δt is the simulation time step. Canopy transpiration (3) is calculated on the basis of LAI, soil moisture content (θ) and the distribution of plant roots with depth (after Kristensen and Jensen 1975):

$$T = f_1(LAI) f_2(\theta) RDF * E_p \quad (3)$$

where T is canopy transpiration, $f_1(LAI)$ is a function of LAI, $f_2(\theta)$ is a function of soil moisture content and RDF is a function of rooting depth; the maximum value of each function is unity. The $f_1(LAI)$ function (4) is computed using input LAI and two empirical parameters, C_1 and C_2, that influence the ratio of transpiration to soil evaporation (DHI 2000). The C_1 and C_2 parameters are the slope and intercept, respectively, of Eq. (4) which describes a linear relationship between ET_a / E_p and LAI for LAI between zero and LAI' = (1- C_2) / C_1 (Kristensen and Jensen 1975). The value of C_2 establishes a minimum amount of soil evaporation that occurs regardless of canopy leaf area and soil dryness conditions, as long as soil moisture content (θ) is above the wilting point (θ_w). Consequently, $f_1(LAI)$ is greater than or equal to C_2 whenever $\theta \geq \theta_w$. The value of $f_1(LAI)$ rises above C_2 as LAI increases to LAI', after which point $f_1(LAI)$ is equal to unity.

$$f_1(LAI) = C_2 + C_1 LAI' \quad (4)$$

The soil moisture function, $f_2(\theta)$, expresses the dependence of ET_a / E_p on soil dryness, as the ability of vegetation to extract water from the soil is assumed to decline as moisture content in the root zone is reduced (Kristensen and Jensen 1975). The root distribution function, RDF, is determined by the input root depth

and a vertical root density distribution (logarithmic). Soil evaporation is calculated as a function of soil moisture in the upper layer of the soil column, and is added to E_{can} and T in order to compute ET_a (Refsgaard and Storm 1995, DHI 2000).

2.2. Study site

The Jameson catchment (34 km^2), located in the San Rafael Mountains north of Santa Barbara, California, USA (Figure 3-1), is one of the few remaining non-urbanized catchments in this region. The semi-arid climate of this area is characterized by cool, wet winters and warm, dry summers. Average water year (October – September) precipitation and streamflow are 780 mm and 233 mm, respectively. Elevation ranges from 677 m at the catchment outlet to 1771 m at the highest point in the catchment. Sandy-loam soils are typically found on the rugged hillslopes (average slope ~ 43%), while somewhat deeper sandy-loam and loam soils are found on gentler slopes. The combination of stands in different stages of post-fire succession with spatial variability in physical site characteristics (e.g., terrain and soils) produces a complex vegetation mosaic dominated by evergreen shrubs (chaparral) intermixed with oak woodlands, summer deciduous sub-shrubs (coastal sage scrub), conifer forest and grassland (Stephenson and Calcarone 1999).

2.3. Input data

A brief description of the time series and spatial datasets required for MSHE_m is given here (see Chapter Two and Appendix A for a more detailed explanation of dataset compilation procedures). Daily temperature and precipitation data from water years 1961 to 1993 were obtained from National Climate Data Center (NCDC) gages in and around the Jameson catchment. Less than one percent of the temperature and precipitation values were missing and had to be interpolated. MSHE_m also requires daily inputs of potential evapotranspiration, however, observed values were not available. Therefore, we used the Hargreaves-Samani (1985) model (calibrated and validated for regional conditions) to calculate daily values of potential evapotranspiration for each of twelve topographically-defined catchment zones (derived using three slope and four aspect classes). Existing digital vegetation (Franklin *et al*. 2000), soils (O'Hare and Hallock 1988) and elevation maps were used to delineate and characterize vegetation, soil and topographic units within the catchment. An average LAI recovery trajectory was calculated from the set of 10 sequences derived in Chapter One and used as the 'baseline' (i.e., 'no uncertainty') LAI input sequence for MSHE_m in both the uncertainty analysis and sensitivity analysis studies described below. As discussed in Chapter Two, this sequence does not represent intra-annual variation in LAI, with the notable exception of the immediate post-fires years when winter/spring LAI is augmented to account for the presence of herbaceous

vegetation. The use of fall-based LAI values may underestimate growing season LAI and, thus, contribute additional uncertainty to model predictions.

2.4. GLUE-based uncertainty analysis

Implementing a GLUE-based uncertainty analysis requires making Monte Carlo simulations using a large number of parameter sets, assessing the relative performance of each set by comparing model estimates with observed data, and retaining only those parameter sets that provide behavioral (acceptable) predictions. The suite of behavioral model predictions is then used to compute the 5% and 95% uncertainty bounds, i.e., prediction limits, for the given model application. The reader is referred to Binley and Beven (1991), Zak and Beven (1999), Ratto *et al*. (2001) and Chapter Two for additional details on this procedure.

A previous GLUE-based application of MSHE_m in the Jameson catchment yielded 109 behavioral parameter sets for a period in which mature chaparral stands dominated the landscape (Chapter Two). These parameter sets were then used to make simulations for a second period containing a fire which burned nearly 78% of the Jameson catchment in July 1985. Greater than two-thirds of the observed monthly streamflow values (comprising over 90% of the total observed flow) in each period were contained within the calculated 5% and 95% prediction limits, an acceptable level of model performance relative to total period flow (Chapter Two). However, most estimation errors were associated with

key catchment events, i.e., large storms and fire, particularly in the second period where nearly half of the under-estimation error occurred in the first post-fire year.

In this study we examined the impacts of uncertainty in LAI inputs on MSHE_m predictive uncertainty for the second period (described above) when inter-annual changes in canopy leaf area were most rapid. The 109 behavioral parameter sets identified in Chapter Two were used to make seven sets of model simulations for this 'recovery' period, one for the baseline LAI sequence (section 2.3) and one for each of six 'uncertainty scenarios'. The six LAI uncertainty scenarios were generated by increasing and decreasing the baseline sequence by 10, 20 and 40%, increments selected to cover the potential range of (unknown) error levels associated with remote sensing-based estimates of LAI. The 90% uncertainty interval (i.e., the range of acceptable model predictions) was computed for all seven cases as the total distance between the 95% and 5% uncertainty bounds. The effect of uncertainty in LAI inputs on predictive uncertainty was examined by comparing uncertainty intervals between each uncertainty scenario and the baseline case, as well as among uncertainty scenarios.

2.5. Generalized sensitivity analysis

Conducting a GSA involves following many of the same procedures used in the GLUE methodology described above. Specifically, Monte Carlo simulations are made for a large number of randomly selected parameter sets which are subsequently divided into behavioral and non-behavioral subsets. These subsets

are further analyzed in GSA to distinguish between sensitive and insensitive parameters by comparing the behavioral and non-behavioral cumulative distribution functions (CDFs) for each individual parameter. It is assumed that model predictions are not influenced by parameters whose behavioral and non-behavioral CDFs are very similar (Hornberger *et al*. 1985, Beven 2001). The non-parametric Kolmogorov-Smirnov *d* statistic, the maximum vertical distance between a pair of CDFs, may be used to quantify the difference between CDFs (Beven 2001, Makino *et al*. 2001, Wade *et al*. 2001). While this test statistic is not robust for large numbers of simulations, relative sensitivity may be assessed by grouping parameters into low, medium and high sensitivity classes on the basis of their associated *p* values (Madsen 2000).

In this research GSA was used to examine the sensitivity of predicted monthly streamflow to eleven model parameters (Table 3-1) for three different input LAI sequences. The eleven parameters examined in the GSA component of this study are the same as those used in the GLUE-based calibration of MIKE-SHE for the Jameson watershed (Chapter Two and Appendix B). Parameter sensitivity was examined for two periods with contrasting post-fire recovery dynamics (the mature and recovery periods described in section 2.4) using the minimum, average and maximum LAI recovery sequences from Chapter One as model inputs. As in the uncertainty analysis, the average LAI sequence was used here as the baseline case for GSA. The minimum and maximum sequences were used to represent the extreme remote sensing-based LAI estimates for this study area. One thousand

Monte Carlo simulations were made for each combination of input LAI and time period, for a total of 6000 runs. The performance of each parameter set was evaluated following each simulation using two different, but related, performance measures: the coefficient of efficiency, E, and E calculated using the natural log of observed and estimated values, lnE. The coefficient of efficiency (5) is a standard performance metric used to evaluate the accuracy of both the magnitude and timing of predicted flows (e.g., Andersen *et al*. 2001, Beven 2001, Vasquez *et al*. 2002). The lnE metric places increased emphasis on the frequent low flows observed in this semi-arid catchment.

$$E = \frac{\sum (O - \overline{O})^2 - \sum (O - P)^2}{\sum (O - \overline{O})^2} \qquad (5)$$

The first two water years in each simulation period were used to spin-up model storages and, thus, were excluded from the calculation of E and lnE. The behavioral threshold value of E used in this application of MSHE_m followed Andersen *et al*. (2001), where 'good' model runs were those with $E \geq 0.80$; for consistency, the same threshold value was used for lnE.

3. Results and discussion

3.1. Uncertainty analysis

For ease of discussion the six LAI uncertainty scenarios were labeled using either a '+' or '-', depending upon whether simulated uncertainty of 10, 20 and 40% was added to (+10, +20 and +40) or subtracted from (-10, -20 and -40) the baseline LAI sequence. The 90% uncertainty interval (UI) was calculated for all seven LAI sequences as the difference between the 95% and 5% uncertainty bounds (i.e., the total distance between the bounds). The relative change in the UI (UI_{rc}) between an uncertainty scenario and the baseline case was calculated as: $UI_{rc} = (UI_{scenario} - UI_{baseline}) / UI_{baseline}$. Positive (negative) values of UI_{rc} indicated an increase (decrease) in predictive uncertainty resulting from uncertainty in LAI inputs.

The relative change in MSHE_m predictive uncertainty (UI_{rc}) associated with each uncertainty scenario is shown in Figure 3-2. Overall, the amount of uncertainty associated with monthly streamflow predictions increased when input LAI was lowered below the baseline (-10, -20 and -40 scenarios), while predictive uncertainty decreased for LAI inputs above the baseline sequence (+10, +20 and +40 scenarios). (Absolute) values of UI_{rc} generally followed the expected directional trends, with values increasing as input errors progressed from 10 to 40%. The largest (absolute) values of UI_{rc} over the post-fire recovery period (1986-1993) occurred for LAI inputs below the baseline, especially with the -40 uncertainty scenario. (Absolute) values of UI_{rc} were less than 10% for the -10, -20, +10 and +20 uncertainty scenarios over this period, with the exception of the -

20 scenario in 1987 and 1990 (two very dry years). Values of UI_{rc} for the -40 and +40 scenarios were much more variable.

Values of UI_{rc} associated with the +10, +20 and +40 uncertainty scenarios were much smaller than values related to the -10, -20 and -40 scenarios in the first year following fire (1986, Figure 3-2). LAI inputs above the baseline had little effect on values of UI_{rc} in 1986, suggesting that the baseline LAI sequence represented sufficient canopy leaf area for the available soil moisture that year. That is, all available soil moisture was apparently utilized under the baseline LAI scenario, leaving no reserves to support LAI values in excess of baseline values. In contrast, lowering input LAI below the baseline resulted in higher predicted flows and larger (absolute) values of UI_{rc} in 1986 for the -10, -20 and -40 uncertainty scenarios. Modified LAI inputs in the second post-fire year (1987) produced proportional changes in predictive uncertainty for the ± 10, 20 and 40% scenarios (Figure 3-2). Moreover, UI_{rc} values for this year were generally much larger than in 1986, possibly due to the extremely dry conditions in 1987 (272 mm). These results imply that streamflow dynamics are very sensitive to LAI in dry years. In 1987, raising LAI above the baseline apparently drained already low soil moisture reserves, reducing predicted streamflow values and narrowing the uncertainty bounds. In contrast, predictive uncertainty increased when input LAI was below the baseline sequence by even a small percentage. Raising LAI inputs above the baseline had an increasingly smaller effect on UI_{rc} values in the third through eighth post-fire years (Figure 3-2). This may be explained, at least in part,

by the formulation of the transpiration function $f_1(LAI)$ in MSHE_m which tends to limit the effect of increasing LAI after a threshold value determined by the C_1 and C_2 parameters (Eq. 4). The effects of reducing LAI inputs below the baseline during this period varied with rainfall conditions and were generally largest in drier years.

(Absolute) values of UI_{rc} were highest in wet season months (November – April), decreasing into the transition (May – June) and dry (July – October) season months (Figure 3-3). UI_{rc} values associated with the ± 10 and 20% uncertainty scenarios were less than 10% in all months, as were values corresponding to the +40 scenario. However, values UI_{rc} for the -40 scenario were greater than 10% in six of twelve months, including all wet season months except April. Overall, uncertainty in LAI inputs had the greatest impact on catchment water balance in wet season months as canopy leaf area directly affects the partitioning of rainfall into evapotranspiration and streamflow in MSHE_m. The potential under-estimation of LAI values in the growing season (section 2.3) may also have contributed to greater relative predictive uncertainty in these months.

Differences in the UIs between LAI uncertainty scenarios and the baseline sequence were largely the result of changes in the 95% uncertainty bound (Figure 3-4a), particularly for the -10, -20 and -40 scenarios. The difference between the 95% bound for each uncertainty scenario and the baseline sequence was calculated as: $\Delta 95\%$ = (scenario_95% - baseline_95%) / baseline_95%; a similar calculation was performed using the 5% uncertainty bounds. Values of $\Delta 95\%$ were highest in

the driest years (1987 and 1990) and smallest in the two wettest years (1992 and 1993). These results indicate that uncertainty in LAI inputs has a greater impact on predicted high flows (which control the 95% bound) when rainfall is limited, especially when input LAI was less than the baseline. Uncertainty in LAI inputs under very wet conditions may have little impact on predicted high flows since there is an upper limit on the ability of vegetation to utilize incoming rainfall. Values of Δ5% were largest in the first year following fire (Figure 3-4b), and were greater than values of Δ95% that year for all uncertainty scenarios except -40. Overall, values of Δ5% were greatest in the first few post-fire years, generally decreasing with increasing stand age. It appears that uncertainty in LAI inputs has a greater impact on predicted low flows (which control the 5% bound) in the early stages of post-fire recovery when the development of canopy leaf area may be most tightly coupled to available water resources.

3.2. Generalized sensitivity analysis

Each of the parameter sets used to make MSHE_m simulations in the GSA was classified as either behavioral or non-behavioral based on the 0.80 threshold for both E and lnE. The number of behavioral parameter sets identified for each of the three LAI scenarios was low for both performance measures in both the periods (Table 3-2). However, in some cases the proportion of behavioral parameter sets (i.e., ~10%) was comparable to that found in other hydrological modelling studies (e.g., Spear 1997, Brazier *et al*. 2000, Beven and Freer 2001). In the first period

substantially more behavioral parameter sets were identified based on E than on lnE, while very few behavioral parameter sets were identified in the second period using either measure. The sensitivity of individual parameters was only assessed for those cases (i.e., combination of performance measure and period) where at least 5% of the 1000 parameter sets were classified as behavioral. This criterion was adopted to ensure that the behavioral CDFs were calculated using a reasonable number of parameter sets. Hence, parameter sensitivity was evaluated for each LAI scenario in the first period only, and only as a function of the E performance measure. Behavioral and non-behavioral CDFs were computed for each parameter under each of the LAI scenarios examined; corresponding values of d and p are given in Table 3-3. Parameter sensitivity was assessed using the following classes (after Madsen 2000) (a) $p \geq 0.100$, low sensitivity, (b) $0.010 < p < 0.100$, medium sensitivity, and (c) $p \leq 0.010$, high sensitivity.

For ease of discussion, individual parameters were placed into one of three groups according to their role in regulating catchment hydrologic processes (after Vazquez and Feyen 2003). Water balance parameters (C_1, C_2 and C_3) are those that affect the partitioning of rainfall into evapotranspiration and streamflow. Water routing parameters are subdivided into those that regulate processes in the unsaturated zone (*n_Loam*, K_s*_Loam*, *n_Sandy Loam* and K_s*_Sandy Loam*) and the saturated zone (IF_t, IF_h IF_v and GW_h).

3.2.1. Water balance parameters

Model performance was highly sensitive to values of the C_2 parameter for all three LAI uncertainty scenarios (Table 3-3). Values of the *d*-statistic and *p*-value were similar for each scenario, indicating that C_2 sensitivity was not affected by uncertainty in LAI inputs. In contrast, the sensitivity of C_1 declined as input LAI increased, while the C_3 parameter was characterized by low sensitivity for all three uncertainty scenarios.

As previously mentioned, C_1 and C_2 are the slope and intercept, respectively, of the LAI function used in the calculation of canopy transpiration (section 2.1). The fact that C_2 was not dependent on input LAI may be a result of its role in establishing the minimum soil evaporation that occurs whenever soil moisture is greater than the wilting point, regardless of canopy leaf area. Once LAI ≥ LAI', the LAI function is always equal to one and increasing LAI has no additional affect on transpiration. A possible explanation for the high sensitivity of C_1 under the minimum LAI scenario is tied to its role in determining the value of LAI', and the fact that input LAI values remain below LAI' for the longest period of time under the minimum LAI scenario. Overall, these results support previous MIKE-SHE work that demonstrated the sensitivity of model output to both C_1 and C_2 (Xevi *et al*. 1997, Vazquez and Feyen 2003).

The low sensitivity of model output to C_3, which influences the linear relation between ET_a/E_p and relative soil dryness (i.e., $f_2(\theta)$), might be explained as follows. The value of C_3 does little to influence the value of $f_2(\theta)$ when plant

available water is at or near its maximum value. However, at lower moisture contents, C_3 strongly influences the value of $f_2(\theta)$, such that smaller values of C_3 lead to lower values of $f_2(\theta)$ (DHI 2000). That is, the ratio of ET_a to E_p is smaller for lower values of C_3 at a given moisture content. Kristensen and Jensen (1975) recommend larger values of C_3 for light soils and vegetation with dense, shallow roots, and smaller values for heavy soils and deep-rooted vegetation. Previous work with MIKE-SHE has shown C_3 to be a sensitive parameter for study areas characterized by sandy loam soils and agricultural crops, i.e., light soils and shallow rooted vegetation (Xevi *et al*. 1997, Vazquez and Feyen 2003). In contrast, MSHE_m predictions for the Jameson catchment, where soils are light and chaparral rooting depth is substantial, were relatively insensitive to C_3 regardless of input LAI values. This combination of soil texture and rooting habit is not discussed in the MIKE-SHE User's Manual (DHI 2000) or Kristensen and Jensen (1975), suggesting that it may fall outside of the range of conditions best represented by the soil moisture function, $f_2(\theta)$.

3.2.2. Water routing parameters – unsaturated zone (UZ)

Two soils types were used in MSHE_m to represent soil characteristics in the study catchment, a moderately deep 'upland' soil and a deeper 'lowland' soil. Both horizons in the upland soil were characterized as 'Sandy Loam', while the lowland soil type had a 'Sandy Loam' upper horizon and a 'Loam' lower horizon. Model output was highly sensitive to *n_Sandy Loam* for each LAI uncertainty

scenario at very similar values of *d* and *p* (Table 3-3). The *n* parameter influences the reduction of saturated hydraulic conductivity (K_s) to actual hydraulic conductivity (K_{act}) as a function of the effective saturation (S): $K_{act} = K_s * S^n$. Larger values of *n* lead to greater reductions in K_s for a given value of S, thus influencing soil percolation rates, soil evaporation and transpiration. Suggested values of *n* are lower for sandy soils than for clayey soils (DHI 2000), implying that the sensitivity of model output to *n_Sandy Loam* is largely a function of soil properties – and is independent of uncertainty in LAI inputs.

Model output was highly sensitive to K_s*_Sandy Loam* for the minimum and maximum LAI scenarios only. Values of *d* and *p* were very similar for these two scenarios, but very different from values associated with the average LAI scenario. The use of the simplified Richard's equation to model UZ flow means that vertical water movement is primarily a function of K_s, which explains why model output would be sensitive to this parameter. However, it is not clear why K_s was only highly sensitive under the minimum and maximum LAI uncertainty scenarios. Perhaps it is the result of a 'compensating effect', where model output becomes increasingly sensitive to K_s as LAI inputs diverge from baseline values. That is, K_s may play a larger role in regulating UZ flows when input LAI values are too large or too small. Model performance was not sensitive to either of the UZ routing parameters corresponding to the Loam soil type (*n_Loam* and K_s*_Loam*), most likely due to its limited presence in the Jameson catchment.

3.2.3. Water routing parameters – saturated zone (SZ)

Model performance was highly sensitive to IF_t, IF_h and IF_v for all but one of the LAI uncertainty scenarios, while it was relatively insensitive to GW_h in each case (Table 3-3). Thus, the sensitivity of model output to SZ parameters was essentially independent of uncertainty in LAI inputs, which was expected given the absence of feedbacks between the saturated and unsaturated zones in MSHE_m. The sensitivity of model predictions to the interflow reservoir threshold and timing parameters suggests that interflow dynamics strongly influenced the routing of stormflow following a rainfall event. The low sensitivity of model output to GW_h was somewhat surprising given the high frequency of low flows in the study catchment, though this might be related to the use of E which is somewhat biased towards higher flows.

3.3. GSA revisited - modifying the lnE threshold for behavioral parameter sets

One of the original objectives of this study was to examine the impact of uncertainty in LAI inputs on parameter sensitivity using two different performance measures, E and lnE. However, there were insufficient behavioral parameter sets available to make this comparison (for all combinations of LAI uncertainty scenario and time period) when the 0.80 threshold was used for both performance measures. Upon completion of the GSA described above, we decided to re-examine our choice to use the same behavioral threshold for both performance measures.

As noted previously values of E tend to be biased by larger flows, whereas the use of lnE lessens this bias by logarithmically transforming observed and estimated values prior to calculating E. Therefore, it could be argued that the behavioral threshold for lnE should, in fact, be lower than the value used for E. Working under this assumption we selected a new behavioral threshold for lnE of 0.65, a value which produced nearly the same number of behavioral parameter sets for each LAI uncertainty scenario in the first period as did the 0.80 threshold for E (Table 3-4).

New CDFs were calculated for each model parameter based on the modified behavioral threshold for lnE. Table 3-5 shows the resulting *d* and *p* values for each model parameter under each of the LAI uncertainty scenarios in Period One. A number of important differences in parameter sensitivity were observed between Table 3-4 (E) and Table 3-5 (modified lnE, lnE_m) which appeared to be related to the different emphasis given to high flows by each performance measure. For example, GW_h was identified as having low sensitivity using the E performance measure, but was classified as highly sensitive based on lnE_m. The interflow reservoir parameters IF_t and IF_v were classified as highly sensitive for all LAI uncertainty scenarios using both E and lnE_m, however IF_h was only highly sensitive based on E. These differences between performance measures emphasize the sensitivity of estimated low flows to the vertical interflow contribution to baseflow (which is a function of both IF_t and IF_v). Horizontal interflow (determined by IF_t and IF_h) contributes directly to streamflow

(bypassing the groundwater reservoir) and, consequently, is more likely linked to the timing of larger flows. As before, the sensitivity of SZ parameters was independent of uncertainty in LAI inputs. These results highlight the fact that the choice of performance measure and corresponding threshold value affects the separation of behavioral from non-behavioral parameter sets (Beven and Binley 1992, Freer and Beven 1996), which, in turn, directly impacts the calculation of CDFs and the assessment of parameter sensitivity.

4. Conclusions

Overall, MSHE_m predictive uncertainty was not greatly influenced by uncertainty in remote sensing-based LAI inputs. Relative changes in UI between five of the six LAI uncertainty scenarios (i.e., -10, -20, +10, +20 and +40) and the baseline LAI sequence were less than 10% in all but the two driest years. These results suggest that remote sensing-derived estimates of LAI are generally appropriate for distributed modelling in chaparral-dominated catchments. However, given that some of the larger (absolute) changes in UI_{rc} occurred in the first few years following fire, future remote sensing efforts should focus on refining LAI estimates for this initial recovery period. Additional work is also needed to incorporate intra-annual variability in LAI inputs as a step towards reducing predictive uncertainty in wet season months.

Model output was highly sensitive to many individual parameters across all three LAI uncertainty scenarios (i.e., it was independent of uncertainty in LAI

inputs); this was particularly true for saturated zone parameters. However, model sensitivity did vary between LAI uncertainty scenarios for a number of key parameters in the evapotranspiration and unsaturated zone modules – highlighting the importance of LAI in partitioning rainfall in this model. While these results are based on a relatively small number of behavioral parameter sets, they underscore the need for refining our remote sensing-based estimates of LAI. The current study could be expanded in future work to examine how different performance measures and thresholds, modified parameter ranges, and additional Monte Carlo simulations influence GSA results.

In this study we focused on the effects of uncertainty in *remote sensing-based* LAI inputs on the performance of MSHE_m in a chaparral shrubland catchment. Results from this study are expected to facilitate future applications of MSHE_m in this region and will be used to improve remote sensing-based estimates of LAI. In addition, we hope they illustrate the importance of examining the effects of uncertainty in LAI inputs on distributed model performance – *regardless of the technique* used to estimate input LAI.

Acknowledgements

Funding for this research was provided in part by a NASA Land Use Land Cover Change Grant (No. NAG5-11141), a NASA Earth System Science Fellowship (No. NGT5-30335), and a NSF Doctoral Dissertation Research Improvement Grant (No. BCS-0000233). The authors would like to thank: Robyn Clark, W. Casey McMichael, and Jared Aldstadt for assistance with data processing, Harry Johnson for designing the study area map, and the software technical support staff at the Danish Hydraulic Institute.

References

Abbott, M.B., Bathurst, J.A., Cunge, P.E., O'Connell, J., and Rasmussen, J., 1986a. An introduction to the European Hydrological System – Systeme hydrologique Europeen 'SHE 1: history and philosophy of a physically based distributed modeling system. Journal of Hydrology 87, 45-59.

Abbott, M.B., Bathurst, J.A., Cunge, P.E., O'Connell, J., and Rasmussen, J., 1986b. An introduction to the European Hydrological System – Systeme Hydrologique Europeen 'SHE' 2: structure of a physically based distributed modelling system. Journal of Hydrology 87, 61-77.

Andersen, J., Refsgaard, J.C., and Jensen, K.H., 2001. Distributed hydrological modelling of the Senegal River Basin – model construction and validation. Journal of Hydrology 247, 200-214.

Andersen, J., Dybkjaer, G., Jensen, K.H., Refsgaard, J.C., and Rasmussen, K., 2002. Use of remotely sensed precipitation and leaf area index in a distributed hydrological model. Journal of Hydrology 264, 34-50.

Anderton, S., Latron, J., and Gallart, F., 2002. Sensitivity analysis and multi-response, multi-criteria evaluation of a physically based distributed model. Hydrological Processes 16, 333-353.

Baret, F., Olioso, A., Luciani, J.L., and Hanocq, J.F., 1989. Estimation de l'énergie photosynthétiquement active absorbée par une culture de blé à partir de données radiométriques. Agronomie 9, 885-895.

Beven, K.J., 2001. Rainfall-Runoff Modelling: the Primer. John Wiley & Sons Ltd., West Sussex, England, 360 pp.

Beven, K., and Binley, A., 1992. The future of distributed models: model calibration and uncertainty prediction. Hydrological Processes 6, 279-298.

Beven, K., and Freer, J., 2001. Equifinality, data assimilation, and uncertainty estimation in mechanistic modelling of complex environmental systems using the GLUE methodology. Journal of Hydrology 249, 11-29.

Brazier, R.E., Beven, K.J., Freer, J., and Rowan, J.S., 2000. Equifinality and uncertainty in physically based soil erosion models: an application of the GLUE methodology to WEPP- the Water Erosion Prediction Project – for sites in the UK and USA. Earth Surface Processes and Landforms 25, 825-845.

Chen, J.M., and Chilar, J, 1996. Retrieving leaf area index of boreal conifer forests using Landsat TM images. Remote Sensing of Environment 55, 53-162.

Christiaens, K., and Feyen, J., 2001. Analysis of the uncertainties associated with different methods to determine soil hydraulic properties and their propagation in the distributed hydrological MIKE SHE model. Journal of Hydrology 246, 63-81.

Davis, F.W., and Michaelsen, J., 1995. Sensitivity of fire regime in chaparral ecosystems to global climate change. In Global Change and Mediterranean-Type Ecosystems, Oechel, W.C., and Moreno, J.M. (eds). Springer-Verlag: New York, pp. 435-456.

Davis, G.W., Richardson, D.M., Keeley, J.E., and Hobbs, R.J., 1996. Mediterranean-type ecosystems: the influence of biodiversity on their functioning. In Functional Roles of Biodiversity: a Global Perspective, Mooney, H.A., Cushman, J.H., Medina, E., Sala, O.E., and Schulze, E-D. (eds). John Wiley and Sons Ltd., pp. 151-183.

de Jong, S.M., 1994. Derivation of vegetative variables from a Landsat TM image for modelling soil erosion. Earth Surface Processes and Landforms 19, 165-178.

DHI Water and Environment, 2000. MIKE-SHE: Pre- and Post-processing User Manual.

Eckhardt, K., Breuer, L., and Frede, H.-G., 2003. Parameter uncertainty and the significance of simulated land use changes effects. Journal of Hydrology 273, 164-176.

Franklin, J., Woodcock, C.E., and Warbington, R., 2000. Digital vegetation maps of forest lands in California: integrating satellite imagery, GIS modeling, and field data in support of resource management. Photogrammetric Engineering and Remote Sensing 66, 1209-1217.

Freer J, and Beven K. 1996. Bayesian estimation of uncertainty in runoff prediction and the value of data: an application of the GLUE approach. Water Resources Research 32, 2161-2173.

Gamon, J.A., Field, C.B., Goulden, M.L., Griffin, K.L., Hartley, A.E., Joel, and G., Penuelas, J., Valentini, R., 1995. Relationships between NDVI, canopy structure, and photosynthesis in three Californian vegetation types. Ecological Applications 5, 28-41.

Hargreaves G.H., and Samani, Z.A., 1985. Reference crop evapotranspiration from temperature. Applied Engineering in Agriculture 1, 96-99.

Hill, J., Megier, J., and Mehl, W., 1995. Land degradation, soil erosion and desertification monitoring in Mediterranean ecosystems. Remote Sensing Reviews 12, 107-130.

Hoff, C., Bachelet, D., Rambal, S., Joffre, R., and Lacaze, B., 1995. Simulating leaf area index of Mediterranean evergreen oak ecosystems: comparison with remotely sensed estimation. In: Proceedings of the International Colloquium Photosynthesis and Remote Sensing, Montpellier, France, 28-30 August 1995, pp. 313-321.

Hornberger, G.M., Spear, R.C., 1981. An approach to the preliminary analysis of environmental systems. Journal of Environmental Management 12, 7-18.

Hoyt, W.G., and Troxell, H.C., 1932. Forests and streamflow. Proceedings of the American Society of Civil Engineers 58, 1037-1066.

Keeley, J.E., Fotheringham, C.J., and Morias, M., 1999, Reexamining fire suppression impacts on brushland fire regimes. Science 284, 1829-1832.

Keeley, J.E., 2002, Fire management of California shrubland landscapes. Environmental Management 29, 395-408.

Kristensen, K.J., and Jensen, S.E., 1975. A model for estimating actual evapotranspiration from potential evapotranspiration. Nordic Hydrology 6, 170-188.

Lavabre, J., Sempere-Torres, D., and Cernesson, F., 1993. Changes in the hydrological response of a small Mediterranean basin a year after a wildfire. Journal of Hydrology 142, 273-299.

Loaiciga, H.A., Pedreros, D., and Roberts, D., 2001. Wildfire-streamflow interactions in a chaparral watershed. Advances in Environmental Research 5, 295-305.

Mackay, D.S. and Band, L.E., 1997. Forest ecosystem processes at the watershed scale: dynamic coupling of distributed hydrology and canopy growth. Hydrological Processes 70, 1197-1217

Madsen, H., 2000. Automatic calibration and uncertainty assessment in rainfall-runoff modelling. In: Proceedings Joint Conference on Water Resources Engineering and Water Resources Planning and Management, Minneapolis, USA, 30 July – 2 August.

Makino, H., McKenna, S.A., and Wakasugi, K., 2001. Sensitivity analysis of Monte Carlo simulation results using the Kolomogorov-Smirnov d statistic. In: Proceedings International Association of Mathematical Geology, Cancun, Mexico, 6-12 September.

Mittermeier, R.A., Meyers, N., Thomsen, J.B., da Fonseca, G.A.B., and Olivieri, S., 1998. Biodiversity hotspots and major tropical wilderness areas: approaches to setting conservation priorities. Conservation Biology 12, 516-520.

Moreno, J.M., and Oechel, W.C., 1995. Global change and Mediterranean-type Ecosystems. Springer-Verlag: New York.

O'Hare, J.P., and Hallock, B.G., 1988. Soil Survey of the Los Padres National Forest Area, California. United States Department of Agriculture, Forest Service and Soil Conservation Service: University of California, 148 p.

Poole, D.K., Roberts, S.W., and Miller, P.C. 1981. Water utilization. In: Miller, P.C. (Ed), Resource use by chaparral and matorral: a comparison of vegetation function in two Mediterranean-type ecosystems. Ecological Studies No. 39. Springer-Verlag: Berlin, pp. 123-149.

Ratto, M., Tarantola, S., and Saltelli, A., 2001. Sensitivity analysis in model calibration: GSA-GLUE approach. Computer Physics Communications 136, 212-224.

Refsgaard, J.C., and Storm, B., 1995. MIKE-SHE. In: Singh VP (Ed). Computer Models of Watershed Hydrology. Water Resources Publications, Colorado, USA, pp. 809-846.

Riggan, P.J., Goode, S., Jacks, P.M., and Lockwood, R.N., 1988. Interaction of fire and community development in chaparral of southern California (USA). Ecological Monographs 58, 155-176.

Rundel, P.W., and Parsons, D.J., 1979. Structural changes in chamise, *Adenostoma fasciculatum*, along a fire-induced age-gradient. Journal of Range Management 32, 462-466.

Ryan, K.C., 1991. Vegetation and wildland fire: implications of global climate change. Environment International 17, 169-178.

Sandholt, I., Andersen, J., Dybkjær, G., Lo, M., Rasmussen, K., Refsgaard, J.C., and Høgh-Jensen, K., 1999. Use of remote sensing data in distributed hydrological models: applications in the Senegal River basin. Danish Journal of Geography 99, 47-57.

Schlesinger, W.H., and Gill, D.S., 1980. Biomass, production, and changes in the availability of light, water, and nutrients during the development of pure stands of the chaparral shrub, *Ceanothus megacarpus*, after fire. Ecology 61, 781-789.

Scott, D.F., 1993. The hydrological effects of fire in South African mountain catchments. Journal of Hydrology 150, 409-432.

Spear, R.C., and Hornberger, G.M., 1980. Eutrophication of the Peel Inlet, II, identification of critical uncertainties via generalized sensitivity analysis. Water Resources 14, 43-49.

Spear, R.C., 1997. Large simulation models: calibration, uniqueness and goodness of fit. Environmental Modelling and Software 12, 219-228.

Stephenson, J.R., and Calcarone, G.M., 1999. Southern California mountains and foothills assessment: habitat and species conservation issues. General Technical Report GTR-PSW-172, Pacific Southwest Research Station, Forest Service, U.S. Department of Agriculture.

Turner, D.P., Cohen, W.B., Kennedy. R.E., Fassnacht, K.S., and Briggs, J.M., 1999. Relationships between leaf area index and Landsat TM spectral vegetation indices across three temperate zone sites. Remote Sensing of the Environment 70, 52-68.

Vachaud, G., and Chen, T., 2002. Sensitivity of a large-scale hydrologic model to quality of input data obtained at different scales: distributed versus stochastic non-distributed modelling. Journal of Hydrology 264, 101-112.

Vasquez, R.F., Feyen, L., Feyen, J., and Refsgaard, J.C., 2002. Effect of grid size on effective parameters and model performance of the MIKE-SHE code. Hydrological Processes16, 355-372.

Vazquez, R.F., and Feyen, J., 2003. Effect of potential evapotranspiration estimates on effective parameters and performance of MIKE SHE-code applied to a medium-size catchment. Journal of Hydrology 270, 309-327.

Verstraete, M.M., and Schwartz, S.A., 1991. Desertification and global change. Vegetatio 91, 3-13.

Wade, A.J., Hornberger, G.M., Whitehead, P.G., Jarive, H.P., and Flynn, N., 2001. On modeling the mechanisms that control in-stream phosphorus, macrophyte, and epiphyte dynamics: an assessment of a new model using generalized sensitivity analysis. Water Resources Research 37, 2777-2792.

Watson, F.G.R., Vertessy, R.A., and Grayson, R.B., 1999. Large scale modelling of forest hydrological processes and their long term effect on water yield. Hydrological Processes 13, 689-700.

Xevi, E., Christiaens, K., Espino, A., Sewnandan, W., Mallants, D., Sorensen, H., and Feyen, J., 1997. Calibration, validation and sensitivity analysis of the MIKE-SHE model using Neuenkirchen catchment as case study. Water Resources Management 11, 219-242.

Zak, S.K., and Beven, K.J., 1999. Equifinality, sensitivity and predictive uncertainty in the estimation of critical loads. The Science of the Total Environment 236, 191-214.

TABLES

Table 3-1. Parameters and associated ranges used in the GSA sensitivity analysis.

Parameter*	Minimum value	Maximum value
Vegetation		
C_1	0.01	1
C_2	0.01	1
C_3 (mm day^{-1})	1	60
Interflow/Groundwater reservoirs		
IF_t (m)	0.0001	0.3
IF_h (days)	0.0001	3
IF_v (days)	0.0001	80
GW_h (days)	0.05	100
Soil		
K_s_Sandy Loam (m s^{-1})	$1.0x10^{-6}$	$5.0x10^{-4}$
n_Sandy Loam	1	30
K_s_Loam (m s^{-1})	$1.0x10^{-6}$	$5.0x10^{-4}$
n_Loam	1	30

* Parameter definitions: (a) *Vegetation*: C1, C2, and C3 (see Section 2.1); (b) *Interflow (IF) / Groundwater (GW) reservoirs*: IF_t (storage threshold), IF_h (horizontal time constant), IF_v (vertical time constant), and GW_h (horizontal time constant);(c) *Soil*: K_s (saturated hydraulic conductivity), and n (exponential coefficient). Please see Appendix B for more a more detailed explanation of each parameter.

Table 3-2. Number of behavioral parameter sets for each LAI scenario – by period and performance measure.

Period One	**No. sets E ≥ 0.80**	**No. sets lnE ≥ 0.80**	***Period Two***	**No. sets E ≥ 0.80**	**No. sets lnE ≥ 0.80**
Minimum LAI	95	15	*Minimum LAI*	1	0
Average LAI	109	16	*Average LAI*	4	0
Maximum LAI	95	22	*Maximum LAI*	7	0
TOTAL	299	53	TOTAL	12	0

Table 3-3. Values of the d-statistic and *p*-value for each model parameter in Period One – by LAI scenario.

PERIOD ONE				
E ≥ 0.80				
Parameter		***Minimum LAI****	***Average LAI****	***Maximum LAI****
C_1	*d*	**0.251**	0.134	0.122
	p	**0.000**	0.055	0.146
C_2	*d*	**0.257**	**0.280**	**0.278**
	p	**0.000**	**0.000**	**0.000**
C_3	*d*	0.094	0.121	0.074
	p	0.421	0.109	0.718
IF_t	*d*	**0.504**	**0.538**	**0.570**
	p	**0.000**	**0.000**	**0.000**
IF_h	*d*	**0.285**	**0.305**	**0.286**
	p	**0.000**	**0.000**	**0.000**
IF_v	*d*	**0.185**	**0.163**	0.169
	p	**0.005**	**0.010**	0.013
GW_h	*d*	0.075	0.106	0.099
	p	0.696	0.212	0.353
n_Loam	*d*	0.077	0.090	0.064
	p	0.664	0.393	0.863
K_s_Loam	*d*	0.123	0.091	0.092
	p	0.136	0.376	0.443
n_Sandy Loam	*d*	**0.226**	**0.221**	**0.252**
	p	**0.000**	**0.000**	**0.000**
K_s_Sandy Loam	*d*	**0.222**	0.101	**0.252**
	p	**0.000**	0.258	**0.000**

*Numbers in 'bold' type indicate highly sensitive parameters.

Table 3-4. Number of behavioral parameter sets for each LAI scenario in Period One – by performance measure.

Period One	**No. sets E ≥ 0.80**	**No. sets lnE ≥ 0.65**
Minimum LAI	95	89
Average LAI	109	100
Maximum LAI	95	103
TOTAL	299	292

Table 3-5. Modified lnE: values of the d-statistic and *p*-value for each model parameter in Period One – by LAI scenario.

PERIOD ONE

lnE >= 0.65

Parameter		*Minimum LAI**	*Average LAI**	*Maximum LAI**
C_1	*d*	**0.344**	**0.230**	**0.192**
	p	**0.000**	**0.000**	**0.002**
C_2	*d*	**0.327**	**0.340**	**0.347**
	p	**0.000**	**0.000**	**0.000**
C_3	*d*	0.123	0.115	0.086
	p	0.161	0.174	0.485
IF_t	*d*	**0.348**	**0.357**	**0.370**
	p	**0.000**	**0.000**	**0.000**
IF_h	*d*	0.102	0.104	0.089
	p	0.354	0.269	0.436
IF_v	*d*	**0.275**	**0.341**	**0.290**
	p	**0.000**	**0.000**	**0.000**
GW_h	*d*	**0.427**	**0.547**	**0.511**
	p	**0.000**	**0.000**	**0.000**
n_Loam	*d*	0.084	0.124	0.128
	p	0.598	0.115	0.091
K_s_Loam	*d*	0.120	0.073	0.068
	p	0.179	0.707	0.767
n_Sandy Loam	*d*	**0.203**	0.138	0.122
	p	**0.002**	0.060	0.117
K_s_Sandy Loam	*d*	0.075	**0.588**	0.089
	p	0.743	**0.000**	0.447

*****Numbers in 'bold' type indicate highly sensitive parameters.

FIGURES

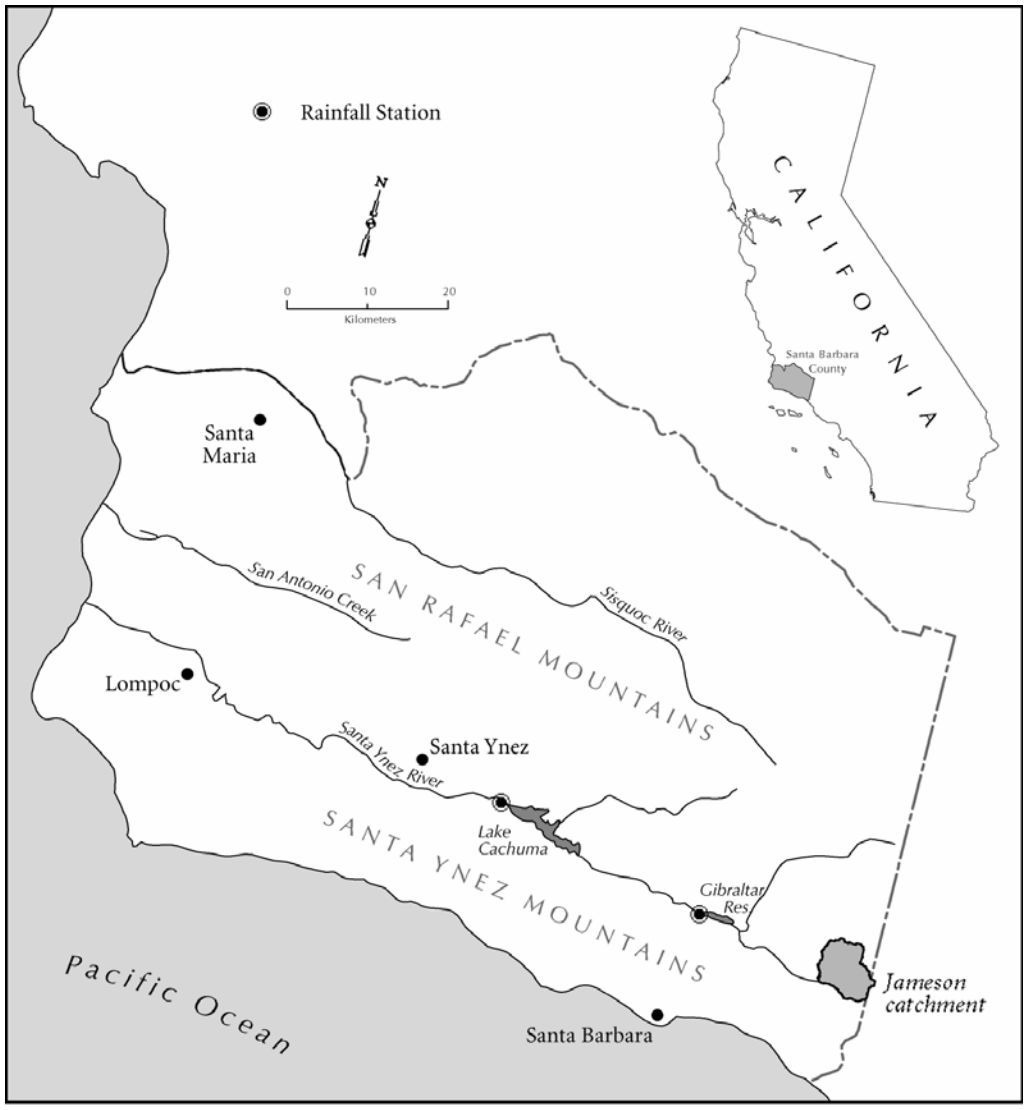

Figure 3-1. The study site – Jameson catchment near Santa Barbara, California.

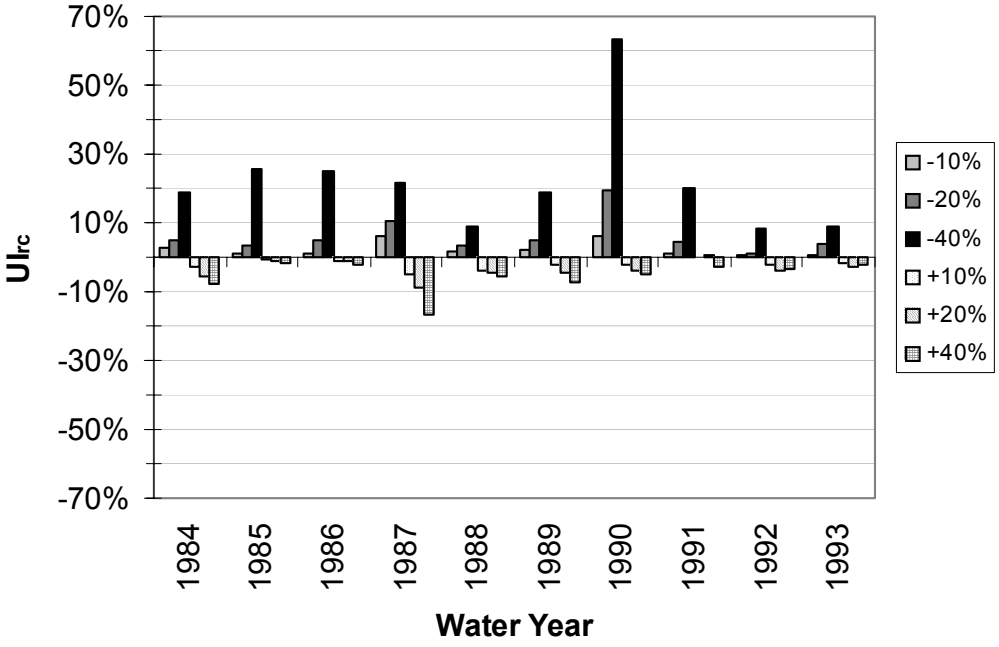

Figure 3-2. Relative changes in predictive uncertainty (UI_{rc}) for each LAI uncertainty scenario over the study period.

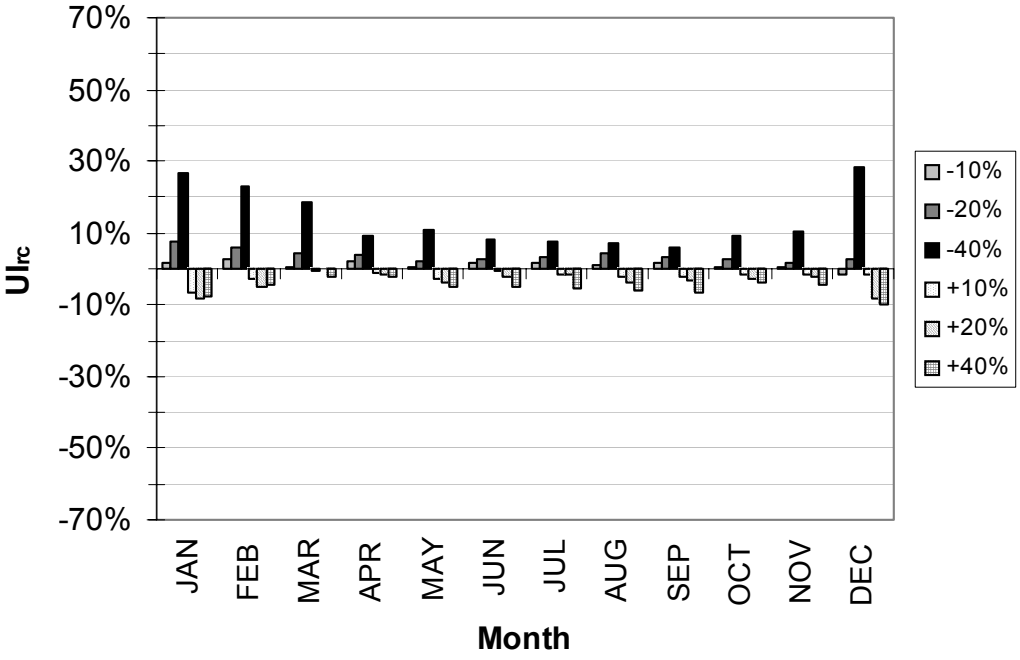

Figure 3-3. Relative changes in predictive uncertainty (UI_{rc}) for each LAI uncertainty scenario over the study period – by month.

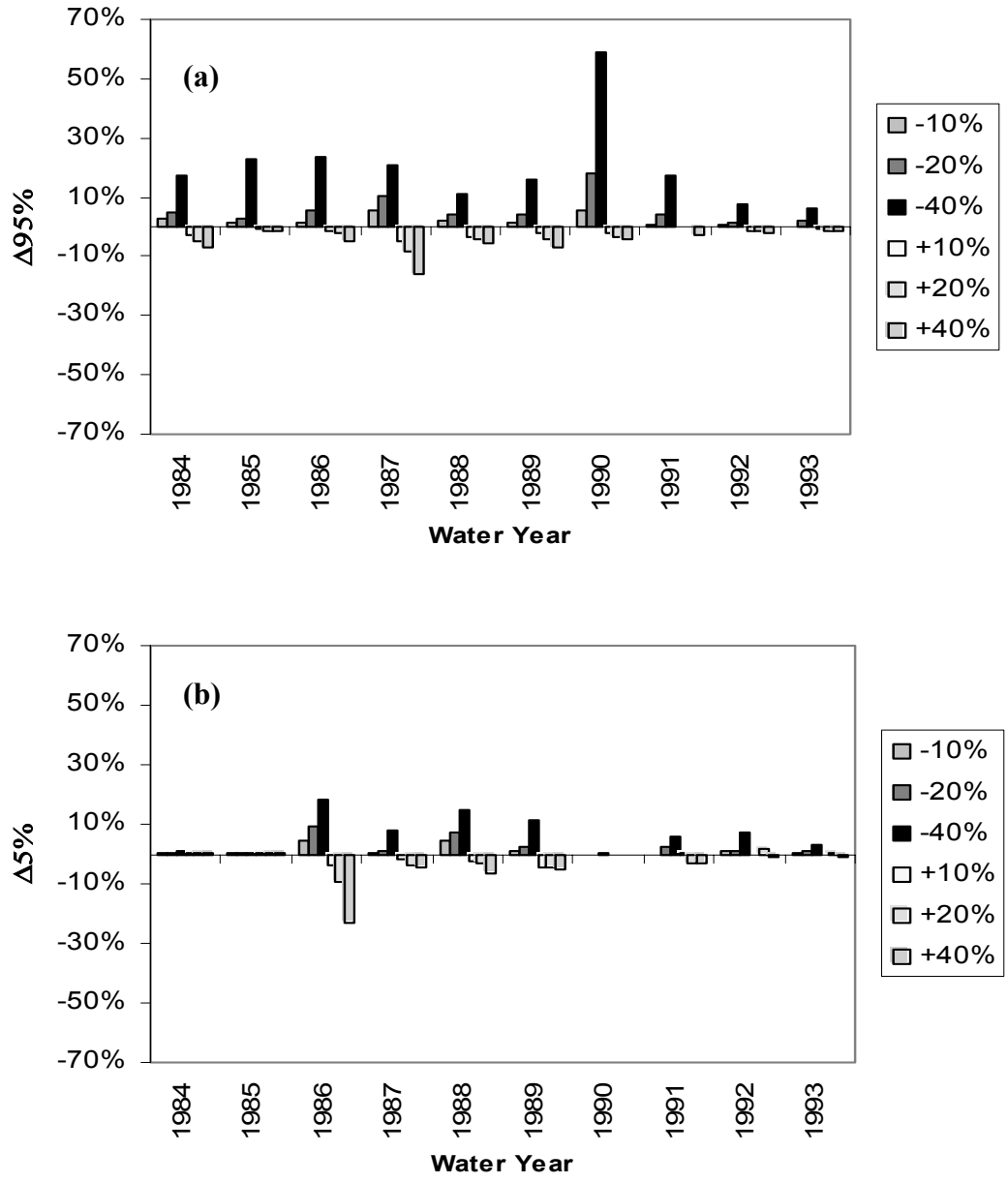

Figure 3-4. Relative changes in predictive uncertainty for each LAI uncertainty scenario over the study period for the (a) 95% and (b) 5% uncertainty bounds (Δ95% and Δ5%, respectively).

CHAPTER FOUR

Modeling the effects of fire size on streamflow in a chaparral watershed

Abstract. Fire is a primary agent of land cover transformation in chaparral-dominated watersheds, however few studies have examined the impacts of fire and post-fire succession on streamflow dynamics in these basins. While it may seem intuitive that larger fires will have a greater impact on streamflow response than smaller fires in chaparral catchments, the actual nature of these relationships has not been determined. The effects of fire size on seasonal and annual streamflow responses were investigated for a medium sized chaparral catchment in central California using a modified version of the MIKE-SHE model (MSHE_m) [which had been previously calibrated and tested for this catchment using the Generalized Likelihood Uncertainty Estimation (GLUE) methodology]. Model simulations were made for two contrasting periods, wet and dry, in order to assess whether fire size effects varied with weather regime. Results indicated that seasonal and annual streamflow response increased nearly linearly with fire size in both periods. The sensitivity of annual streamflow response varied with both annual rainfall conditions and stand age. Moreover, model predictions were largely indistinguishable from the inherent predictive uncertainty associated with the calibrated model - a key finding that highlights the importance of analyzing hydrologic predictions for altered land cover conditions in the context of model

uncertainty. Future work will investigate whether the effect of fire size on streamflow varies with fire location, given that different catchment locations are characterized by different combinations of attributes (e.g., soil type and terrain).

1. Introduction

Fire is a major agent of land surface transformation in California semi-arid shrublands (i.e., chaparral) – a region predicted to be among the most sensitive to global change (Moreno and Oechel 1995). However, little attention has been given to the effects of fire and post-fire succession on streamflow response in this water-limited environment. The need to understand and predict these effects is driven by a variety of issues related to water supply, water quality, ecosystem hydro-ecology, prescribed burning and flood hazard management. Moreover, it is anticipated that future climate change and increasing anthropogenic pressures will alter the current fire regime in this region (Ryan 1991, Moreno and Oechel 1995, Davis and Michaelsen 1995, Lenihan *et al*. 2003) and, subsequently, streamflow dynamics.

Chaparral ecosystems are, by definition, resilient to fire. That is, following fire community structure tends to return to its pre-fire state fairly rapidly (Keeley 1986). However, if the fire return-interval is very short, or fire intensity is too high, rapid shifts in community composition are possible (Zedler *et al*. 1983, Haidinger and Keeley 1993, Zedler 1995). The fire rotation interval in California chaparral shrublands is generally on the order of three to six decades (Keeley *et al*.

1999). Available moisture is very often the dominant factor affecting fuel flammability so fires tend to occur most often during late summer and early fall when fuel moisture has been depleted; large, catastrophic fires occur when dry conditions are coupled with high winds (Moritz 1997). Although fires can typically kill all aboveground biomass, much of the belowground biomass remains intact. Overall vegetation mortality is variable and results from a number of interacting factors including fire intensity, seasonality, elevation, soil moisture, plant size, physiological condition, and life history strategy.

Herbaceous species dominate the immediate post-burn environment, but most generally disappear after three to four years as they are shaded out by the recovering shrubs and trees (Keeley *et al*. 1981, Keeley and Keeley 1981). Evergreen shrub/tree cover tends to reach pre-fire levels within the first decade following fire depending upon species' life history strategies (i.e., resprouting or seedling recruitment) and site characteristics (Horton and Kraebel 1955, Keeley and Keeley 1981). Growth rates for most evergreen species level off after 20-30 years and remain small for the balance of the shrubs' life-span (Horton and Kraebel 1955, Hanes 1971, Black 1987).

Research that has examined the impacts of fire and post-fire succession on streamflow in chaparral and other semi-arid shrubland ecosystems indicates that storm flow dynamics (Hoyt and Troxell 1932, Lavabre *et al*. 1993), summer flows (Hoyt and Troxell 1932), and annual water yields (Hoyt and Troxell 1932, Scott 1993, Lavabre *et al*. 1993) are all modified following fire. Loaiciga *et al*. (2001)

demonstrated that mean annual streamflow in 'fire' years was statistically significantly greater than in 'non-fire' years, and that mean annual streamflow increased by 20-30% in 'fire-impacted' vs. 'non-impacted' years. All of these authors suggest that the modified streamflow patterns they observed following fire were primarily due to the removal of the vegetation cover, and the concomitant reductions in total evapotranspiration. However, extrapolation of these results is constrained by the limited space and/or time scales examined. For example, most of these studies were carried out in *small* experimental catchments that were *completely* (or almost completely) *burned* (Hoyt and Troxell 1932, Scott 1993, Lavabre *et al*. 1993). In contrast, fires in larger chaparral catchments rarely burn the entire landscape, rather a sample of catchment attributes (e.g., vegetation, soil, terrain) is usually treated by a given fire – with larger fires sampling through a greater range of characteristics than smaller fires. Consequently, post-fire streamflow in chaparral catchments is usually impacted by a combination of the newly regenerating area and the unburned portion of the landscape (which itself is a complex mosaic of vegetation types in different stages of recovery and with different fire histories). While it may seem intuitive that larger fires will have a greater impact on streamflow response than smaller fires in these catchments, the actual nature of these relationships has not been determined.

1.1. Research objectives

It is not feasible to conduct the field experiments required to improve our understanding of the effects of fire size on streamflow dynamics at the space (tens to hundreds of square kilometers) and time (seasonal and annual) scales most relevant to water resource managers in this semi-arid environment. Rather, a distributed hydrological modeling approach is required, one capable of representing changes in vegetation patterns following fire and their effects on integrated catchment response. In this study we utilized a modified version of the distributed MIKE-SHE model (Andersen *et al*. 2001) to investigate the impacts of fire size on the seasonal and annual hydrologic responses of a medium-sized chaparral catchment in central California. Model simulations were made for two contrasting periods, wet and dry, in order to assess whether fire size effects varied with weather regime. It is recognized that other factors (e.g., fire location, intensity, frequency and seasonality) may interact with fire size (and with each other) to impact post-fire streamflow dynamics, however examination of these variables is beyond the scope of the current study.

The modified version of MIKE-SHE utilized in this study (MSHE_m) was previously calibrated and tested for the study catchment using the Generalized Likelihood Uncertainty Estimation (GLUE) methodology of Beven and Freer (2001) (Chapter Two). GLUE is a Bayesian Monte Carlo-based approach that recognizes the equifinality of parameter sets, i.e., that multiple parameter sets may provide acceptable model results, and provides a strategy for distributed model

calibration and uncertainty estimation. Implementing GLUE requires making Monte Carlo simulations using a large number of parameter sets, assessing the relative performance of each set by comparing model estimates with observed data, and retaining only those parameter sets that provide behavioral (acceptable) predictions. The suite of behavioral predictions is then used to compute the 5% and 95% uncertainty bounds, i.e., prediction limits, which capture the uncertainty in model predictions arising from uncertainties in model parameterization (Binley and Beven 1992, Beven 2001). It is suggested here that these prediction limits represent the 'inherent predictive uncertainty' associated with using the calibrated MSHE_m model in this catchment, and that it is important to understand how predictions for altered conditions (e.g., due to fire) relate to the inherent uncertainty of the model used to make them. Therefore, an additional objective of this study was to evaluate the effects of fire size on catchment hydrologic response *relative* to the inherent predictive uncertainty of MSHE_m.

2. Methods

Detailed descriptions of the MSHE_m model, the study site and input data can be found in Chapter Two (and Appendix A); therefore, only summaries are provided in the first three sections below. The remaining sections describe the set up and execution of the fire size scenarios, including the random generation of fires, the selection of wet and dry weather regimes, and the approach used to make scenario-based model simulations.

2.1. MSHE_m model

MIKE-SHE is a physically-based, distributed hydrological model capable of representing all major phases of the hydrologic cycle (Refsgaard and Storm 1995). Spatial variation in catchment characteristics is represented using equally sized grid cells, each of which is vertically discretized into a number of sub-layers to represent the soil profile. Following Chapters Two and Three, model grid cell size in this study was fixed at 270 m and model predictions of daily streamflow were aggregated to monthly values. A modified version of the MIKE-SHE model, developed by Andersen *et al*. (2001) for use in catchments with limited data on subsurface processes, was used in this study. The major differences between the original (MIKE-SHE) and modified (MSHE_m) versions of the model are found in the representations of flow in the unsaturated and saturated zones.

2.2. Study site

Jameson is a medium size catchment (34 km^2) located in the mountains just north of Santa Barbara, California, USA (Figure 4-1). This non-urbanized area is dominated by evergreen chaparral shrubs, followed by drought-deciduous sub-shrubs (coastal sage scrub), oak woodland, conifer forest and grassland (Franklin *et al*. 2000). Sandy-loam soils cover the generally rugged terrain. Mean water year (October-September) precipitation and streamflow in this semi-arid region are approximately 780 mm and 233 mm, respectively.

2.3. Input data

Observed daily precipitation and temperature data were obtained for the study period from National Climate Data Center (NCDC) gages in and around the Jameson catchment. Time-varying, spatially distributed inputs of precipitation were estimated by redistributing daily observed (point) values across the catchment based on computed patterns of mean annual precipitation. Together, the temperature data and estimated values of solar radiation were used to predict daily, spatially distributed inputs of potential evapotranspiration via application of the Hargreaves-Samani (1985) model (calibrated for regional conditions). Existing digital maps were used to characterize spatially varying vegetation, soil, and topographic units within the catchment. The average LAI recovery trajectory described in Chapter Two was used to represent post-fire LAI dynamics in this study. As discussed in Chapter Two, this sequence does not represent intra-annual variation in LAI, with the exception of the first four years after fire when growing season LAI is augmented to account for the presence of herbaceous vegetation (Keeley *et al*. 1981).

2.4. Fire size scenarios

Approximately 85% of the Jameson catchment is covered by chaparral (75%) and coastal sage scrub (10%) vegetation types. Given the predominance of shrub vegetation in this catchment, and the propensity of fires in this region to favor shrub-covered hillslopes over wooded riparian areas, model simulations were

made for five different fire sizes ranging from 0% to 100% of the shrub-covered catchment area. Specifically, each fire size scenario corresponded to 0% (No Fire), 25%, (Small Fire), 50% (Medium Fire), 75% (Large Fire), and 100% (Total Fire) of the shrub-covered area, which translated into 0%, 21%, 43%, 64% and 85% of the total catchment area, respectively (Table 1).

A rule-based program was written in MATLAB to generate fire 'shapes' of different sizes located randomly in the Jameson catchment. It should be noted that this program does not model fire spread dynamics; instead, the algorithm creates a user-specified number of shapes for each fire size. A few simple rules govern the selection of grid cells included in each fire shape. First, a cell must fall within the defined catchment boundary. Second, only cells designated 'chaparral' or 'coastal sage scrub' may be selected. Subject to these rules, a fire shape is created via the following steps. Initially, a 'seed' cell is randomly selected from all available grid cells and its location is recorded in a log file. The second cell to be included in the shape is then randomly selected from among the eight neighboring grid cells and, providing it meets the criteria, its location is recorded in the log file. Based upon the specified fire size, additional cells are randomly selected, one at a time, for inclusion in the fire shape provided they: a) are adjacent to an existing shape cell, b) meet all of the abovementioned criteria, and c) have not been previously selected (this is determined by having the program examine the log file before adding new cells to the existing shape).

The fire shape program was used in this study to generate 30 fire shapes for each of the three intermediate fire sizes, i.e., small, medium and large – each shape being randomly located in the catchment; one shape from each group was randomly selected for use in model simulations. Fire shapes for the No Fire and Total Fire scenarios (one each) were generated manually by selecting either none or all of the shrub-covered grid cells in the catchment, respectively. Each of the five fire shapes was converted into MSHE_m format using customized ARC/INFO scripts and ARCVIEW extension files and used to 'burn' the corresponding grid cells in the Jameson catchment prior to each scenario-based simulation.

2.5. Weather regimes

Dry and wet weather regimes were selected by examining five-year trends in water year (October-September) rainfall totals for the period 1961- 1981 (the calibration period from Chapter Two). Observed daily rainfall values for the driest and wettest (non-overlapping) five-year periods were used in model simulations. The five-year rainfall total for the 1965-1969 wet regime (5071 mm) was much higher than that for the 1970-1974 dry regime (3353 mm) (Table 2). The mean (standard deviation) water year rainfall was 1014 mm (649 mm) and 670 mm (248 mm) in the wet and dry period, respectively. A five year 'sampling' period was used in this research based on the assumption that, given the rapid recovery of chaparral in the first five years following fire (Chapter One), fire size effects would be greatest and most different within this time frame.

2.6. Model simulations

The GLUE-based calibration of MSHE_m in the Jameson catchment yielded 109 behavioral parameter sets for the period October 1961 – September 1981 (Chapter Two). These parameter sets were used in the present study to make five sets of model simulations for each weather regime (for a total of 1090 runs), one for the baseline No Fire scenario and one each for the Small Fire, Medium Fire, Large Fire and Total Fire scenarios. Prior to running the simulations, two additional water years were added to the beginning of each period in order to allow model storages to 'spin up' prior to 'burning' the catchment; these additional years were excluded from subsequent analyses. The 5% and 95% uncertainty bounds were calculated for each group of 109 model predictions using the GLUEWIN software package (Ratto *et al*. 2001). The 90% uncertainty interval was computed for each fire size scenario (in each weather regime) as the difference between the 95% and 5% uncertainty bounds.

The effects of fire size on seasonal and annual streamflow were assessed by comparing median flow responses between the baseline case and the remaining fire size scenarios, both within and between weather regimes; median flow was calculated as the midpoint of the corresponding 90% uncertainty interval. The inherent predictive uncertainty (IPU) of MSHE_m was represented using the 90% predictive uncertainty interval from those portions of the calibration period in Chapter Two (1961-1981) that corresponded to the wet (1970-1974) and dry (1965-1969) periods used in this study. Median flows for each fire size – weather

regime combination were evaluated relative to the corresponding IPU interval; predicted values falling *outside of* the IPU interval were regarded as more 'reliable' than those valued found *within* the IPU interval. That is, model predictions greater than the 95% inherent uncertainty bound were considered indicative of periods when fire-induced alterations in shrub cover resulted in flow estimates that were most distinguishable from the inherent predictive uncertainty associated with the use of MSHE_m in the Jameson catchment.

3. Results and discussion

3.1. Effects of fire size on streamflow

3.1.1. Cumulative flow

Trends in cumulative median flow were similar for all fire size scenarios within each period, with more total flow predicted as fire size increased (Figure 4-2). Differences in cumulative median flow between scenarios in a given period were nearly proportional to changes in fire size at every time step. That is, doubling (Small Fire → Medium Fire), tripling (Small Fire → Large Fire) and quadrupling (Small Fire → Total Fire) fire size generated approximately two-, three-, and four-fold increases in cumulative median flow for a given time step. [Hereafter, median flow (Q) is referred to as Q_{med}.] Total cumulative Q_{med} in the dry period was lower than for the wet period for all fire size scenarios (Figure 4-2).

3.1.2. Annual flow

The absolute change in Q_{med} (Q_{ac}) between each fire size scenario (Small Fire (SF), Medium Fire (MF), Large Fire (LF) and Total Fire (TF)) and the baseline case (No Fire (NF)) increased approximately linearly with fire size in each year of the wet and dry periods (Figure 4-3). For a given scenario-baseline pair (e.g., TF-NF), larger values of Q_{ac} were often associated with higher annual rainfall totals in both periods, however the effect of time-since-fire (i.e., stand age) appeared to confound a clear trend with respect to annual rainfall. Values of Q_{ac} in the wet period were smallest for all scenario-baseline pairs in the first and fourth water years following fire (the two driest years in the period), yet the largest values of Q_{ac} were not seen in the wettest year (the fifth water year following fire) (Figure 4-3a). In fact, values of Q_{ac} in the wet period were greatest, and nearly equal, for all scenario-baseline pairs in second and third water years following fire (two years with quite different rainfall totals). The smallest and largest values of Q_{ac} for each scenario-baseline pair in the dry period (Figure 4-3b) were found in the first (very dry) and the fourth (very wet) post-fire water years, respectively. On the other hand, very different values of Q_{ac} were observed in the second and fifth water years following fire, despite similar values of annual rainfall. Finally, it is important to note that the small values of Q_{ac} in the first post-fire water year in each period may be a consequence of over-estimating model inputs related to vegetation re-growth (i.e., LAI) for this year.

To better understand the effect of stand age on the relationship between fire size and Q_{med}, each Q_{ac} value in Figure 4-3 was divided by the corresponding annual rainfall total; Figure 4-4 shows the result of this calculation (i.e., normalization) for the wet and dry periods. Examination of Figure 4-4 reveals that 'normalized' annual streamflow peaked for all scenario-baseline pairs in the second and third post-fire years in the wet and dry period, respectively. Values of the normalized response in both periods were generally less than 10% by the fifth year following fire.

3.1.3. Seasonal flow

The relative change in Q_{med} between a fire size scenario and the baseline (No Fire) case was calculated for each month as: $Q_{rc} = (Q_{med}(\text{Scenario}) - Q_{med}(\text{No Fire})) / Q_{med}(\text{No Fire})$. Positive (negative) values indicated an increase (decrease) in Q_{rc} resulting from a change in fire size relative to the baseline case. Values of Q_{rc} for each fire size scenario were largest in the early part of the wet season (November-April), declining into the transition (May-June) and dry (July-October) seasons for both periods (Figure 4-5). Q_{rc} values in the wet period increased steadily with fire size over all months and were nearly proportional to changes in fire size in six of the twelve months (October, November, December, January, March and April) (Figure 4-5a); similar seasonal trends were observed for Q_{ac} (results are not shown). The month with the largest values of Q_{rc} across all fire size scenarios in the dry period was December, one month later than that observed in the wet

period. Values of Q_{rc} were nearly proportional to changes in fire size in four of the twelve months (December, January, March and September) in the dry period (Figure 4-5b); similar seasonal trends were observed for Q_{ac} (results are not shown).

3.2. Inherent model uncertainty

Only 29 of the 300 Q_{med} values (5 years * 12 months * 5 fire sizes), or 10%, fell outside of the IPU interval in the wet period, i.e., were considered 'reliable' (Figure 4-6a); all values of Q_{med} associated with the No Fire and Small Fire scenarios fell within the IPU interval. The largest number of reliable Q_{med} values (14) was found in the driest year in this period (1968), the greatest proportion of which was associated with the Total Fire size (8). In the dry period, forty-nine of the 300 Q_{med} values (16%) fell outside of the IPU interval and were regarded as reliable predictions (Figure 4-6b). Reliable Q_{med} predictions were observed concurrently for all fire size scenarios (except No Fire) in only six months of this period; all values of Q_{med} associated with the No Fire scenario in this period fell within the IPU interval.

Reliable predictions of Q_{med} in wet season months within the wet period were often, but not always, associated with high rainfall totals. With the exception of 1968, no Q_{med} values fell outside of the IPU interval in transition and dry season months in the wet period. Reliable values of Q_{med} in the dry period were generally concentrated in wet season months, although they occurred in nine of 12 months in

1972 (the driest year). Overall, the Total Fire size scenario was associated with the highest number of reliable Q_{med} values, followed by the Large and Medium Fire size scenarios.

3.3. Discussion

Results from this study are in agreement with previous research that demonstrated increases in seasonal and annual flows following fire in chaparral-dominated catchments (Hoyt and Troxell 1932, Loaiciga *et al*. 2001). As expected, total Q_{med} increased with fire size in both the wet and dry periods (Figure 4-2), i.e., larger fires produced more streamflow than smaller fires. Absolute changes in Q_{med} (Q_{ac}) were generally proportional to changes in fire size for a given month or annual time step. However, this proportionality was not constant *between* time steps, but varied with monthly and annual rainfall conditions. For example, annual Q_{med} increased approximately 10 mm for every 25% increase in fire size in 1965 (597 mm precipitation), while it increased nearly 60 mm for every 25% increase in fire size in 1966 (810 mm precipitation). Mean annual streamflow increased approximately 38 mm per 25% change in fire size in both periods, though this represented a much larger relative increase in flow in the dry period (22%) than in the wet period (9%). This value is somewhat larger than that reported by Bosch and Hewlett (1982) who, summarizing information from 94 paired-catchment studies around the world, found a 10 mm change in annual water yield for each

10% change in shrub cover. Nevertheless, the similarity in these two values provides a measure of confidence in the realism of our simulation results.

Absolute changes in Q_{med} (Q_{ac}) for each scenario-baseline pair increased with fire size in a near linear fashion under both weather regimes (Figure 4-3) [recall that Q_{ac} values in the first post-fire year may be artificially low due to over-estimating input LAI values immediately following fire]. Note that the range of Q_{ac} values for each fire size scenario under the wet regime is comparable to that observed in the dry regime, despite the variability in annual rainfall totals between periods. This finding helps explain why the average annual change in Q_{med} with increasing fire size was approximately the same in both periods (i.e., 38 mm for each 25% increase in fire size).

Values of Q_{ac} for a given scenario-baseline pair were also shown to vary with annual rainfall condition and stand age. For example, the largest values of Q_{ac} in the wet period were not found in the wettest year (1969), but in two years with quite different rainfall totals (1966 and 1967). A possible explanation for this result may be related to observed differences in intra-annual rainfall patterns between these two years. Rainfall in the drier year (1966) was concentrated in just a few, large storms early in the wet season, while a greater number of large storms in 1967 were fairly evenly distributed over the wet season. These patterns suggest that if rainfall is concentrated in a few storms, and there is a fire, relatively more of the annual rainfall will become streamflow. In contrast, if rainfall is more evenly distributed, and there is a fire, relatively less of the annual rainfall will be

partitioned into streamflow. Additionally, a larger fraction of incoming rainfall may have been partitioned into evapotranspiration in 1967, compared with 1966, as a result of increased leaf area, potentially reducing predicted flows in the wetter year. The fact that values of Q_{ac} were smaller in 1969 (the wettest year) than in 1966 and 1967 may be a function of higher leaf areas in 1969 (the fifth year following fire) and the fact that, after a certain threshold, the vegetation cannot utilize additional rainfall.

Trends in the normalized annual streamflow response in both periods were generally similar, peaking in the second or third water year following fire and then steadily decreasing through the fifth post-fire year (Figure 4-4). [As previously mentioned, LAI may have been overestimated in the first post-fire year – such that the peak response did not occur in the first year following fire.] The difference in the timing of the peak response between periods may be the result of very different rainfall conditions in the third following fire in each period. The third post-fire year in the dry period experienced very little rainfall (416 mm), compared to the third post-fire year in the wet period (1206 mm). Hence, the value of Q_{ac} in the dry period represented a relatively larger percentage of the corresponding annual rainfall total than in the wet period. Following its peak in each period, the normalized response continued to decline through the fifth post-fire year as the vegetation recovered (i.e., LAI increased).

The relative change in Q_{med} (Q_{rc}) increased with increasing fire size for every month in each period (as did Q_{ac}; results not shown). Values of Q_{rc} were

greatest in wet season months for all fire size scenarios in both periods (Figure 4-5), while Q_{rc} values in transition and dry season months were much lower. This set of results highlights the importance of leaf area in partitioning incoming rainfall into evapotranspiration and streamflow in the wet season, such that burning larger and larger areas of the catchment produces increasingly higher flows in wet months. The relative insensitivity of Q_{rc} to changes in fire size in the transition and dry seasons should be expected since chaparral evapotranspiration rates steadily decline as soil moisture reserves are depleted through the summer and fall months (Poole and Miller 1975, Poole *et al*. 1981).

This research has demonstrated that streamflow response in the Jameson catchment varies with fire size, rainfall condition and stand age. However, evaluating these responses relative to the inherent predictive uncertainty (IPU) of MSHE_m revealed that only a small percentage of modeled flows (Q_{med}) could be considered 'reliable' in either the wet (10%) or dry (16%) periods (Figure 4-6). It was rare for these flows to occur for the Small, Medium, Large and Total fire size scenarios in the same month; in fact, almost all values of Q_{med} associated with the No Fire and Small Fire scenarios fell within the inherent uncertainty of the model (i.e., were uncertain). The majority of reliable Q_{med} estimates occurred in early wet season months in both periods, usually in conjunction with very large storms. The driest year in each period contained the greatest number of reliable Q_{med} predictions, and the only occurrences of reliable Q_{med} values in transition and dry season months. Overall, the greatest proportion of reliable Q_{med} values were

associated with the Total Fire size scenario, followed by the Large Fire, Medium Fire and Small Fire size scenarios. The greater proportion of reliable Q_{med} values in the dry period, and in the driest year in both periods, is likely a function of the smaller inherent uncertainty interval found in drier years and in the dry versus wet period.

4. Conclusions

As expected, modeled (seasonal and annual) streamflow in the Jameson catchment increased with fire size in both the wet and dry periods. The relationship between fire size and streamflow response was approximately linear for all years examined, although the sensitivity of catchment response to fire size varied with annual rainfall condition and stand age. While these results enhance our understanding of the effects of fire size on hydrologic response in chaparral catchments, it is crucial to remember that very few model predictions actually fell outside of the model's inherent uncertainty interval (i.e., were considered reliable). That is, the effects of fire size on streamflow response were usually indistinguishable from the predictive uncertainty associated with MSHE_m. This is a key finding, one which highlights the importance of analyzing hydrologic predictions for altered land cover conditions in the context of model uncertainty.

The inherent uncertainty interval used in this study was itself a function of the many subjective decisions that were made during the GLUE-based calibration of MSHE_m in the Jameson catchment (Chapter Two). For example, the choice of

both the likelihood measure and corresponding threshold value has been shown to influence the number of behavioral parameter sets retained following Monte Carlo simulations which, in turn, directly impacts the calculation of prediction limits (Beven and Binley 1992, Freer and Beven 1996). More recently, research has shown that GLUE-based predictive uncertainty is also affected by the number of free parameters used in calibration (A. Hope, personal communication). Thus, any comparison between model predictions for altered conditions and inherent predictive uncertainty is predicated on the appropriateness of the subjective decisions made during the GLUE-based calibration process. Additional work is needed to examine how different likelihood measures and thresholds, modified parameter ranges, and additional Monte Carlo simulations influence MSHE_m predictive uncertainty and, in turn, our confidence in model predictions of streamflow following different size fires.

Future work should also investigate whether the effect of fire size on streamflow varies with fire location, given that different catchment locations are characterized by different combinations of attributes (e.g., soil type and terrain). Moreover, the interacting effects of annual rainfall and stand age on modeled flows indicate that future work should strive to refine remote sensing-based model inputs of leaf area index to include variability arising from both intra- and inter-annual rainfall dynamics. Finally, while this study examined the effects of fire size on streamflow using median flow values (Q_{med}), each set of Monte Carlo simulations actually produced a range of model predictions for each fire size

scenario, i.e., a 90% uncertainty interval (95%-5% uncertainty bounds). Additional efforts are needed to investigate how the upper (95%) and lower (5%) uncertainty bounds for each scenario vary with both rainfall condition and stand age.

Acknowledgements

Funding for this research was provided in part by a NASA Land Use Land Cover Change Grant (No. NAG5-11141), a NASA Earth System Science Fellowship (No. NGT5-30335), and a NSF Doctoral Dissertation Research Improvement Grant (No. BCS-0000233). The authors would like to thank W. Casey McMichael, Dr. Zachary Bortolot, and Joseph Grubb for assistance with data processing and Harry Johnson for designing the study area map.

References

Andersen, J., Refsgaard, J.C., and Jensen, K.H., 2001. Distributed hydrological modelling of the Senegal River Basin – model construction and validation. Journal of Hydrology 247, 200-214.

Beven, K.J., 2001. Rainfall-Runoff Modelling: the Primer. John Wiley & Sons Ltd., West Sussex, England, 360 pp.

Beven, K., and Binley, A., 1992. The future of distributed models: model calibration and uncertainty prediction. Hydrological Processes 6, 279-298.

Beven, K., and Freer, J., 2001. Equifinality, data assimilation, and uncertainty estimation in mechanistic modelling of complex environmental systems using the GLUE methodology. Journal of Hydrology 249, 11-29.

Black, C.H., 1987. Biomass, nitrogen, and phosphorus accumulation over a Southern California fire chronosequence. In: Plant response to stress – functional analysis in Mediterranean ecosystems. Springer-Verlag, Berlin, pp. 445-58.

Bosch, J.M., and Hewlett, J.D., 1982. A review of catchment experiments to determine the effect of vegetation changes on water yield and evapotranspiration. Journal of Hydrology 55, 3-23.

Davis, F.W., and Michaelsen, J., 1995. Sensitivity of fire regime in chaparral ecosystems to global climate change. In: Oechel, W.C., Moreno, J.M. (Eds), Global Change and Mediterranean-Type Ecosystems. Springer-Verlag, New York, pp. 435-456.

Franklin J., Woodcock, C.E., and Warbington, R., 2000. Digital vegetation maps of forest lands in California: integrating satellite imagery, GIS modeling, and field data in support of resource management. Photogrammetric Engineering and Remote Sensing 66, 1209-1217.

Freer, J., and Beven K., 1996. Bayesian estimation of uncertainty in runoff prediction and the value of data: an application of the GLUE approach. Water Resources Research 32, 2161-2173.

Haidinger, T.L., and Keeley, J.E., 1993. Role of high fire frequency in destruction of mixed chaparral. Madroño 40, 141-147.

Hanes, T. L., 1971. Succession after fire in the chaparral of southern California. Ecological Monographs 41, 27-52.

Hargreaves G.H., and Samani, Z.A., 1985. Reference crop evapotranspiration from temperature. Applied Engineering in Agriculture 1, 96-99.

Horton, J.S., and Kraebel, C.J., 1955. Development of vegetation after fire in the chamise chaparral of southern California. Ecology 36, 244-262.

Hoyt, W.G., and Troxell, H.C., 1932. Forests and streamflow. Proceedings of the American Society of Civil Engineers 58, 1037-1066.

Keeley, J.E., and Keeley, S.C., 1981. Post-fire regeneration of southern California chaparral. American Journal of Botany 68, 524-530.

Keeley, S.C., Keeley, J.E., Hutchinson, S.M., and Johnson, A.W., 1981. Post-fire succession of the herbaceous flora in southern California chaparral. Ecology 62, 1608-1621.

Keeley, J.E., 1986. Resilience of Mediterranean shrub communities to fires. In: Dell, B., Hopkins, A.J.M. (Eds), Resilience in Mediterranean-type ecosystems. Dr. W. Junk Publishers, Dordrecht, Netherlands.

Keeley, J.E., Fotheringham, C.J., and Morias, M., 1999. Reexamining fire suppression impacts on brushland fire regimes. Science 284, 1829-1832.

Lavabre, J., Sempere-Torres, D., and Cernesson, F., 1993. Changes in the hydrological response of a small Mediterranean basin a year after a wildfire. Journal of Hydrology 142, 273-299.

Lenihan, J.M., Drapek, R., Bachelet, D., and Neilson, R.P., 2003. Climate change effects on vegetation distribution, carbon and fire in California. Ecological Applications 13, 1667-1681.

Loaiciga, H.A., Pedreros, and D., Roberts, D., 2001. Wildfire-streamflow interactions in a chaparral catchment. Advances in Environmental Research 5, 295-305.

Moreno, J.M., and Oechel, W.C. (Eds)., 1995. Global change and Mediterranean-type Ecosystems. Springer-Verlag, New York, USA.

Moritz, M., 1997. Analyzing extreme disturbance events: fire in the Los Padres National Forest. Ecological Applications 7, 1252-1262.

Poole, D.K., and Miller, P.C., 1975. Water relations of selected species of chaparral and coastal sage scrub. Ecology 56, 118-1128

Poole, D.K., Roberts, S.W., and Miller, P.C., 1981. Water utilization. In: Miller, P.C. (Ed), Resource use by chaparral and matorral: a comparison of vegetation function in two Mediterranean-type ecosystems. Ecological Studies No. 39. Springer-Verlag: Berlin, pp. 123-149.

Ratto, M., Tarantola, S., and Saltelli, A., 2001. Sensitivity analysis in model calibration: GSA-GLUE approach. Computer Physics Communications 136, 212-224.

Refsgaard, J.C., and Storm, B., 1995. MIKE-SHE. In: Singh VP (Ed). Computer Models of Catchment Hydrology. Water Resources Publications, Colorado, USA, pp. 809- 846.

Ryan, K.C., 1991. Vegetation and wildland fire: implications of global climate change. Environment International 17, 169-178.

Scott, D.F., 1993. The hydrological effects of fire in South African mountain catchments. Journal of Hydrology 150, 409-432.

Zedler, P.H., Gautier, C.R., and McMaster, G.M., 1983. Vegetation change in response to extreme events: the effect of a short interval between fires in California chaparral and coastal scrub. Ecology 64, 809-818.

Zedler, P.H., 1995, Fire frequency in southern California shrublands: biological effects and management options. In: Brushfires in California Wildlands: Ecology and Resource Management, Keeley, J.E., and Scott, T.A. (eds). International Association of Wildland Fire, Fairfield, WA, pp. 101-112.

TABLES

Table 4-1. Key attributes of each of fire shape used in model simulations.

Attribute		*Small Fire*	*Medium Fire*	*Large Fire*	*Total Fire*
Catchment area	[%]	21	43	64	85
Fraction chaparral	[%]	91	87	85	85
Fraction coastal sage scrub	[%]	9	13	15	15
Mean elevation (SD)	[m]	1210 (178)	1236 (225)	1148 (283)	1145 (268)
Mean slope (SD)	[%]	25 (6)	24 (7)	22 (9)	22 (9)
Mean aspect (SD)	[^{0}]	209 (34)	215 (42)	213 (52)	217 (62)

Table 4-2. Water year rainfall totals for the WET (1965-1969) and DRY (1970-1974) periods.

WET Period	**Rainfall [mm]**	**DRY Period**	**Rainfall [mm]**
1965	597	1970	463
1966	810	1971	631
1967	1206	1972	416
1968	410	1973	1132
1969	2048	1974	709
Sum	5071	*Sum*	3353
Average	1014	*Average*	670
Standard Deviation	649	*Standard Deviation*	284

FIGURES

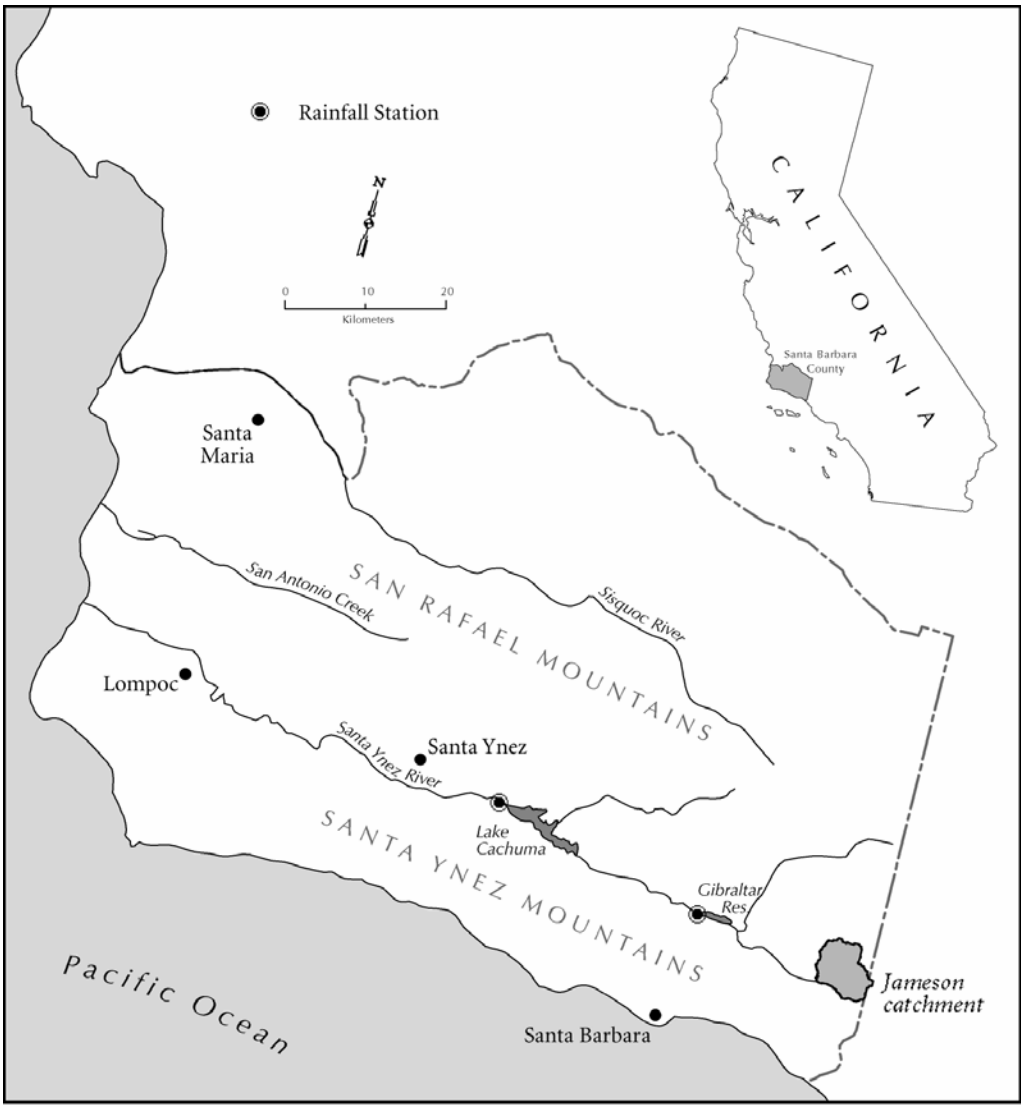

Figure 4-1. The study site - Jameson catchment near Santa Barbara, California.

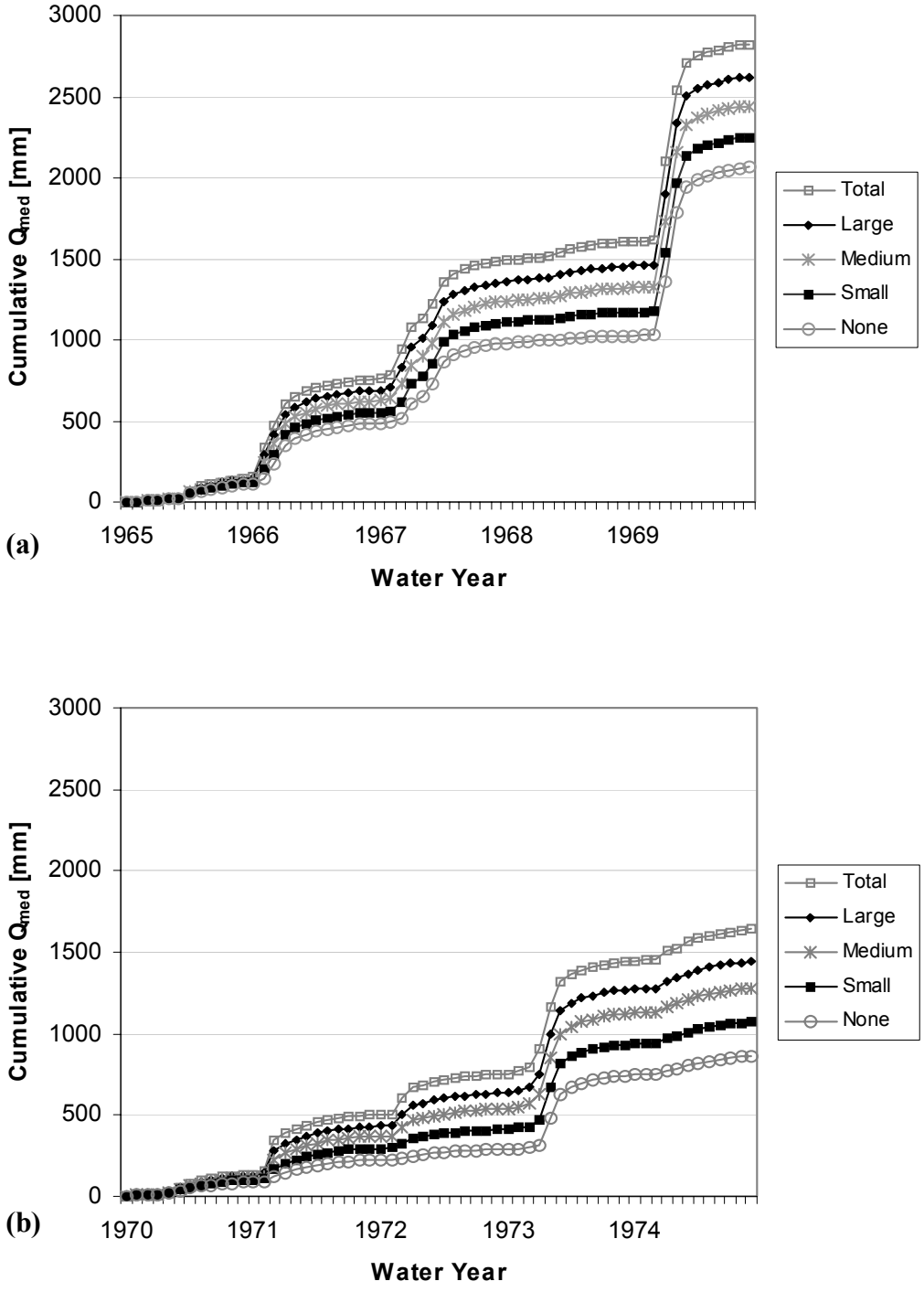

Figure 4-2. Cumulative median flow (Q_{med}) for each fire size scenario for the (a) wet and (b) dry periods.

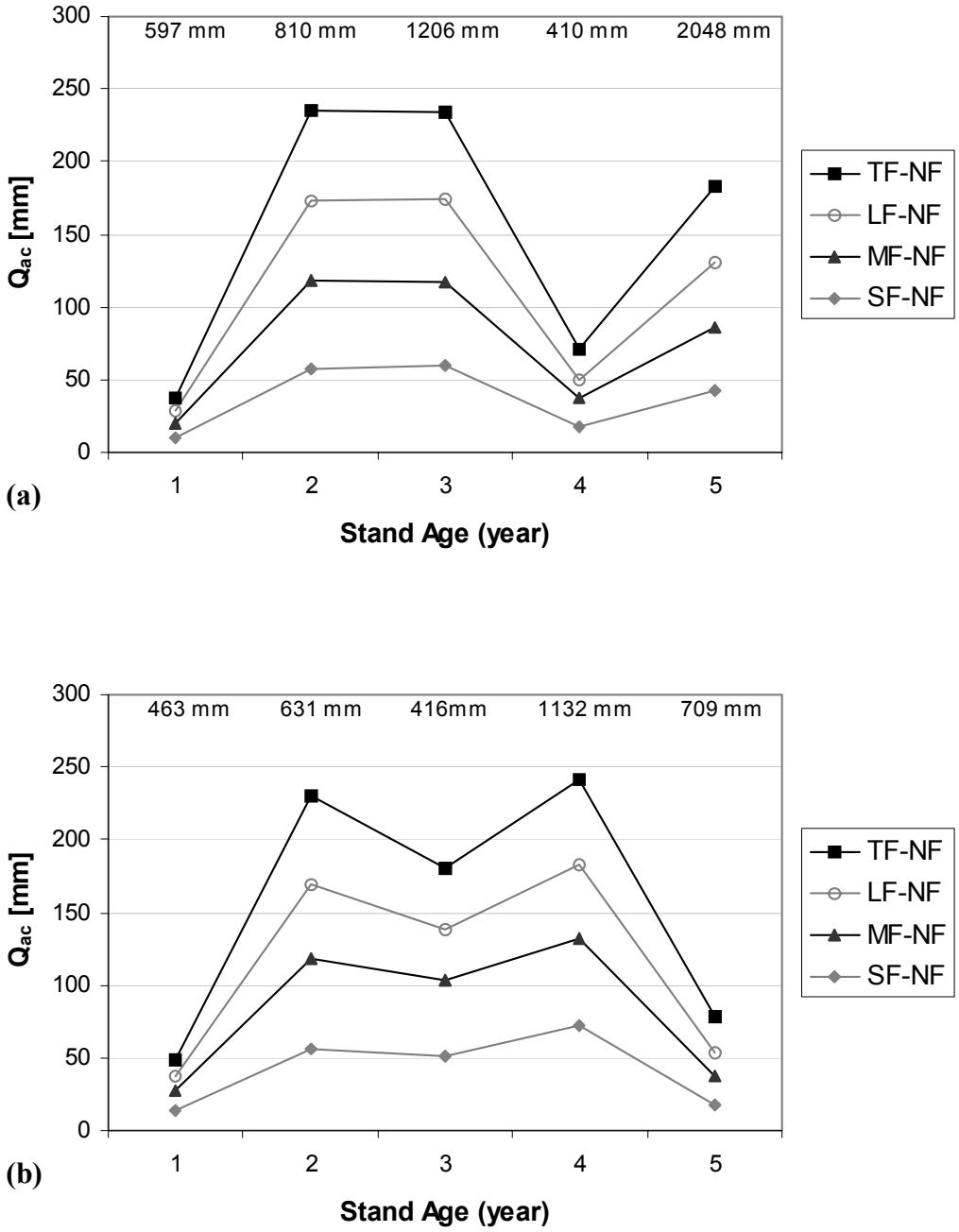

Figure 4-3. Absolute change in median flow (Q_{ac}) for each fire size-baseline pair, by water year, for the (a) wet and (b) dry periods. Total precipitation is shown for each water year at the top of the graph. [NF = No Fire; SF = Small Fire; MF = Medium Fire; LF = Large Fire; TF = Total Fire.]

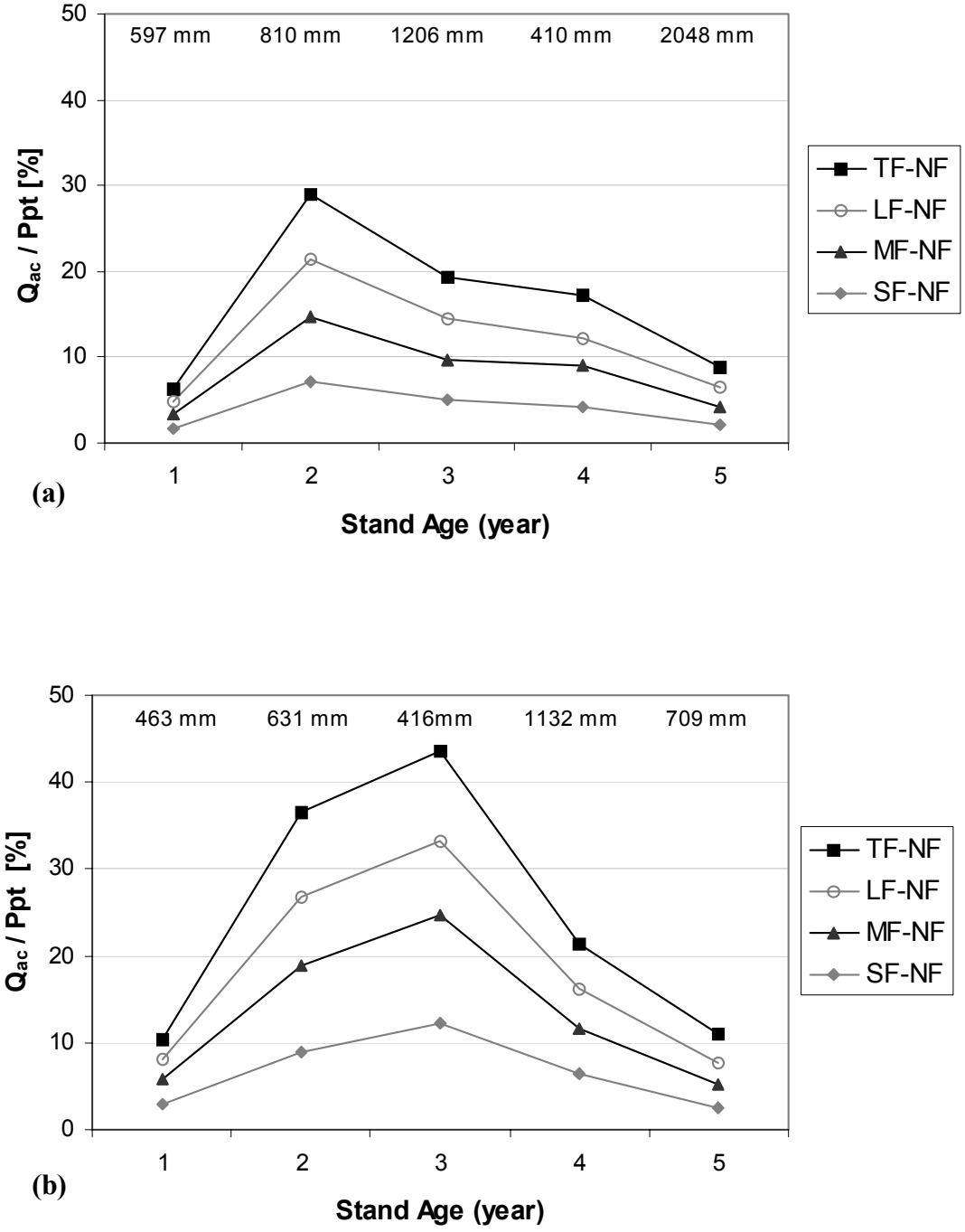

Figure 4-4. 'Normalized' change in median flow (Q_{ac} / Ppt) for each fire size-baseline pair, by water year, for the (a) wet and (b) dry periods. Total precipitation (Ppt) is shown for each year at the top of the graph. [NF = No Fire; SF = Small Fire; MF = Medium Fire; LF = Large Fire; TF = Total Fire.]

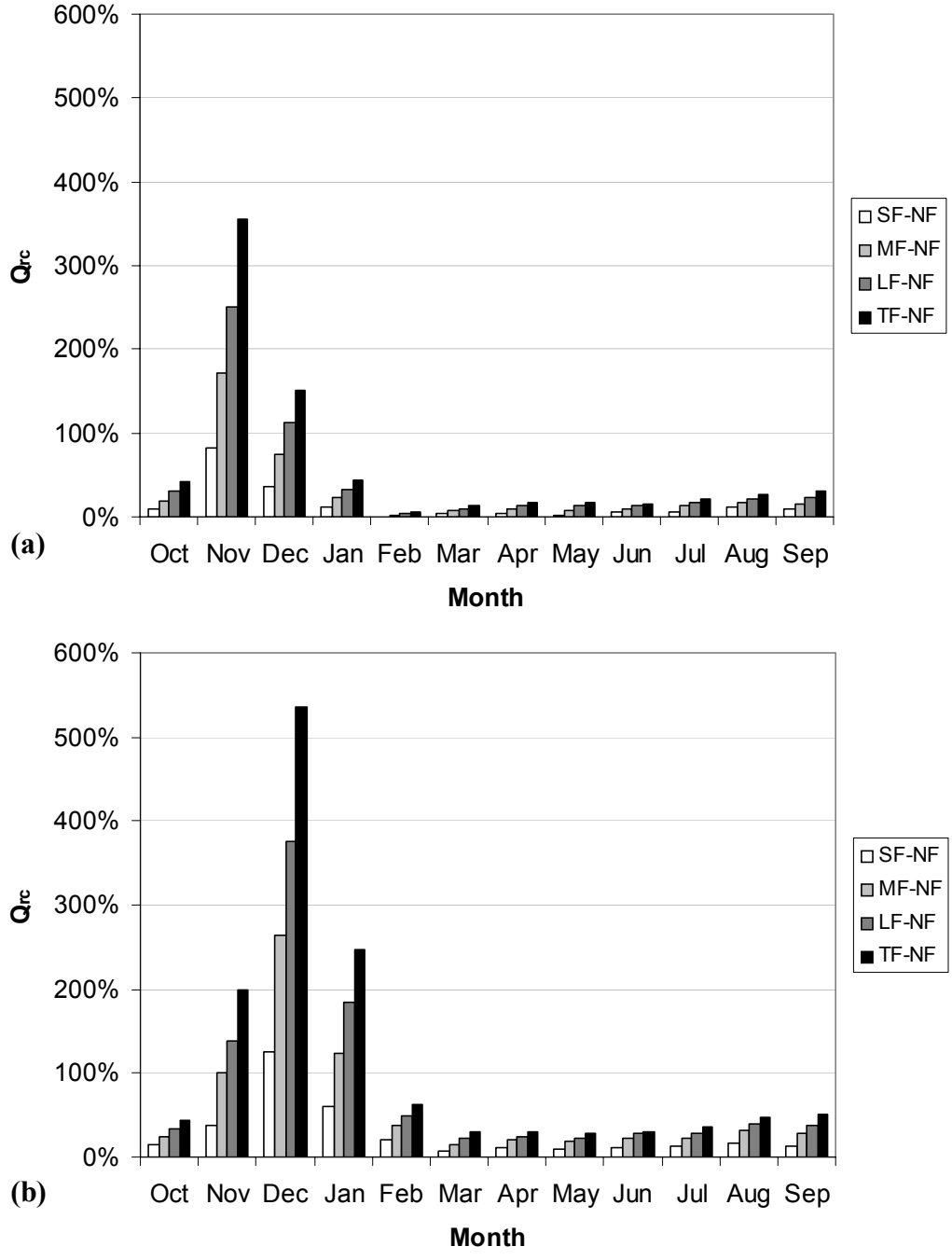

Figure 4-5. Relative change (Q_{rc}) in monthly median flow (Q_{med}) for each fire size-baseline pair (e.g., SF-NF) for the (a) wet and (b) dry periods. [NF = No Fire; SF = Small Fire; MF = Medium Fire; LF = Large Fire; TF = Total Fire.]

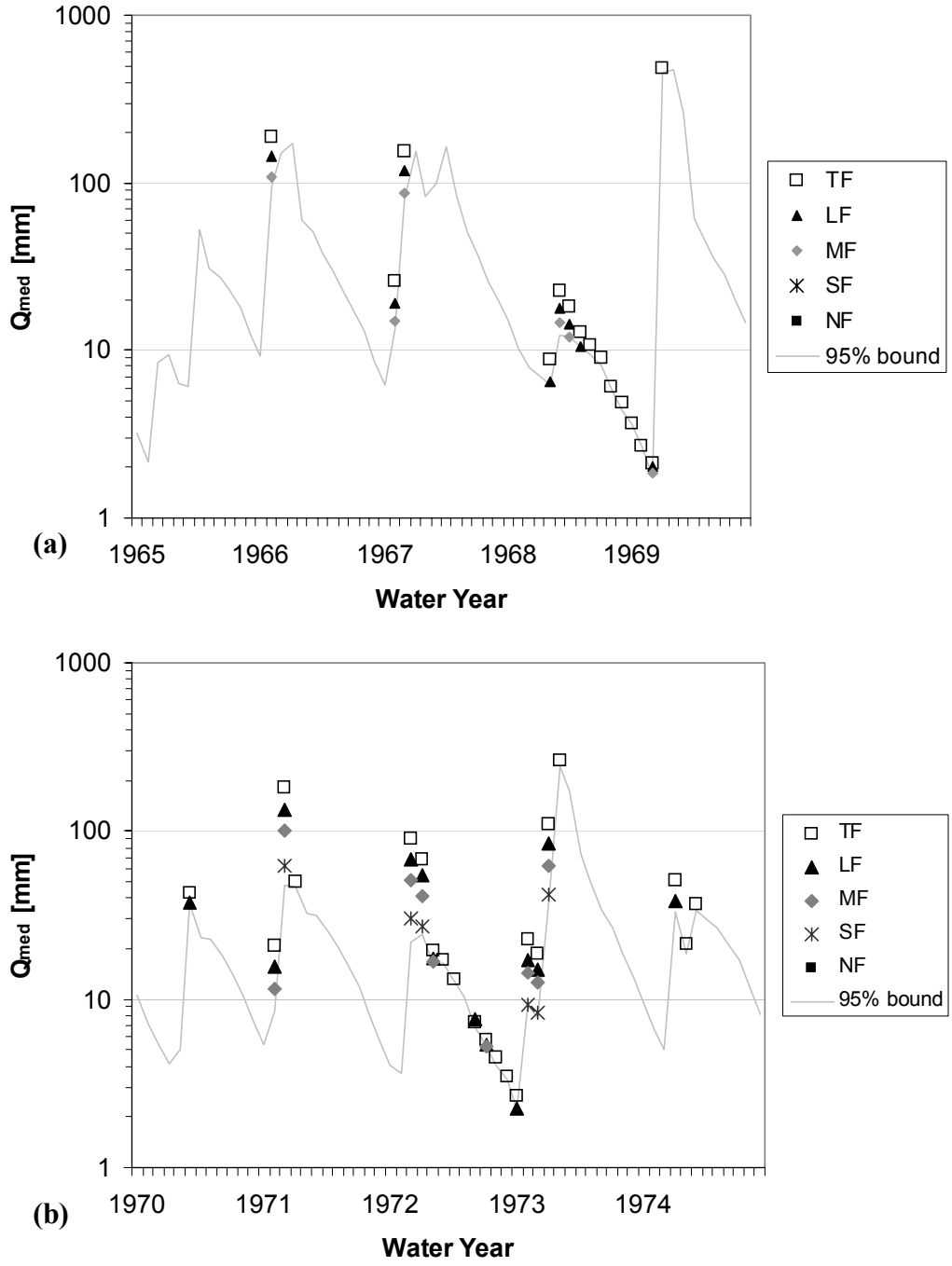

Figure 4-6. 'Reliable' median flow (Q_{med}) predictions for the (a) wet and (b) dry periods – by fire size scenario. Points represent Q_{med} values falling outside of the inherent predictive uncertainty (IPU) interval; line represents the upper (95%) bound of the IPU. Note the y-axis is plotted using a logarithmic scale. [NF = No Fire; SF = Small Fire; MF = Medium Fire; LF = Large Fire; TF = Total Fire.]

CONTRIBUTIONS OF THE DISSERTATION

This dissertation has made important contributions in the fields of chaparral eco-hydrology and distributed hydrological modeling. These contributions are discussed in the corresponding sections below, as are areas for future research.

Chaparral Eco-Hydrology

The remote sensing-chronosequence approach developed in this research provides a reasonable estimate of the post-fire LAI recovery sequence for the chaparral-dominated study area in central California. This sequence represents new information about this ecosystem, and provided key input data for the hydrological modeling component of this study. Additional work is needed to refine this sequence to account for the seasonal development of LAI and the effects of inter-annual rainfall conditions, however it represents an important advance in our understanding of post-fire vegetation re-growth dynamics in California chaparral ecosystems.

The demonstration of a near-linear relationship between fire size and streamflow response in the study watershed contributes new information about chaparral eco-hydrology that is expected to assist forest and watershed scientists in, e.g., planning prescribed burns, managing the water supply, and protecting wildlife habitat. Additional work is needed to better understand the interacting effects of stand age and annual rainfall conditions on this relationship, and to investigate whether the hydrologic effects of fire size vary with fire location –

given that different watershed locations are characterized by different combinations of attributes (e.g., soil, terrain, and fire history).

Distributed Hydrological Modeling

There were number of important 'firsts' in this research associated with the hydrologic modeling component of the study. The use of (a modified version of) the MIKE-SHE model in this research was the first application of a physically-based, spatially distributed hydrological model in chaparral-dominated watersheds. Another 'first' was the coupling of MIKE-SHE with the GLUE methodology for model calibration, testing and uncertainty estimation. Moreover, using the GLUE-based behavioral parameter sets to evaluate how uncertainty in LAI inputs affected model output represents an extension of the GLUE framework in the arena of distributed hydrological modeling. In addition, this study was the first to evaluate model predictions related to land cover modifications (e.g., fire) in the context of 'inherent predictive uncertainty'. It is expected that this comparison, and the related finding that model predictions were generally indistinguishable from the predictive uncertainty of the calibrated model used to make them, will stimulate other modelers to make similar assessments in their own research. Finally, it is hoped that results from this research encourage model developers to incorporate the flexibility to conduct GLUE-based modeling and uncertainty estimation – especially since distributed model predictions are widely used as a basis for environmental decision-making.

APPENDIX A: DATASETS AND DATA PROCESSING

Precipitation

Daily precipitation data were obtained from the National Climate Data Center for two gages in the Gibraltar watershed (Gibraltar and Juncal). These gages were selected on the basis of record length (> 40 years) and completeness (> 95%). The Gibraltar and Juncal precipitation series were quality checked and missing data values were 'patched' using daily precipitation data from neighboring gages maintained by the Santa Barbara County Water Agency. The resulting time series contained complete records of daily precipitation for each gage for the period 1952-1997.

The spatial distribution of daily precipitation is a required MIKE-SHE model input. However, there are only two available gages in the Gibraltar watershed, and both are located at lower elevations along the stream channel. Therefore, an approach was developed to augment the existing gages, and thereby generate the required spatial patterns of precipitation for this basin. This strategy involved two major steps: 1) calculating the ratio of mean annual precipitation between a given site in the basin and an existing gage (i.e. the normal ratio method) and 2) generating a new daily precipitation time series for the selected site by multiplying daily observed precipitation values at the existing gage by this MAP ratio. Implementing this strategy required a digital MAP map of the area and daily precipitation values for each of the existing gages.

A digital map of mean annual precipitation (MAP) was obtained for Santa Barbara County with a grid cell resolution of approximately 0.92 km (J. Michaelsen, personal communication). All mapped MAP grid cells for the Gibraltar watershed were grouped into one of seven classes as a means of delineating the spatial distribution of precipitation in this basin. Classes were created via an equal-value division of the MAP histogram – the mapped range of MAP from 37 cm to 72 cm was subdivided into 5 cm increments. The value of MAP for each class midpoint was assigned as the class MAP value.

The classified MAP map was examined to determine the class association for each of the two existing precipitation gages. A point coverage of the existing gages was overlain on the raster-based MAP map of Gibraltar in ARC/INFO and each gage (point) was assigned to the class of the corresponding grid cell. The MAP for each gage was calculated and compared to that from the MAP map (i.e., the corresponding grid cell). In each case the gage-based value of MAP was somewhat smaller than the map-based MAP (approximately 10% less at Juncal and 7% less at Gibraltar). Reasons for this discrepancy likely relate to the particular method used to calculate MAP in each case. MAP map values were modeled as a function of geographic (e.g., latitude, distance from coast) and topographic attributes (e.g., elevation) and daily precipitation data (November-April) from the period 1961-1990. MAP values for the Gibraltar and Juncal gages were calculated directly from daily precipitation data (October – September) covering the 1952-1997 period. Despite these differences in MAP, the relative

spatial patterns displayed in the MAP map were assumed to be accurate given the expertise involved in creating the map.

MAP ratios were calculated between the class corresponding to the Gibraltar gage and the remaining classes using the class midpoint MAP values. The Gibraltar gage was selected as the 'base station' because it is located at the basin outlet. The observed daily precipitation series at the base station was assigned to the class corresponding to the Gibraltar gage. New daily precipitation time series were generated for the remaining classes by multiplying daily base station values by the appropriate MAP ratio. The accuracy of the resulting precipitation values was evaluated by comparing daily precipitation values recorded at the Juncal gage with those predicted using the MAP ratio method. A plot of predicted versus observed daily precipitation reveals some scatter around the 1:1 line with an R^2 of 0.83). A plot of the residuals (observed – predicted) versus observed values shows a fairly random scatter around the zero line (line of no difference).

MIKE-SHE requires precipitation input in millimeters per hour. Given that only daily precipitation data are available for the Gibraltar watershed, each of the seven precipitation time series were converted from [mm/day] to [mm/hr] by dividing the daily values by 24. This method assumes that precipitation falls uniformly throughout a day – which is generally not the case in this environment. However, as there is no information available on the actual distribution of hourly

precipitation over individual days for this watershed, this assumption holds. The final precipitation inputs for MIKE-SHE comprise a map depicting the spatial arrangement of the seven MAP classes and the seven corresponding time series containing hourly precipitation values for each day of record.

Streamflow

Monthly streamflow data for the Gibraltar watershed (and Jameson Lake sub-watershed) over the period 1960-2000 were transcribed from annual USGS data reports and double-checked for accuracy. Missing data values were patched using monthly streamflow data obtained from the Santa Barbara County Water Agency for the Gibraltar watershed (and Jameson Lake sub-watershed) (J. Ahlroth, personal communication). Scatterplots of precipitation and streamflow were analyzed for accuracy.

Temperature/Potential Evaporation

A long-term daily maximum/minimum temperature dataset was needed for the Gibraltar watershed as input into the Hargreaves-Samani model of potential evaporation (a required MIKE-SHE input). However, the temperature dataset from the only station within the watershed boundary (Gibraltar station) contained a total of 244 values for the 1952-1998 period. Therefore, a simulated temperature time series for the Gibraltar watershed was generated using daily maximum/minimum temperature data from a nearby station (Cachuma Dam) in combination with calculated lapse rates.

Daily minimum, maximum and mean air temperature data [C] for the Cachuma Dam station were obtained for the period 1952-1998. Missing temperature data were patched by developing a linear regression equation between the stations at Cachuma Dam and the Santa Barbara airport. While these two stations are on opposite sides of the Santa Ynez mountains (Cachuma Dam = leeward/valley, airport = windward/coast), the coastal airport station was the only nearby station with a record that was both long and complete enough for use in a regression analysis. Separate regression equations were developed for the minimum and maximum temperature datasets. The resulting R^2 values were 0.67 and 0.44, respectively. These lower than ideal R^2 values are likely the result of differences in microclimate factors between stations (e.g. fog, cold air drainage, winds). However, as the coastal station was the only long-term dataset available for this analysis, and as only one percent of the temperature data were missing, the Cachuma Dam temperature datasets were patched using these regression equations.

The patched Cachuma Dam temperature dataset was then used as the basis for creating a daily temperature dataset for the Gibraltar watershed. The first step in this process was to calculate the minimum and maximum temperature lapse rates between the Gibraltar (472 m) and Cachuma Dam (238 m) stations. The 244 Gibraltar values were grouped into 'winter' (213 points) and 'summer' (31 points) periods for lapse rate calculations, as were the corresponding data points for Cachuma Dam. Overall, lapse rates for maximum temperature (winter = -4.15

C/km; summer = 2.61 C/km) and winter minimum temperature (-7.26 C/km) were within acceptable limits. However, the lapse rate for summer minimum temperature was extremely large (18 C/km) and considered unrealistic. Therefore, only a daily maximum temperature dataset was generated via this process (which necessitated modifying the Hargreaves-Samani PE model before generating a daily PE time series for the Gibraltar basin - see below). Since the actual lapse rate applied to the Cachuma Dam maximum temperature dataset was 'per kilometer', the resulting maximum temperature dataset was actually representative of a site located at approximately the mean elevation of Gibraltar basin (1212m) – not of the Gibraltar station itself.

The Hargreaves-Samani (HS) model (1) requires daily inputs of solar radiation (RS) and mean temperature (T) to estimate values of potential evaporation (ETo):

$$ETo = 0.0135 * RS (T + 17.8) \qquad (1)$$

Before applying this model to estimate ETo for the Gibraltar watershed, it was evaluated to determine its 'fitness' for making ETo predictions in this environment. Daily RS, T and ETo data obtained from a nearby CIMIS station (No. 107) for the period 1995-97 were used in (1) to calibrate the model for this station (and, in theory, this region). The calibrated coefficient was 0.0126 (close to the initial value of 0.0135) and the coefficient of efficiency was 0.992. Satisfied

that the HS model was generally applicable in this region, it was used to generate a daily ETo dataset for the Gibraltar watershed.

There was no observed daily solar radiation data available for the Gibraltar watershed. Instead, it was derived using an equation (2) provided in Hargreaves-Samani (1985) which required daily values of extra-terrestrial radiation (RA) and temperature range (TD). Prior to applying it in Gibraltar, this equation was calibrated using observations of RA, TD and RS from the abovementioned CIMIS station.. Calibration results were good and the equation was used to estimate daily value of RS for Gibraltar.

$$RS = K_{RS} * RA * TD^{0.50} \qquad (2)$$

RA was calculated using a computer program written to incorporate equations from Dingman (19XX) which calculate RA as a function of slope-aspect. This was an important consideration given that microclimate conditions in chaparral (e.g., soil moisture, available energy) are controlled largely by the distribution of slope-aspect. Slope and aspect grids generated from a 90m digital elevation model of the Gibraltar watershed were classified into twelve slope-aspect combinations (3 slope classes (low, moderate and high) and 4 aspect classes (N, S, E, W). Given the uncertainties related to the summer minimum temperature lapse rate, the same lapse rates (maximum temperature - summer and winter) were applied to both the maximum and minimum temperature data from Cachuma Dam in order to

calculate TD for the Gibraltar basin. [Actually, no lapse rates needed to be applied in this case, given that the same rates were applied to both temperature datasets - TD would be the same before and after applying the same lapse rates to the two temperature datasets.] TD was assumed constant over the watershed (i.e., the same at all elevations) in order to reduce the number of slope-aspect-elevation combinations for which ETo had to be calculated – while still retaining enough classes to be representative of the range of basin characteristics. RS was calculated for each of the twelve slope-aspect-elevation classes given daily inputs of TD and RA.

Originally, mean daily temperature inputs for the HS ETo model (1) were to be calculated using lapse-rate adjusted minimum and maximum temperature data (from Cachuma Dam). However, given the uncertainties related to the summer minimum temperature lapse rate, only simulated maximum temperature estimates were deemed reliable. Therefore, the HS ETo model was re-calibrated for CIMIS station 107 using maximum temperature in place of mean temperature values. [The step assumes that maximum temperature is the primary driver of ETo dynamics over a day, on average, for this area.] The new model coefficient was 0.011 and the coefficient of efficiency was 0.99. Given this result, lapse rate adjusted maximum temperature data and estimated solar radiation data for Gibraltar were used in (1) to generate a daily ETo time series for each of the twelve slope-aspect-elevation classes in the watershed.

Fire History Map

A digital fire history map (ARC/INFO regions coverage) for the Los Padres National Forest was obtained from Max Moritz (Cal Poly – SLO), along with an AML script used for deriving 'stand age' maps from the coverage. This script was used to generate a stand age map (90m grid cells) for each year of Landsat TM imagery (1988, 1990, 1997 and 1998). This grid cell resolution was selected to match that of the imagery. Each of the resulting stand age maps was subset to the Gibraltar watershed and the areal coverage for each fire within the basin was calculated.

Vegetation Type

A digital vegetation type map of the southern California region (30m grid) was obtained from Stephenson and Calcarone (1999). This map was subset to an area just surrounding the Gibraltar watershed. A 3x3 block majority filter (Arc/Info) was used to smooth the 30m map. The resulting map was aggregated to 90m and now contained 19 mapped vegetation types. Vegetation types with similar 'hydrologic functioning' (e.g., northern mixed chaparral and chamise chaparral) were placed into the same class. Five vegetation type classes resulted: grassland (1.1%), coastal sage scrub (9.7%), chaparral (75.7%), oak woodland (10.0%) and conifer (2.9%) – and two miscellaneous classes: water (0.2%) and barren (0.4%).

Vegetation Succession

Representing the temporal dynamics of vegetation succession/growth in MIKE-SHE requires information on vegetation type and vegetation age. Each mapped

vegetation type in the watershed (except 'grassland') comprised stands of different ages (as determined from the fire history maps). In order to represent each type/age combination in MIKE-SHE it was necessary to sub-divide mapped vegetation types into multiple 'sub-types' based on stand age, e.g., chaparral-age1, chaparral-age2, etc. LAI values were then attached to each sub-type using information from the literature and the remote sensing-based LAI curves (XXX). In fact, only the chaparral and coastal sage scrub types were divided into sub-types in this manner – grassland, conifer and oak types were not. The reasons for this are three-fold. First, the literature suggests that LAI is a function of stand age in chaparral and coastal sage scrub communities. Therefore, it was important to represent the intra- and inter-annual LAI dynamics for these vegetation types. Second, as the grassland type was assumed to be comprised solely of annual species, the same LAI values could be applied from year to year (i.e., annual grasses don't 'age'). And third, the very limited information on conifer and oak LAI for this region suggested that LAI was not a function of age for these two types. This, combined with the fact that much of the conifer and oak covered areas in the basin had not burned in over 30 years, led to the use of a constant LAI for each type.

Soils

A digital version of a 3rd order soil survey for the Los Padres National Forest was obtained from the Geography Department at UCSB (O'Hare and Hallock, National Cooperative Soil Survey, USDA, 1980). This soils coverage identifies soil

associations and soil complexes – map units composed of two or more major soil families (or subgroups). This 3rd order survey was compiled for use as a management tool and for determining the suitability and potential of a particular soil type for specific uses. The report that accompanies the digital data describes the general region, individual soil families/subgroups and provides detailed attribute information (e.g., texture, drainage class, soil profile depths, slope, etc.) for each map unit.

This soils coverage was clipped to the Gibraltar watershed boundary and converted to a 90m grid in Arc/Info, comprising 17 different soil associations. During a field visit to the watershed it was decided to generalize these 17 soils into 2 classes (upland and lowland), as the soils along a trial from valley bottom to ridge top appeared very similar - varying mainly in depth. The first step in the generalization process was to classify each of the 17 soil associations into either 'upland' or 'lowland'. The NCRS Soil Survey Manual describes slopes classes for use in soil type classification (Table 3-1, NRCS Soil Survey Manual). From this table, slopes less than/equal to 8% are described as 'nearly level' to 'gently sloping' and slopes greater than 8% are characterized as 'strongly sloping' to 'very steep'. This '8%' criteria was used as the basis for subdividing a slope map of the watershed (derived from a 90m DEM) into two classes, upland and lowland. Soil associations were then assigned to either the upland or lowland soil class by overlaying the slope map on the soil association map. Two of the 17 mapped soil

associations fell predominantly within the 'lowland' area (and were classified as such), while the remaining 15 associations were classified as upland.

In addition to soil type and distribution information, MIKE-SHE requires descriptions for each soil horizon (depth and texture) in the lowland and upland soil classes. These attributes were derived by examining the depth and texture descriptions for the soil associations comprising the upland and lowland soil classes. As mentioned above, each soil association is composed of a number of soil families. The 3rd order soil survey provided information on the depth and texture of each horizon for each soil family in each association. As a simplification, it was assumed in this study that each soil family had only two horizons (in some cases there were three horizons – in which case the 2nd and 3rd horizon attribute information was combined).

Determining the depth of each horizon for the lowland and upland soil classes required a number of steps. First, the depth of each horizon for each family in each soil association was established. Second, using information in the soil survey report, the total area of each family in each association was expressed as a percentage of the total area occupied by that association. These values were termed 'family weighting factors'. The weighted average depth of the upper horizon for each soil association was calculated by multiplying the depth of each family's upper horizon by the corresponding family weighting factor. The same procedure was used to determine the weighted average depth of the lower horizon for each soil association. Third, the percent area occupied by each soil association

within each soil class (upland or lowland) was calculated and termed the 'association weighting factor'. For each association, the weighted average depths of the upper and lower horizons were multiplied by the corresponding association weighting factor to determine the weighted average depths of each horizon for the soil association as a whole. Finally, the total depth of the upper and lower horizons for the lowland and upland soil classes were calculated by summing up the appropriate association-based horizon depths. The total depths of the upper/lower horizon for the lowland and upland soil classes were 15.03cm/92.85cm and 12.55cm/57.97cm, respectively.

The dominant soil texture (e.g., sandy loam) for each horizon for each soil class (lowland and upland) was established in the following manner. First, the dominant texture of each horizon for each soil family was assumed to be the texture that was mentioned first in the horizon description. A total of seven texture types were identified using this approach. Next, the number of occurrences of a given soil texture were tabulated by horizon (upper/lower) and soil class (lowland/upland). The texture type found most often in a given horizon/soil class was assigned as the texture type for that horizon/soil class. The 'sandy loam' texture type was assigned to the upper/lower horizons of the upland soil class and to the upper horizon of the lowland soil class. A 'loam' texture type was assigned to the lower horizon of the lowland soil class.

For each horizon for each soil class MIKE-SHE requires information on the hydraulic conductivity, the soil moisture characteristic curve and various other

physical characteristics (e.g., soil moisture content at saturation, residual soil moisture content). A review of the literature provided baseline values for these parameters/curves. For each horizon in each soil class parameter values were set on the basis of the assigned soil texture.

Topography

A 30m digital elevation model (DEM) of the Santa Barbara region was compiled in Arc/Info using 20 individual digital topo-quads obtained from the USGS. Sinks were filled to 'smooth' the surface and remove artifacts related to DEM compilation and aggregation. A variety of input datasets for MIKE-SHE were then generated using this DEM. Topographic slope, aspect and elevation were derived from the DEM and used in the production of basin geometry (boundary, elevation) rainfall, potential evaporation and soil input datasets (see Sections 1, 3 and 7, respectively). The river channel was then identified using a set of Arc/Info commands. The elevation of each cell in the channel was extracted into a digitized file and input into a utility program used to create the final river file in MIKE-SHE format.

The linear reservoir (LR) module in MIKE-SHE requires the user to specify the number and spatial distribution of watershed sub-basins and topographic zones. Two sub-basins were delineated for the Jameson sub-basin using a series of Arc/Info commands. Seven sub-basins were delineated for Gibraltar in the same manner. Each sub-basin was then sub-divided into three 'topographic zones': a) cells bordering the river, b) hillslope cells and c) ridgetop

cells. Water within a sub-basin is 'moved' through these zones from ridgetop to hillslope to river channel.

Fire Shape Simulation

Testing the research hypotheses involves running model simulations using a range of fire sizes found in different parts of the watershed. A simple, rule-based program (SHAPEGEN) was written in MATLAB to generate (fire) shapes of different sizes located randomly across the watershed. This program is not a fire simulator, rather it attempts to encompass the range of possible fire sizes and locations for a given watershed. A number of simple rules govern the selection of shape cells. First, a cell must fall within the watershed boundary. Second, the cell cannot contain a NODATA value. Third, only cells designated 'chaparral' or 'coastal sage scrub' may be selected (these vegetation types dominate the watersheds). Subject to these rules, a shape is created via the following set of steps. First, a 'seed' cell is randomly selected from all available cells and its location is recorded in a 'log' file. The second cell to be included in the shape is then randomly selected, provided that it is adjacent to the seed cell (eight possible cells border a given cell) – its location is also recorded in the log file. Based on a user-defined size, additional cells are then randomly selected, one at a time, for inclusion in the shape provided they: a) meet all of the abovementioned criteria and b) have not previously been selected (this is determined by having the program examine the log before selecting each new cell). All resulting shapes are

converted into an Arc/Info grid file using a customized .aml script and then imported into MIKE-SHE for use in model simulations.

APPENDIX B: MIKE-SHE CALIBRATION PARAMETERS – DEFINITIONS

The following table lists each of the parameters used in the calibration of the modified MIKE-SHE model (MSHE_m) in Chapter Two, and in the sensitivity analysis in Chapter Three (parameter definitions can be found following the table); parameter ranges are also shown in the table.

Parameter		Minimum value	Maximum value
Interflow/Groundwater reservoirs			
IF_t	(m)	0.0001	0.3
IF_h	(days)	0.0001	3
IF_v	(days)	0.0001	80
GW_h	(days)	0.05	100
Soil			
K_s_Sandy Loam	($m\ s^{-1}$)	1.0×10^{-6}	5.0×10^{-4}
n_Sandy Loam		1	30
K_s_Loam	($m\ s^{-1}$)	1.0×10^{-6}	5.0×10^{-4}
n_Loam		1	30
Vegetation			
C_1		0.01	1
C_2		0.01	1
C_3	($mm\ day^{-1}$)	1	60

Interflow/Groundwater Parameters

IF_t: Interflow (IF) reservoir threshold (depth) in meters.

IF_h: Interflow reservoir horizontal time constant in days.

IF_v: Interflow reservoir vertical time constant in days.

GW_h: Groundwater (GW) horizontal time constant in days.

Soil

K_s*_Sandy Loam*: Saturated hydraulic conductivity for the Sandy Loam soil type.

Ks_Loam: Saturated hydraulic conductivity for the Loam soil type.

n_Sandy Loam: exponent in the unsaturated hydraulic conductivity equation.

n_Loam: exponent in the unsaturated hydraulic conductivity equation.

Vegetation

C_1: Constant in the f(1) leaf area index (LAI) function used in the calculation of transpiration.

C_2: Constant in the f(1) leaf area index (LAI) function used in the calculation of transpiration.

C_3: Constant in the f(2) soil moisture function used in the calculation of transpiration.